MOLECULAR MEAN FIELD THEORY FOR LIQUID WATER AND HYDROPHOBIC FORCE

By

Jampa Maruthi Pradeep Kanth

PHYS10200604007

THE INSTITUTE OF MATHEMATICAL SCIENCES, CHENNAI

A thesis submitted to the
Board of Studies in Physical Sciences

In partial fulfillment of requirements
For the Degree of

DOCTOR OF PHILOSOPHY

of

HOMI BHABHA NATIONAL INSTITUTE

May, 2012

Homi Bhabha National Institute
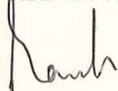
Recommodation of the Viva Voce Board

As members of the Viva Voce Board, we certified that we have read the dissertation prepared by Jampa Maruthi Pradeep Kanth entitled "Molecular Mean Field Theory for Liquid Water and Hydrophobic Force" and recommend that it may be accepted as fulfilling the dissertation requirement for the Degree of Doctor of Philosophy.
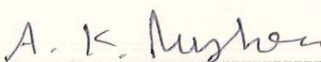
-- Date: 8/5/2012

Dean, Physical Sciences : T.R. Govindarajan

-- Date: 8/5/2012

Convener / Guide : Ramesh Anishetty

-- Date: 8/5/2012

Chairman : A.K. Mishra

-- Date: 8/5/2012
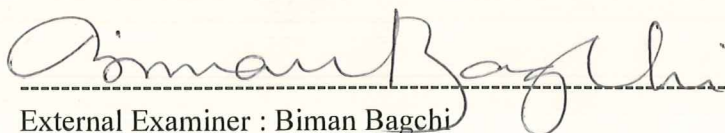
Member : Vani Vemparala

-- Date: 08/05/2012

Member : Purusattam Ray

-- Date: 8/5/2012
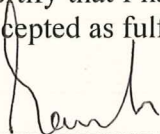
External Examiner : Biman Bagchi

Final approval and acceptance of this dissertation is contingent upon the candidate's submission of the final copies of the dissertation to HBNI.

I hereby certify that I have read this dissertation prepared under my direction and recommend that it may be accepted as fulfilling the dissertation requirement.

Convener / Guide: Ramesh Anishetty

Date : 8/5/2012

Place: Chennai

STATEMENT BY AUTHOR

This disseration has been submitted in partial fulfillment of requirements for an advanced degree at Homi Bhabha National Institute (HBNI) and is deposited in the Library to be made available to borrowers under rules of the HBNI.

Brief quotations from this dissertation are allowable without special permission, provided that accurate acknowledgment of source is made. Requests for permission for extended quotation from or reproduction of this manuscript in whole or in part may be granted by the Competent Authority of HBNI when in his or her judgement the proposed use of the material is in the interests of scholarship. In all other instances, however, permission must be obtained from the author.

Jampa Maruthi Pradeep Kanth

DECLARATION

I, hereby declare that the investigation presented in the thesis has been carried out by me. The work is original and has not been submitted earlier as a whole or in part for a degree/diploma at this or any other Institution/University.

Jampa Maruthi Pradeep Kanth

. . . to my Grandmother and my mother . . .

ACKNOWLEDGEMENTS

Abstract

The thesis aims at understanding the role of hydrogen-bond fluctuations in liquid water in bringing about a solvent-induced interaction between hydrophobic moieties, called hydrophobic force. This interaction plays a significant role in many oft-studied biological phenomena like protein folding, cell membrane formation etc. Surface force apparatus measurements reveal that hydrophobic force is long-ranged and monotonic in nature. We provide a statistical description of hydrogen-bond fluctuations in liquid water and address the long-distance nature of hydrophobic force and also attempt to provide a consistent picture of its dependence on the size of hydrophobes. The hydrogen-bond interaction is essentially orientation-dependent and specific in nature. The features imply for a system of water molecules that the density of dangling bonds and hydrogen bonds are to be commensurate with molecular density, which can be stated as "sum rule" for water. These aspects necessitate the statistical description of water in terms of both density and orientational degrees of freedom of the molecules. We define and analyze density and orientational correlations in popular water models in terms of a complete orthonormal set of orientational fields. Large-scale molecular dynamics simulations reveal that the density correlations vanish beyond few molecular diameters, whereas (longitudinal part of) dipolar orientational correlation shows long-distance behavior, at least up to 75 Å. Two correlation lengths of order 5.2 Å and 24 Å are inferred for the correlation function. It is seen to be predominantly influenced by the hydrogen-bond interaction. Coulomb interactions, surprisingly, have little effect on its long-distance behavior. The orientational correlation function is utilized to deduce interaction free energy for two mesoscopic hydrophobic surfaces in water. The restricted orientational fluctuations of water molecules in the vicinity of a hydrophobe are envisaged in a local interaction Hamiltonian and in presence of two such hydrophobes, the deduced force shows exponential decay with a correlation length half that of orientational correlations. The range of the force is strikingly consistent with that seen in experiments. The magnitude of the force is also shown to depend on shape and mutual orientations of the surfaces.

We take a theoretical route to understand hydrophobic force between large surfaces, by envisaging a simple lattice model for water and investigating the thermodynamic consequences of confining hydrogen-bond fluctuations. The model

incorporates the essential density and orientational degrees of freedom of water molecules. The restrictions on network formation, due to the nature of hydrogen-bond interaction, are handled in terms of dual lattice fields. A mean field analysis consistent with the sum rule for water is carried out and fluctuations in dual fields about the mean field are analyzed. The analytical framework is called molecular mean field theory. Monte Carlo simulations in compliance with constraints and restrictions in the model are also carried out to attest the mean field results. The sum rule manifests as an equation of network, i.e., a relation between molecular density and hydrogen-bond density. It correctly predicts density saturation and bond saturation within the model and is in quantitative agreement with the simulation results. The mean field analysis is pursued at arbitrary densities in the model. However, it is seen to be a good approximation only at densities corresponding to liquid phase or above. Correlation functions are also deduced in terms of dual field correlations. The density correlation vanishes within a short lattice distance, whereas orientational correlations show long-distance behavior. The correlation length deduced here is consistent with the shorter length inferred in molecular dynamics simulations. Coulomb interactions are seen to have little effect on the correlation length.

We then envisage large hydrophobic surfaces confining hydrogen-bond fluctuations in their intervening region. Casimir-like forces are known to arise in various contexts where fluctuating fields are confined between surfaces. The free energy of the system is increased due to restriction imposed on fluctuations by the boundaries, thereby system tends to minimize the separation in order to reduce the free energy cost. We investigate hydrophobic force to be a manifestation of Casimir-like force due to density and orientational fluctuations in liquid water. The discretization of fluctuation modes in confinement direction gives rise to a Casimir part of free energy. The modified orientational fluctuations in the interfacial region of hydrophobic surfaces, in addition, give rise to interfacial free energy and interfacial flucutations-induced free energy, both of which depend on nature of the surfaces. The Casimir part of free energy is the leading contribution and varies as $\frac{1}{L}$ for large distances. However, it is seen to be numerically small for distances beyond four times the orientational correlation length in the model. Interfacial free energy is also seen to vary with separation distance, albeit weakly and it reaches a constant value, asymptotically. The interfacial fluctuations-induced part is effectively cor-

relation between modified interfacial fluctuations at both surfaces. Its asymptotic behavior is dominated by orientational correlations in water and is analogous to hydrophobic force between mesoscopic surfaces. The collective consequences of these effects are analyzed for both hydrophobic and hydrophilic types of surfaces. The quantitative details of hydrophobic interaction are consistent with experiments. Transverse density profile of water is also addressed in our calculation and is seen to be qualitatively concomitant with results of confined water simulations.

For both mesoscopic surfaces and macroscopic surfaces, hydrophobic interaction is seen to be largely influenced by orientational correlations in water. Our mean field framework provides a direction to elucidate the size dependence of the interaction in terms of water properties.

Publications and preprints

[1] Jampa Maruthi Pradeep Kanth, Satyavani Vemparala, and Ramesh Anishetty. *Long-distance correlations in molecular orientations of liquid water and shape-dependent hydrophobic force.* Phys. Rev. E, 81(2):021201, 2010.

[2] Jampa Maruthi Pradeep Kanth and Ramesh Anishetty. *Molecular mean field theory for liquid water.* Physica A, 391:439-455, 2012.

[3] Jampa Maruthi Pradeep Kanth and Ramesh Anishetty. *Hydrophobic force a Casimir-like effect due to hydrogen-bond fluctuations.* arXiv:1109.2733, 2011.

Contents

List of Figures

List of Tables

Introduction

"Hydrophobic interaction is arguably the most important non-specific interaction in biological systems and is responsible for the creation of enclosed compartments by proteins and lipid bilayers in water, which was fundamental for the evolution of cells and therefore life."

J. N. Israelachvili

Liquid water provides matrix for many ubiquitous physical, chemical and biological phenomena. Interesting among them is *hydrophobic effect* which manifests at macroscopic scale as tendency of apolar chemical species to minimize contact with water. Some well known consequences are oil-water demixing and formation of near-spherical water droplets on a lotus leaf. The effect manifests at microscopic scale as a force of attraction between apolar moeities in aqueous medium, called *hydrophobic force*. This interaction is dominantly prevalent in biology and is known to be responsible for micellar aggregation, cell membrane formation, assembly of proteins into functional complexes [1]. Its occurence as a solvent-induced interaction was first suggested by Frank and Evans [2] and later elucidated in biological context by Kauzmann [3]. The former study noted that transferring small hydrophobes such as hydrocarbons into water was accompanied by unfavorable free energy change [4], dominated by entropy reduction due to reorganization of vicinal water molecules [2]. Hence, two hydrophobes show tendency to coalesce in order to minimize the unfavorable free energy. The low solubility of pure hydrocarbons in water, however, hampered efforts to directly measure or infer the interaction at this scale in experiments.

In early 1980s, employing large hydrophobic surfaces the first direct measurement of hydrophobic force was carried out using surface force apparatus (SFA) [5]. Amphiphilic molecules were chemisorbed on activated mica surfaces with their hydrophobic tails left open to interact with water. Two such surfaces were employed in a cross-cylinder geometry inside water medium and the measured force between them was related to interaction free energy using Derjaguin approximation [6].

Hydrophobic interaction was seen to be influential upto hundreds of Angstroms and stronger than inter-surface van der Waal (vdW) interaction. The qualitative nature of the interaction i.e., long range and monotonic decay, withstood the test of time [7–9].

A quantitative understanding of hydrophobic force from statistical description of liquid water is essential for many biophysical problems, eg., protein folding [10]. We briefly discuss essential degrees of freedom to be envisaged in the description of water and past attempts in this direction. The water molecules are uniquely set up with a geometry and intermolecular interaction that facilitate diverse molecular and orientational arrangements. Each molecule has two positively polarized hydrogen atoms (covalently bonded to oxygen atom) and two negatively polarized lone-pair of electrons, distributed at tetrahedral angles about oxygen nucleus. The geometry is a consequence of sp^3 hybridization (of $2s$ and $2p$ orbitals) in oxygen atom and the associated charge distribution is due to electronegative nature of oxygen [11]. In the background of this knowledge, x-ray diffraction studies on structure of ice and quantum-mechanical studies on water dimer in gas phase [11] indicate that a *hydrogen bond* occurs when two water molecules suitably orient such that a hydrogen arm of one molecule interacts with a lone-pair arm of the other. The orientation dependence and the specificity of hydrogen bonding impart importance to both density and orientational degrees of freedom in statistical analysis of water. There are models galore which were proposed and analyzed to reproduce anomalous thermodynamic properties of water [12, 13]. Theoretical attempts to envisage fluctuations in water are limited to Ornstein-Zernike-like phenomenological approaches, wherein integral equations only in terms of molecular density correlation were heuristically proposed and are numerically solved using different closure approximations [14, 15]. Wertheim's theory for associating fluids envisages similar density correlations to be solved in compliance with steric constraints imposed by formation of molecular clusters [16]. Other approaches specific to molecular fluids, such as reference interaction-site model, were seen to be less predictive in case of associating fluids [17]. Hydrophobic interaction at both small and large lengthscales has also been conventionally addressed in terms of density fluctuations in water. In case of small solutes, phenomenological approaches based on scaled particle theories envisage density exclusion caused by small solutes and estimate hydration free energies [17]. The accompanying change in density fluctuations of water is

considered small and using Ornstein-Zernike approach, the interaction free energy is derived in terms of density correlation function of bulk water [18]. For extended hydrophobic surfaces, large lengthscale density fluctuations in metastable confined fluid [19], dewetting-induced cavitation under liquid-vapor coexistence conditions [20], and fluid structuring effects [21] are some of the mechanisms suggested for the origin of hydrophobic interaction. These theories are envisaged in narrow range of fluid conditions and besides, were unsuccessful in reproducing generic features of the interaction seen in experiments [7]. There were also other studies that envisage electrostatic mechanisms [22, 23] or specific surface details like charged bilayer patches [22], nanobubbles [24]. The essential nature of hydrophobic interaction is seen to be qualitatively similar between different surface types [25].

The specific nature of hydrogen bonding interaction necessitates the density of hydrogen bonds and dangling bonds (hydrogens and lone-pairs which are not hydrogen bonded) to be commensurate with water density. This can be stated as a sum rule for water. Consequently, the fluctuations of density and orientational fields of water molecules (the latter being inherently connected to the bond fluctuations) are not totally independent; their long wavelength fluctuations especially are to be consistent with the sum rule. The essential features of hydrogen bonding interaction consistent with the sum rule are implicitly incorporated in effective charge models of water designed for numerical simulations (TIP5P, TIP3P, *etc*). A water molecule is often modeled as a polar molecule with charges corresponding to hydrogens and lone-pairs placed at vertices of a tetrahedron. A complete description of molecular correlations can be achieved by defining a set of orthonormal vectors in terms of atomic coordinates and defining correlations among them. We perform large-scale molecular dynamics simulations of the water models at ambient conditions and observe that density correlations are short-ranged, whereas dipolar orientations, which are receptive to bond fluctuations in the neighborhood, are correlated over large distances, at least up to 75 Å. Two correlation lengths of order 5.2 Å and 24 Å are inferred. Coulomb interactions, surprisingly, have little effect on the asymptotic behavior of the correlations [Chapter 2]. We utilize orientational correlation function of bulk water to deduce hydrophobic force between mesoscopic surfaces. The orientational fluctuations of water in the vicinity of a hydrophobe are modified due to unfavorable surface-water interactions. The correlation between modified interfacial fluctuations at two hydrophobic surfaces

gives rise to a long-range attractive force between the surfaces. The magnitude of the force decays exponentially with distance and depends on shape and mutual orientation of the surfaces [Chapter 3]. The exponential decay bears striking consistency with that seen in SFA experiments.

For the case of large hydrophobic surfaces, correlations in confined water need to be ascertained. In this case the desired system size to obtain proper equilibration and small free energy changes that need to be reliably computed are limitations to carry out a simulation study. Alternatively, we propose a simple model for water which incorporates essential features of hydrogen bonding and is envisaged on lattice to account exactly for hard-sphere repulsion. An analytical framework called molecular mean field theory is developed to deduce thermodynamic and fluctuation properties of the system consistent with the sum rule for water [Chapter 4]. In the model study we see that density correlations show hydration peaks and vanish within a short lattice distance, whereas orientational correlations display long-distance behavior, consistent with the results of molecular dynamics simulations. The mean field results are validated using exact Monte Carlo simulations for the lattice model [Chapter 5]. The mean field approximation is envisaged at arbitrary densities. But, within the model the approximation is seen to be self-consistent only for densities corresponding to liquid phase or higher. Qualitative predictions for the correlation functions are verified with exact simulation results. We then envisage large hydrophobic surfaces confining water in their intervening region. The presence of large surfaces substantially disrupts the hydrogen bond network whose fluctuations are suppressed at surface boundaries. The setting is ideally suited for fluctuations-induced force between the surfaces. Forces of this nature are generically called *Casimir forces* as they were first discussed by Casimir in the case of electromagnetic fluctuations confined between conducting plates [26], later studied in detail by Lifshitz [27] and envisaged in widely different contexts [28]. The case of thermal fluctuations-induced force was first discussed by Fisher and de Gennes. They argued that when a binary liquid mixture is confined between surfaces which have specific affinity towards one of the fluid components, Casimir-like density fluctuations in the liquid give rise to an effective force [29]. Origin of the force is entropic in nature; in that, the free energy of the system is increased due to restriction imposed on fluctuations by the boundaries, thereby system tends to minimize the separation in order to reduce the free energy cost. We investigate

hydrophobic force to be a manifestation of Casimir-like force due to density and orientational fluctuations in liquid water [Chapter 6]. The Casimir-like behavior and the modified orientational fluctuations near hydrophobic surfaces collectively give rise to a hydrophobic interaction acting over large distances and consistent with SFA experiments. The analysis is carried out for arbitrary fluid conditions and for generic surface types. We also deduce transverse density profile for water in confinement direction. The density profile shows a characterstic rise near the interfaces, concomitant with simulation studies on confined water and reaches the bulk density value within a hydrogen bond length. For both mesoscopic surfaces and macroscopic surfaces, hydrophobic interaction is seen to be largely influenced by orientational correlations in water. In the concluding chapter, important results from our model studies are summarized [Chapter 7].

Part I

Correlations in bulk water and hydrophobic force between mesoscopic surfaces

2

Correlations in bulk water : A molecular dynamics study

The effective interaction potentials designed for numerical simulations of water [13, 30] provide successful instances of implicitly envisaging hydrogen bonding interaction consistent with its most essential features i.e., orientation-dependent attraction and specific nature of bonding between two water molecules. Here, a water molecule is modeled as a polar molecule with charges corresponding to two hydrogens and two lone-pair of electrons placed at vertices of a tetrahedron, as shown in Fig.(2.1). We define position vectors $\vec{H}_{1,2}$ and $\vec{L}_{1,2}$ corresponding to hydrogens and lone-pairs, respectively, with respect to the position of oxygen O. Angles between the vectors and their lengths fluctuate about respective mean values. A water molecule's orientations can be conveniently described with a choice of vectors defined as

$$\vec{d}_{1(2)}(\mathbf{r}) = \frac{\vec{H}_1 + \vec{H}_2}{|\vec{H}_1 + \vec{H}_2|} - (+) \frac{\vec{L}_1 + \vec{L}_2}{|\vec{L}_1 + \vec{L}_2|} \tag{2.1}$$

where $\mathbf{r}$ is the position of oxygen atom in the bulk. The choice of $\vec{d}_1(\mathbf{r})$ and $\vec{d}_2(\mathbf{r})$ is such that they *do not* depend upon bond lengths of the molecule; they are symmetric under exchange of hydrogen or lone-pair positions of the molecule. The corresponding unit vectors $\hat{d}_1(\mathbf{r})$, $\hat{d}_2(\mathbf{r})$ and $\hat{d}_3 \equiv \hat{d}_1 \times \hat{d}_2$ form an orthonormal set. A set of three orthonormal unit vectors are sufficient to define any direction in three dimensional space. Here, $\hat{d}_1(\mathbf{r})$ is dominantly along the direction of dipole field and $\hat{d}_2(\mathbf{r})$ exists only if the water molecule differs from its mean near-tetrahedral
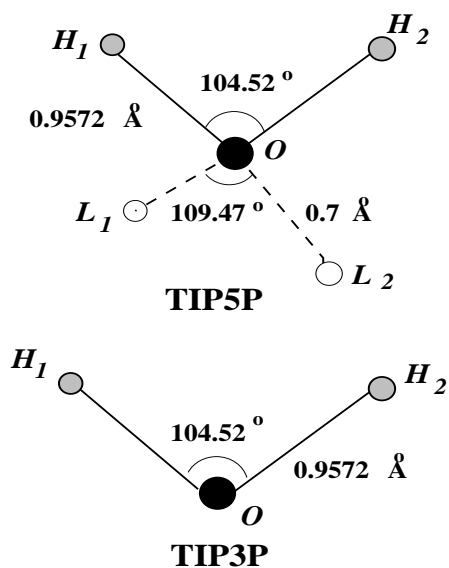
Figure 2.1: Geometry of a water molecule envisaged in TIP5P, TIP3P models.

geometry i.e., it is proportional to the quadrupole moment of the molecule.

The $\hat{d}$-vectors [Eq.(2.1)] form a complete triad with which orientation of any vector ($\vec{H}_{1,2}$ or $\vec{L}_{1,2}$) can be specified. Consequently, dynamics of water can be understood to be an interacting system of the $\hat{d}$-vector fields. In particular molecular dynamics (MD) simulation of water molecules implicitly gives us the dynamics of these fields. Various statistical correlations involving $\hat{d}_1(\mathbf{r})$, $\hat{d}_2(\mathbf{r})$ and $\rho(\mathbf{r}) \equiv (\hat{d}_1(\mathbf{r}))^2 = (\hat{d}_2(\mathbf{r}))^2$ in the liquid phase of water can be formulated as

$$\langle \rho(\mathbf{r}_1)\rho(\mathbf{r}_2)\rangle = g(\mathbf{r}_1, \mathbf{r}_2) \tag{2.2a}$$

$$\left\langle \rho(\mathbf{r}_1)\hat{d}_a(\mathbf{r}_2)\right\rangle = \frac{\mathbf{r}}{r} f_a(\mathbf{r}_1, \mathbf{r}_2) \tag{2.2b}$$

$$\left\langle d_a^i(\mathbf{r}_1)d_b^j(\mathbf{r}_2)\right\rangle = \frac{1}{2}\left(\delta^{ij} - \frac{r^i r^j}{r^2}\right) t_{ab}(\mathbf{r}_1, \mathbf{r}_2) - \frac{1}{2}\left(\delta^{ij} - 3\frac{r^i r^j}{r^2}\right) l_{ab}(\mathbf{r}_1, \mathbf{r}_2) \tag{2.2c}$$

where $\mathbf{r} = (\mathbf{r}_1 - \mathbf{r}_2)$, $r = |\mathbf{r}|$, subscripts $a, b = 1, 2, 3$ denote either of $\hat{d}_1, \hat{d}_2, \hat{d}_3$ and vector indices $i, j = 1, 2, 3$ denote directions in three-dimensional space. $g(\mathbf{r}_1, \mathbf{r}_2)$ is density correlation function, here, of oxygen. The remaining functions capture the correlations among other degrees of freedom of the vector fields. The translational and rotational symmetry of the system enable decomposing the tensorial properties of these correlations explicitly and thus analyze the data in terms of simple scalar
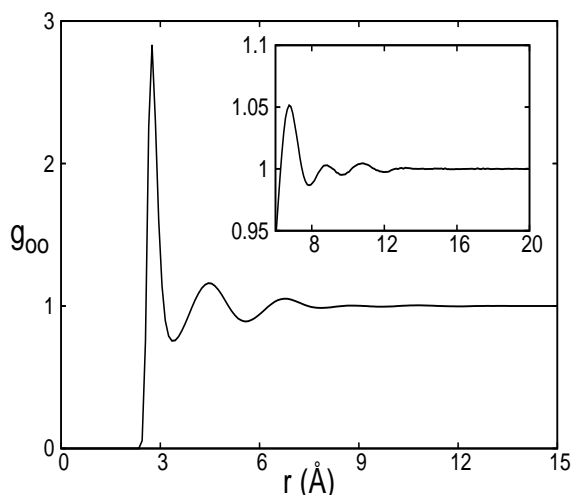
Figure 2.2: TIP5P - $g(r)$. Oxygen-oxygen radial distribution function. (*inset*) additional hydration shells in the end-hydration region.

functions like $g(0, r)$, $f_a(0, r)$, $t_{ab}(0, r)$, $l_{ab}(0, r)$ here after denoted and defined as below.

$$g(r) = \langle \rho(0) \ \rho(r) \rangle \tag{2.3a}$$

$$f_a(r) = \left\langle \rho(0) \ \hat{d}_a(r) \cdot \hat{r} \right\rangle \tag{2.3b}$$

$$t_{ab}(r) = \left\langle \hat{d}_a(0) \cdot \hat{d}_b(r) \right\rangle \tag{2.3c}$$

$$l_{ab}(r) = \left\langle \hat{d}_a \cdot \hat{r} \ \hat{d}_b \cdot \hat{r} \right\rangle \tag{2.3d}$$

TIP5P model [31] possesses all orientational degrees of freedom of a water molecule and has improved accuracy in predicting the structural properties of water at ambient conditions [Fig.(2.1)]. A large system size is chosen to accomodate large correlation lengths and facilitate better statistics (see Methods section 2.3). MD simulations of TIP5P water model are performed in a large cubic box of side 150 Å at ambient conditions i.e., $\rho = 1$ g cm^{-3}, $P = 1$ atm, $T = 300$K.

2.1 Results

The function $g(r)$, scaled with respect to ideal fluid structure at the same density, is called radial distribution function. It is the most conventionally studied correlation
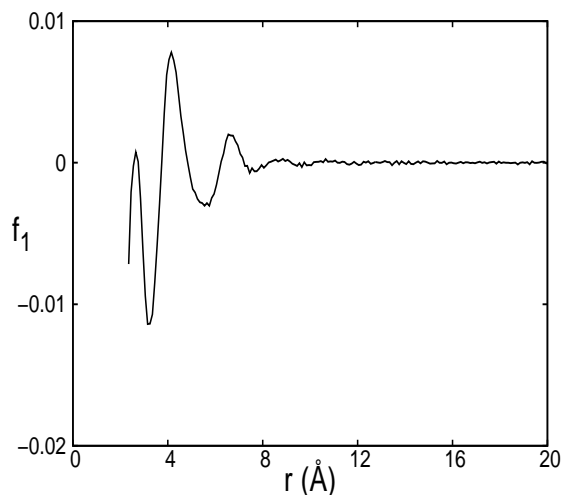
Figure 2.3: TIP5P - $f_1(r)$. Oxygen-dipole correlation function vanishes beyond 14 Å

function in fluid systems, both in experiments and theory [14]. As a consequence of finite size of a molecule, hydration peaks and troughs appear beyond hard-sphere radius (~ 2.5 Å). In our study, due to large system size and hence better statistics, few more prominent troughs are observed at about $r = 8.0$ Å and $r = 10.0$ Å [Fig.(2.2)]. The hydration structure visibly vanishes for distances beyond 12 Å without displaying any long-distance behavior.

$f_1(r)$ is correlation between oxygen atom and component of vicinal dipole along the radial vector separating them. This function also exhibits hydration structure and vanishes beyond 14 Å [Fig.(2.3)].

The orientational correlations of dipolar field are analyzed in terms of transverse trace part $t_{11}(r)$ and longitudinal traceless part $l_{11}(r)$. The longitudinal part measures the correlation between components of two dipoles along the radial vector separating them and transverse part captures the rest. $t_{11}(r)$ correlation solely contributes to Kirkwood dielectric function [32]. It shows oscillatory hydration structure, but vanishes (in compliance with rotational symmetry in the full system) beyond 14 Å, as shown in Fig.(2.4).

The longitudinal part $l_{11}(r)$ is plotted in Fig.(2.5). It is seen to be always positive and furthermore, in the $14 - 75$ Å regime it can be fitted to an Ornstein-
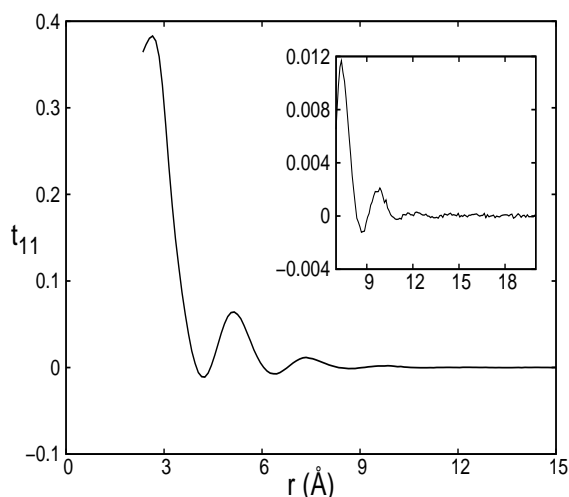
Figure 2.4: TIP5P - $t_{11}(r)$: Transverse part of dipolar orientational correlation. (*inset*) The correlation vanishes beyond the hydration region of 14 Å

Zernike (OZ) form as given below.

$$l_{11}(r) = 0.39(2)\ \frac{\exp(-r/5.2(1)\text{Å})}{r} + 0.027(1)\ \frac{\exp(-r/24(1)\text{Å})}{r} \quad r > 14\text{Å} \quad (2.4)$$

$l_{11}(r)$ shows longest correlation length of 24 Å. Furthermore, it exhibits hydration peaks upto 14 Å [Fig.(2.5)]. The error bars are mentioned as explained in the following illustration. Eg. The precise strength of the first exponential is 0.397541 ± 0.02168 and it is written here as 0.39(2) which expresses the mean value and in bracket, the error in the last significant digit. The statistical sampling errors are dramatically reduced for large distances, as expected [Appendix (2.4.1)].

The orientational correlations have not been measured or inferred in experiments. To ascertain the generality of the long-range correlation we also simulated TIP3P model of water which, by design, has $\hat{d}_1$ degree of freedom only [33]. That is, each water molecule's orientation can be completely described by $\hat{d}_1$ field alone [Fig.(2.1)]. The simulations of TIP3P model are also performed with a large system size and at ambient conditions [see Methods section (2.3)].

Analysis in the case of TIP3P model also shows that $l_{11}(r)$ correlation follows the same asymptotic behavior as described by Eq.(2.4). All other correlations $g(r)$, $f_1(r)$, $t_{11}(r)$ vanish beyond 12 Å and display no long-distance behavior.
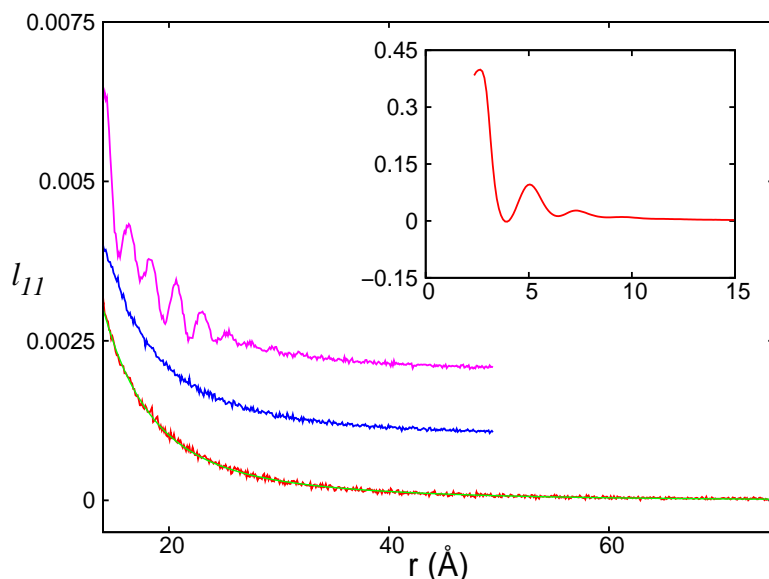
Figure 2.5: Exponential decay in longitudinal part of dipolar orientational correlation $l_{11}(r)$ outside the hydration region. (*red and green, bottom curve*) TIP5P data and fit function given by Eq.(2.4) on top of each other. (*blue, middle curve*) TIP3P data for $l_{11}(r)$. (*pink, top curve*) TIP3P with truncated Coulombic interactions. For clarity, the middle and the top plots are shifted up by 0.001 and 0.002 units respectively. (*inset*) $l_{11}(r)$ inside the hydration region within TIP5P model.

A water molecule in liquid phase is predominantly influenced by hydrogen bonding and furthermore, it has a net dipole moment which interacts through Coloumb force. In the effective charge models, Coulomb interactions are suitably parameterized to envisage both short-range hydrogen bonding and long-range dipolar interactions. To ascertain the cause for the long-distance behavior of $l_{11}(r)$, we truncate the Coulomb interaction potential smoothly in TIP3P model simulations and effectively retain short-range interaction that imitates hydrogen bonding [Appendix (2.4.1)]. The hydration peaks in correlation functions are determined consistent with the hydrogen bonding interaction. Since the peaks extend upto about 12 Å we choose the same distance cut-off in implementing the truncation procedure. The simulations with truncated-Coulomb potential are performed under ambient thermodynamic conditions. There is no noticeable variation in the density of the new model system compared to full-Coulomb case. Our analysis shows that $l_{11}(r)$ remains essentially unchanged in the regions of first few hydration shells and for $r > 30$ Å. This indicates that hydrogen-bond interactions are responsible for

the long-distance behavior of orientational correlations. The intermediate region exhibits over-structuring effects upto 30 Å [34].

It is also found that all correlations involving $\hat{d}_2$, $\hat{d}_3$ vectors in TIP5P model vanish upto statistical errors beyond the first hydration peak itself [Figs.(2.6)-(2.10)]. Therefore, $\hat{d}_2$, the quadrupole moment of the water molecule, fluctuates locally and randomly without any non-local correlations. $\hat{d}_3$ being a pseudovector has vanishing correlations with $\hat{d}_1$ and $\hat{d}_2$, demonstrating that there is no parity violation in the system.
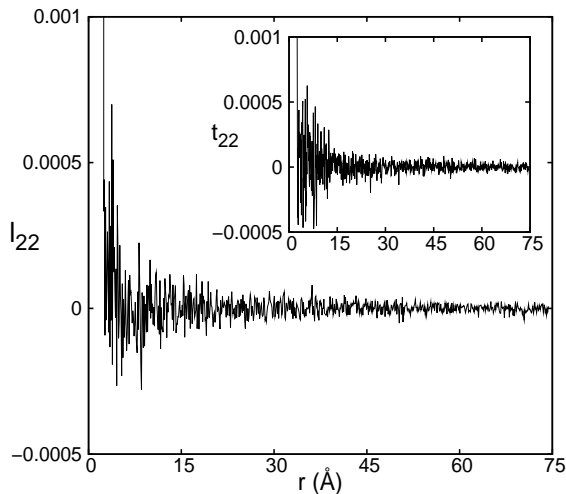
Figure 2.6: TIP5P - l_{22}, $(inset)t_{22}$. Longitudinal and transverse parts of the correlation $< \hat{d}_2\ \hat{d}_2 >$, vanishing upto statistical errors beyond the first hydration peak

2.2   Discussion

The three case studies are in agreement with Eq.(2.4) asymptotically. These observations suggest that (i) the orientational fluctuations in liquid water are dominantly those of dipole degree of freedom; in contrast, the quadrupole has no effect beyond the first hydration peak, (ii) in liquid phase these orientational fluctuations are influenced by local environment of respective molecule through hydrogen bonding, significantly more compared to long-range electrostatic interactions, (iii) furthermore, the orientational fluctuations exhibit long-distance correlations.

$g(r)$ is the conventionally studied correlation function in water. It displays
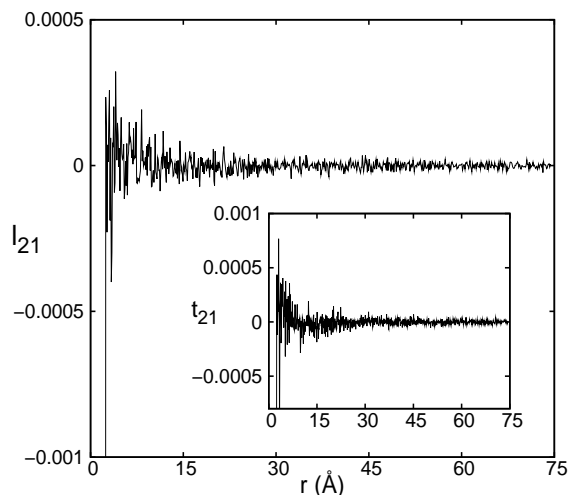
Figure 2.7: TIP5P - l_{21}, $(inset)t_{21}$. Longitudinal and transverse parts of the correlation $< \hat{d}_2\ \hat{d}_1 >$, vanishing upto statistical errors beyond the first hydration peak

only hydration peaks and exhibits no long-distance behavior. Recent small-angle x-ray scattering experiments indicate that $g(r)$ has a correlation length of about 3 Å (300 K) [35] in corroboration with an earlier small-angle neutron-scattering experiment [36]. The origin of this length is speculated to be due to presence of hydrogen-bonded structures of two different densities coexisting in liquid water [35]. This effect is absent in TIP5P and TIP3P models. In MD simulations using spherically symmetric models of water [12, 37] the only interesting correlation is $g(r)$, which exhibits no significant long-distance behavior. These facts support our view that any long-range correlation in water can only be due to orientational degree of freedom.

2.3 Simulation methods

The simulations of TIP5P water system are performed with GROMACS package (version 3.3.1) [38]. In the course of simulations an integration time step of 2 fs is used. The fast-moving bonds $O - H$ are constrained using LINCS algorithm. A large system consisting of 110592 molecules in a 150 Å box is equilibrated for 2 ns in constant pressure and temperature NPT ensemble. A constant pressure is maintained isotropically for the system. In order to compute van der Waals inter-
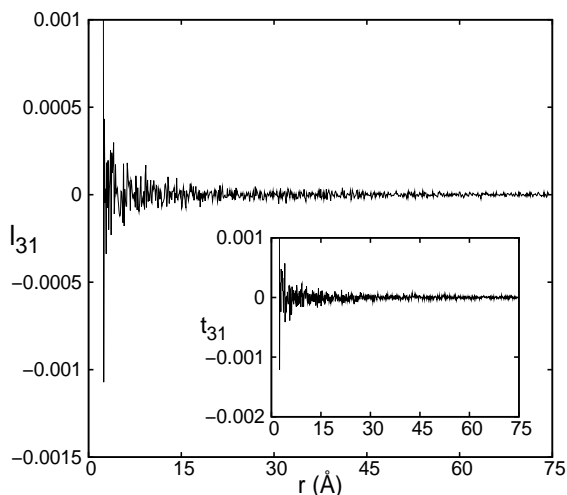
Figure 2.8: TIP5P - l_{31}, $(inset)t_{31}$. Longitudinal and transverse parts of the correlation $< \hat{d}_3 \ \hat{d}_1 >$, vanishing upto statistical errors beyond the first hydration peak

action a cut-off distance of 12 Å is used i.e., the potential is smoothly truncated at 12 Å away from the molecule in question. The smooth truncation allows conservation of energy as against abrupt truncation schemes. The long-ranged electrostatic interaction is handled by incorporation of multiple time-stepping procedure. To reduce the computational cost of handling non-bonded interactions, a non-bonded pair-list is created which contains all pairs of atoms for which non-bonded interactions should be calculated. This list is updated periodically during the dynamics. The pair-list distance is chosen to be greater than cut-off distance to ensure atoms moving in and out of cut-off distances within the period of updation are also included for calculation of non-bonded interactions. A pair-list distance of 15 Å is used in our simulation. Periodic boundary conditions are imposed in all directions. Full electrostatic interactions are computed with particle mesh Ewald method with a tolerance of 10^{-6} and updated every two time steps [39]. The initial equilibriation run is carried out at 1 atm pressure and 300K temperature. The equilibrated volume is noted and at this average volume a production run is carried out for 2 ns in a constant volume NVT ensemble. During the production run, the atomic coordinates of all molecules in the system are saved every 100 ps for analysis.

The simulations on TIP3P water system are performed using NAMD package (version 2.6) [40]. Here, 33105 water molecules are simulated in a cubical box of size
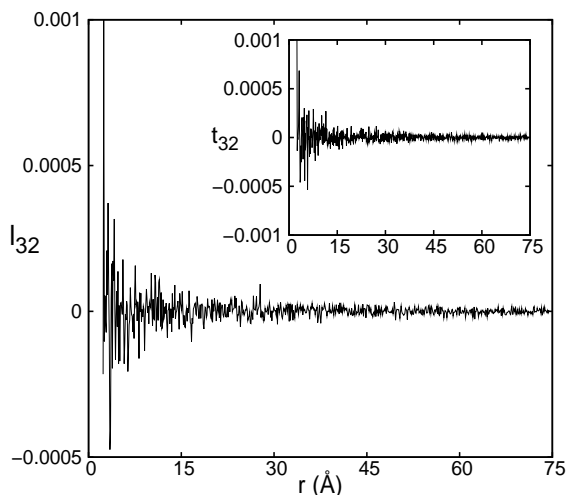
Figure 2.9: TIP5P - l_{32}, $(inset)t_{32}$. Longitudinal and transverse parts of the correlation $< \hat{d_3}\ \hat{d_2} >$, vanishing upto statistical errors beyond the first hydration peak

100 Å and the procedures employed for collecting equilibriated configurations are same as those described in case of TIP5P. The constrained model is implemented using SETTLE algorithm. A cut-off distance of 12 Å and a pair-list distance of 15 Å are used. Simulations are carried out under periodic boundary conditions at ambient conditions.

The TIP3P model with truncated Coulomb potential is simulated using the same procedure as described above in NAMD package. A smooth potential truncation scheme is employed to ensure conservation of energy and charge in the system.

2.4 Appendix

2.4.1 Fit functions for $l_{11}(r)$

For completeness various fitting functional forms are envisaged for $l_{11}(r)$ data obtained from both TIP5P and TIP3P model simulations. The functions and their corresponding root mean square deviations (RMSDs) are summarized in Table (2.1).

Among the exponentials, the bi-exponential OZ function has at least a factor of two better RMSD than other combinations. A single power-law also seems to fit
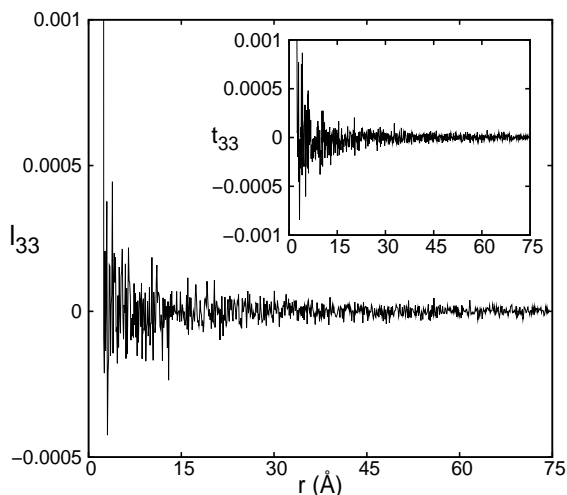
Figure 2.10: TIP5P - l_{33}, $(inset)t_{33}$. Longitudinal and transverse parts of the correlation $< \hat{d}_3 \, \hat{d}_3 >$, vanishing upto statistical errors beyond the first hydration peak

the data very well in this limited distance range upto 75 Å. From numerics point of view the power-law behavior cannot be strictly ruled out. If the r^{-n} behavior is extrapolated asymptotically for large distances, it amounts to the fact that the system is exhibiting critical behavior. In MD simulations, we did not see any concomitant signatures of critical behavior at all. Furthermore, liquid water is certainly not critical at ambient conditions. Therefore, we discard the power-law extrapolation and conclude that the bi-exponential OZ fit function is the correct extrapolation.

There are analytic theories for dipolar fluids which argue that the dipolar correlations behave like r^{-3} asymptotically due to long-range nature of Coulomb interactions [14, 41]. We notice from Fig.(2.5) that the truncation of Coulomb interaction has null effect on the asymptotic behavior of dipolar correlation. Also, the correlation is seen to respond to variation in temperature [Table (2.2)]. Hence, the arguments attributing long-distance dipolar correlations to Coulomb interactions are not justified.

Model	Fit function	RMSD
TIP5P	$0.39(2) \, \dfrac{\exp(-r/5.2(1))}{r} + 0.027(1) \, \dfrac{\exp(-r/24(1))}{r}$	$2.54462e - 05$
TIP3P	$0.34(2) \, \dfrac{\exp(-r/5.4(2))}{r} + 0.029(3) \, \dfrac{\exp(-r/24(1))}{r}$	$2.54122e - 05$
TIP5P	$0.152(2) \, \dfrac{\exp(-r/10.36(9))}{r}$	$5.33897e - 05$
TIP3P	$0.151(2) \, \dfrac{\exp(-r/10.5(1))}{r}$	$5.80041e - 05$
TIP5P	$0.0220(4) \, \exp(-r/6.71(5))$	$6.72991e - 05$
TIP3P	$0.0217(5) \, \exp(-r/6.85(6))$	$7.78593e - 05$
TIP5P	$8.0(1) \, r^{-2.990(8)}$	$2.5292e - 05$
TIP3P	$7.2(1) \, r^{-2.940(8)}$	$2.5860e - 05$

Table 2.1: Numerical fitting of $l_{11}(r)$ obtained from simulations of TIP5P and TIP3P data. The error bars quoted are as per the following illustration : Eg. 0.397541 ± 0.02168 is written as $0.39(2)$ which expresses the mean value and its leading significant deviation.

T (P=1 atm)	Fit function	RMSD
280K	$0.42(3) \dfrac{\exp(-r/5.0(2))}{r} + 0.031(3) \dfrac{\exp(-r/24(1))}{r}$	$3.3018e-05$
	$6.9(1) \ r^{-2.90(1)}$	$3.4272e-05$
	$9.00(1) \ r^{-3}$	$3.8138e-05$
300K	$0.34(2) \dfrac{\exp(-r/5.4(2))}{r} + 0.029(3) \dfrac{\exp(-r/24(1))}{r}$	$2.5412e-05$
	$7.2(1) \ r^{-2.940(8)}$	$2.5870e-05$
	$8.58(1) \ r^{-3}$	$2.7774e-05$
350K	$0.31(2) \dfrac{\exp(-r/5.6(3))}{r} + 0.023(3) \dfrac{\exp(-r/27(3))}{r}$	$3.3624e-05$
	$6.3(2) \ r^{-2.92(1)}$	$3.4253e-05$
	$7.93(1) \ r^{-3}$	$3.6437e-05$

Table 2.2: $l_{11}(r)$ in TIP3P : Temperature dependence and corresponding variation in fit function parameters.

3

Hydrophobic force between mesoscopic surfaces

Hydrophobic force measured in SFA experiments is seen to be influential at large distances upto about 200 Å. Between stable hydrophobic surfaces the force is inferred to be exponentially decaying with a correlation length of 12 Å [5, 7]. We may envisage the situation in a simulation study. The accompanying free energy change at large separation distances could be small and reliable free energy computation schemes are necessary in order to compute the interaction to required precision in simulations. Alternatively, a quantitative theoretic study is considered below. We envisage small hydrophobic surfaces present inside aqueous medium. In the limit of small surface sizes the hydrogen-bond network in water medium is not disrupted significantly. Hence, we utilize the correlation functions of bulk liquid water in order to deduce hydrophobic interaction free energy between mesoscopic surfaces. Our analysis implicates the long-distance orientational correlations responsible for the long-range nature of hydrophobic force [42].

Hydrophobic surfaces cannot form hydrogen-bonds with water. Consequently, water molecules in the vicinity of a hydrophobe rearrange themselves such that they form a sheet of hydrogen-bond network on the surface. Their interactions are such that the directions of lone pairs and hydrogen atoms are perpendicular to the surface normal of the hydrophobe. Owing to the approximate tetrahedral conformation, water molecules cannot have a unique configuration satisfying the above criterion [43]. Consequently, they explore other possible orientations as well by fluctuating at pico-second time scales [44]. These network fluctuations
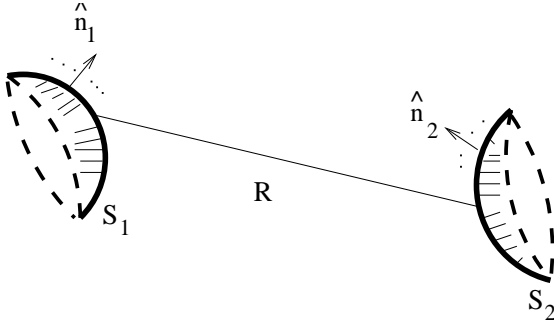
Figure 3.1: S_1, S_2 are hydrophobic surfaces with their local normal vectors $\hat{n}_1$, $\hat{n}_2$. R is the minimum distance between the two surfaces

contribute significantly to the solvation free energy of the hydrophobe. Interaction between a hydrophobic surface and orientation of a vicinal water molecule can be written in terms of $\hat{n}(\mathbf{r})$, the local unit normal vector to the hardcore van der Waals surface of the hydrophobe and $\hat{d}_1(\mathbf{r}')$, the dipole of water molecule near the surface, where $\mathbf{r}' = \mathbf{r} + \delta\mathbf{r}$; $\delta\mathbf{r}$ is typical length of hydrogen arm of water molecule (about 1 Å). A simple local interaction term can be taken as $(\hat{n}(\mathbf{r}) \cdot \hat{d}_1(\mathbf{r}'))^2$ implying that the water dipoles orient orthogonal to the surface normal as seen in simulations [45] (importantly, no linear term in $(\hat{n} \cdot \hat{d}_1)$, for that means a preferential orientation of the water dipole inward/outward to the surface).

The free energy change ΔG due to two small hydrophobic surfaces S_1 and S_2 [Fig.(3.1)] in water can be estimated by

$$\exp(-\Delta G/kT) = \langle \exp(-\Delta\mathcal{H}/kT) \rangle \tag{3.1}$$

$$\text{where} \quad \Delta\mathcal{H} = \frac{\gamma_1}{2}\int_{S_1} d\hat{n}_1 \left(\hat{n}_1(\mathbf{r}_1) \cdot \hat{d}_1(\mathbf{r}_1')\right)^2 + \frac{\gamma_2}{2}\int_{S_2} d\hat{n}_2 \left(\hat{n}_2(\mathbf{r}_2) \cdot \hat{d}_1(\mathbf{r}_2')\right)^2$$

γ is a measure of strength of interaction between hydrophobic solute and water and it can depend upon temperature, density and other parameters defining the thermodynamic system. The brackets $< ... >$ refer to statistical averaging with respect to pure water system and integration is over area of each surface. $\mathbf{R}$ is a vector along minimum distance of separation between them.

When the distance $R \ (= |\mathbf{R}|)$ is large compared to radius of curvature of each surface and the surface areas are sufficiently small, the statistical averaging can be done by cumulant expansion [Appendix (3.2.1)]. The leading term that depends

on distance R is explicitly given below.

$$
\begin{aligned}
\exp(-\Delta G/kT) \;\; = \;\; \exp\Bigg[& \gamma_1 \left\langle \ldots \right\rangle + \gamma_2 \left\langle \ldots \right\rangle + \frac{\gamma_1 \gamma_2}{4(kT)^2} \int_{S_1} \int_{S_2} d\hat{n}_1 \; d\hat{n}_2 \\
& \times \left\langle (\hat{n}_1(\mathbf{r}_1) \cdot \hat{d}_1(\mathbf{r}_1'))^2 \; (\hat{n}_2(\mathbf{r}_2) \cdot \hat{d}_1(\mathbf{r}_2'))^2 \right\rangle + \ldots \Bigg]
\end{aligned}
\qquad (3.2)
$$

In the above equation, terms proportional to γ_1, γ_2 (or their higher orders) only contribute to interfacial free energy for respective hydrophobe-water interface. The term proportional to $(\gamma_1 \gamma_2)$ contributes to the interaction free energy. The above free energy change is a consequence of surface-water interactions. The full solvation free energy in addition comprises hydration free energy of each solute proportional to solute's volume, which can be deduced in the infinite dilution limit [17, 46]. Other forms of short range surface-water interaction such as van der Waal interaction may also be envisaged [18]. They do not, however, affect the long-distance behavior of hydrophobic interaction discussed below.

The interaction term in Eq.(3.2) is analyzed [Appendix (3.2.1)] and the leading expression for force $F(R) = -\partial \Delta G/\partial R$ is given by the following expression.

$$
F(R) \;\; = \;\; \frac{\gamma_1 \gamma_2}{2kT} A_1 A_2 \; \frac{\partial}{\partial R} \mathrm{Tr} \left[\boldsymbol{\Sigma}_{\mathbf{S_1}} \mathbf{E}(\mathrm{R}) \boldsymbol{\Sigma}_{\mathbf{S_2}} \mathbf{E}(\mathrm{R}) \right]
\qquad (3.3)
$$

where A_1, A_2 are areas of the surfaces. $\mathbf{E}$ is a matrix whose elements denote correlation between components of interfacial dipoles. $\boldsymbol{\Sigma}_{\mathbf{S}}$ is a geometric factor characterstic of shape of the surface. The elements of $\mathbf{E}$, $\boldsymbol{\Sigma}_{\mathbf{S}}$ matrices are given by

$$
E^{ij}(R) \;\; \equiv \;\; \left\langle d_1{}^i(\mathbf{r}_1') \; d_1{}^j(\mathbf{r}_2') \right\rangle \;\; \simeq \;\; -\frac{1}{2} \left(\delta^{ij} - 3 \frac{R^i R^j}{R^2} \right) l_{11}(R) \quad \text{for large } R \qquad (3.4)
$$

$$
(\Sigma_S)^{ij} \;\; \equiv \;\; \frac{1}{A} \int_S d\hat{n} \; n^i n^j \qquad (3.5)
$$

where, the integration in Eq.(3.5) is over the direction of surface normal over the extent of surface area.

The above result on hydrophobic force is very general in nature. As discussed in earlier paragraphs, the leading order $(\hat{n} \cdot \hat{d}_1)^2$ is taken to be the interaction energy term for simplicity. By including the non-leading terms in the interaction energy function [Eq.(3.1)] and doing the cumulant expansion, it can be shown that the force equation for large R [Eq.(3.3)] remains unchanged, thus establishing the

generality of the result.

These considerations are valid for distances beyond the solvation region of a typical water molecule. The cumulant expansion allowed decomposing the force equation as a simple convolution of surface-dependent part and solvent-dependent part. Equation (3.3) enables us to conclude that range of the force between hydrophobic surfaces at large distances is always attractive governed by $l_{11}^2(R) \propto \exp(-R/12)$ for large R. Therefore, the hydrophobic force falls off exponentially with a largest correlation length of about 12 Å [see Appendix (3.2.1)], in addition to several other shorter range exponents as well.

$$F(R) \propto (-)\exp(-R/12\text{Å}) \qquad \text{for large } R \qquad (3.6)$$

The strength of attraction is proportional to area and shape of each surface given by the tensor $\mathbf{\Sigma}$, the second moment of surface normal. The final trace operation over the matrices $\mathbf{E}(\mathrm{R})$ and $\mathbf{\Sigma_S}$ implies that the hydrophobic attraction is not just a purely distance-dependent interaction such as van der Waals'. Indeed the orientation of the surfaces relative to each other can modify the magnitude of the force significantly. As an example if two small planar hydrophobic surfaces are mutually perpendicular and are sufficiently far apart, the magnitude of the force is zero. In contrast, the force is maximum when they are parallel to each other [see Appendix (3.2.2)].

3.1 Discussion

A simple-minded theoretical estimate of the force between mesoscopic hydrophobic surfaces done here suggests that the surfaces experience a long-range force albeit the strength is not large and in addition, the proposed force depends on shape and relative orientations of the surfaces. The long-range nature of the force is a consequence of orientational correlations in water. The exponential decay implied in Eq.(3.6) bears a striking consistency with that seen in experiments measuring hydrophobic force [5, 7].

For the case of large hydrophobic surfaces, correlations in water confined between the surfaces need to be ascertained. To simulate such a system the surfaces need to be several times larger than the longest correlation length in the system in

order to obtain proper equilibriation. This requires huge system size that would render the simulation prohibitively resource intensive. In addition, the accompanying free energy change could be very small due to weak nature of correlations at large distances. Instead, we take analytic route to describe hydrogen-bond fluctuations in water and the effect of spatial confinement on them. This study forms the second part of the thesis.

3.2 Appendix

3.2.1 Derivation of force equation

In this section we provide a brief description of intermediate steps in the deduction of the force equation. The technique under consideration is cumulant expansion used to perform statistical averaging in an approximate manner [47]. From Eq.(3.1),

$$
\begin{aligned}
\exp(-\Delta G/kT) \;=\; & \left\langle 1 - \frac{\gamma_1}{2kT} \int_{S_1} d\hat{n}_1 (\hat{n}_1(\mathbf{r}_1) \cdot \hat{d}_1(\mathbf{r}_1^{'}))^2 + \; \gamma_1{}^2(\ldots) \right. \\
& - \frac{\gamma_2}{2kT} \int_{S_2} d\hat{n}_2 (\hat{n}_2(\mathbf{r}_2) \cdot \hat{d}_1(\mathbf{r}_2^{'}))^2 + \; \gamma_2{}^2(\ldots) \\
& \left. + \frac{\gamma_1\gamma_2}{4(kT)^2} \int_{S_1}\int_{S_2} d\hat{n}_1 \; d\hat{n}_2 (\hat{n}_1(\mathbf{r}_1) \cdot \hat{d}_1(\mathbf{r}_1^{'}))^2 \; (\hat{n}_2(\mathbf{r}_2) \cdot \hat{d}_1(\mathbf{r}_2^{'}))^2 + \ldots \right\rangle \\
\;=\; & \exp \left[\gamma_1 \left\langle \ldots \right\rangle + \gamma_2 \left\langle \ldots \right\rangle + \frac{\gamma_1\gamma_2}{4(kT)^2} \int_{S_1}\int_{S_2} d\hat{n}_1 \; d\hat{n}_2 \right. \\
& \left. \times \left\langle (\hat{n}_1(\mathbf{r}_1) \cdot \hat{d}_1(\mathbf{r}_1^{'}))^2 \; (\hat{n}_2(\mathbf{r}_2) \cdot \hat{d}_1(\mathbf{r}_2^{'}))^2 \right\rangle + \ldots \right] \quad (3.7)
\end{aligned}
$$

Force between the surfaces is given by $F(R) = -\partial \Delta G/\partial R$. Only the terms proportional to $(\gamma_1\gamma_2)$ (or its higher order) depend on distance R and contribute to the force. In the above equation we retained only the leading order force term. Employing the notation that any repeated index is summed over, the force term in Eq.(3.7) can be analyzed as below.

$$
(\hat{n}_1 \cdot \hat{d}_1)^2 \equiv n_1{}^i d_1{}^i \; n_1{}^j d_1{}^j
$$
$$
(\hat{n}_2 \cdot \hat{d}_1)^2 \equiv n_2{}^k d_1{}^k \; n_2{}^p d_1{}^p
$$

$$
\begin{aligned}
& \left\langle (\hat{n}_1(\mathbf{r}_1) \cdot \hat{d}_1(\mathbf{r}_1'))^2 \ (\hat{n}_2(\mathbf{r}_2) \cdot \hat{d}_1(\mathbf{r}_2'))^2 \right\rangle \\
& = \quad \left\langle n_1{}^i d_1{}^i(\mathbf{r}_1') n_1{}^j d_1{}^j(\mathbf{r}_1') \ n_2{}^k d_1{}^k(\mathbf{r}_2') n_2{}^p d_1{}^p(\mathbf{r}_2') \right\rangle \\
& = \quad n_1{}^i n_1{}^j n_2{}^k n_2{}^p \left\langle d_1{}^i(\mathbf{r}_1') d_1{}^j(\mathbf{r}_1') \ d_1{}^k(\mathbf{r}_2') d_1{}^p(\mathbf{r}_2') \right\rangle \\
& = \quad n_1{}^i n_1{}^j n_2{}^k n_2{}^p \left[2 \left\langle d_1{}^i(\mathbf{r}_1') d_1{}^k(\mathbf{r}_2') \right\rangle \left\langle d_1{}^p(\mathbf{r}_2') d_1{}^j(\mathbf{r}_1') \right\rangle \right. \\
& \quad \left. + \left\{ \left\langle d_1{}^i(\mathbf{r}_1') d_1{}^j(\mathbf{r}_1') \ d_1{}^k(\mathbf{r}_2') d_1{}^p(\mathbf{r}_2') \right\rangle - 2 \left\langle d_1{}^i(\mathbf{r}_1') d_1{}^k(\mathbf{r}_2') \right\rangle \left\langle d_1{}^p(\mathbf{r}_2') d_1{}^j(\mathbf{r}_1') \right\rangle \right\} \right]
\end{aligned}
$$

(3.8)

where i,j,k,p are vector indices. The last step is tautological as we added and subtracted an important term in the expression. Furthermore, it can be shown that in a system where asymptotic behavior of correlation $\left\langle d_1{}^i(\mathbf{r}_1') d_1{}^k(\mathbf{r}_2') \right\rangle$ is exponentially falling-off, the last term denoted by $\{\dots\}$ in Eq.(3.8) falls-off exponentially even faster than the first term and therefore, it can be neglected in the asymptotic region (i.e., for large R). The vector indices in the remaining expression imply matrix multiplication and a *trace* operation over the product of matrices coming from j index summation. This should be clear if we define the matrices

$$
E^{ij}(R) = \left\langle d_1{}^i(\mathbf{r}_1') \ d_1{}^j(\mathbf{r}_2') \right\rangle \tag{3.9}
$$

$$
(\Sigma_S)^{ij} = \frac{1}{A} \int_S d\hat{n} \ n^i n^j \tag{3.10}
$$

where i,j are generic vector indices and R is the minimum distance of separation. Now the force expression takes the form

$$
F(R) = \frac{\gamma_1 \gamma_2}{2kT} A_1 A_2 \frac{\partial}{\partial R} \operatorname{Tr} [\mathbf{\Sigma_{S_1}} \mathbf{E}(R) \mathbf{\Sigma_{S_2}} \mathbf{E}(R)] \tag{3.11}
$$

where $\operatorname{Tr}[\dots]$ means trace over the product of matrices. The subscripts S_1 and S_2 refer to respective surfaces and Σ matrix defines the second moment of surface normal for the respective surface.

Now, the dipolar correlations from Eq.(2.2) are given as

$$
E^{ij}(r) = \frac{1}{2} \left(\delta^{ij} - \frac{r^i r^j}{r^2} \right) t_{11}(r) - \frac{1}{2} \left(\delta^{ij} - 3\frac{r^i r^j}{r^2} \right) l_{11}(r)
$$
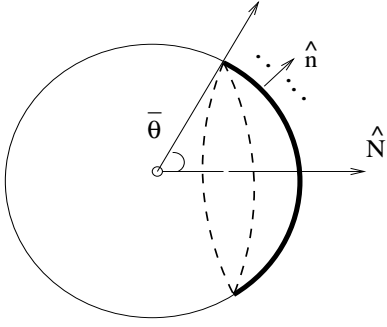
Figure 3.2: A segment of spherical surface (boldened). $\hat{n}$ is local normal vector, and $\bar{\theta}$ is the sector angle for the segment. $\hat{N}$ is the dipole vector of the segment, obtained after integrating $\hat{n}$ over the extent of segment area.

Our analysis from the simulation of bulk liquid water shows that, at large R, only the longitudinal part of the dipolar correlation survives [Eq.(2.4)], i.e.,

$$E^{ij}(R) \simeq (-)\frac{1}{2}\left(\delta^{ij} - 3\frac{R^i R^j}{R^2}\right) l_{11}(R)$$

$$\text{where} \quad l_{11}(R) = 0.39 \frac{e^{-R/5.2}}{R} + 0.027 \frac{e^{-R/24}}{R} \qquad R > 14\text{Å}$$

Hence, the force equation [Eq.(3.11)] will take the form

$$F(R) \propto \frac{\partial}{\partial R}\text{Tr}[\ldots] \, l_{11}^2(R)$$

$$\propto (-)\,\text{Tr}[\ldots] \times \frac{1}{R^2}\,\exp(-R/12\text{Å}) \tag{3.12}$$

where only the long-range exponential's contribution is emphasized, since analysis is for large R.

3.2.2 Surface factor Σ_S

The $\boldsymbol{\Sigma}$ matrix is a geometric factor related to second moment of the surface normal. It is defined as

$$(\Sigma_S)^{ij} \equiv \frac{1}{A}\int_S d\hat{n}\ n^i n^j \tag{3.13}$$

where $\hat{n}(\mathbf{r})$ is the local normal vector at the point $\mathbf{r}$ on the surface; i,j are any two vector components of $\hat{n}$. For a segment of spherical surface, as illustrated in

Fig.(3.2),

$$\hat{n} \; : \; (\sin\theta \; \cos\phi, \; \sin\theta \; \sin\phi, \; \cos\theta); \tag{3.14}$$

$$A_S = \int_S d\hat{n} \; = \; \int_0^{\bar{\theta}} d\theta \sin\theta \int_0^{2\pi} d\phi \; = \; 2\pi(1 - \cos\bar{\theta}) \tag{3.15}$$

The integral $\int n^i n^j$ can be carried out in a similar manner over various pairs of $\hat{n}$ vector components. The $\boldsymbol{\Sigma}$ matrix can be finally expressed in terms of first moment of the surface as

$$\begin{aligned}
(\Sigma_S)^{ij} \; &= \; \frac{1}{A} \int_S d\hat{n} \; n^i n^j \\
&= \; \frac{1}{3} \, \delta^{ij} \; - \; \frac{1}{6} \cos\bar{\theta}(1 + \cos\bar{\theta})(\delta^{ij} - 3N^i N^j)
\end{aligned} \tag{3.16}$$

$$\text{where} \qquad N^i = \frac{M^i}{|M|}, \qquad M^i = \frac{1}{A} \int_S d\hat{n} \; n^i$$

For a spherical surface, $\bar{\theta} = \pi$. Hence $(\Sigma_S)^{ij} \; = \; \frac{1}{3} \, \delta^{ij}$. For a planar surface, $\bar{\theta} = 0$. Hence $(\Sigma_S)^{ij} \; = \; N^i N^j$. The direction of $\hat{N}$ is chosen only with respect to the side of surface under consideration.

We show below that the strength of the force depends on the relative orientations of the surfaces with respect to each other. We consider two planar surfaces separated by large distance. For the surface S_1, $(\Sigma_{S_1})^{ij} \; = \; N_1^i N_1^j$ and similarly for S_2, $(\Sigma_{S_2})^{kl} \; = \; N_2^k N_2^l$ where i, j, k, l are dummy vector indices in coordinate space. For large R, $E^{ij}(R) \; \simeq \; -\frac{1}{2}\left(\delta^{ij} - 3\frac{R^i R^j}{R^2}\right) \; l_{11}(R)$ where i, j are dummy vector indices. So, the part of force expression involving convolution of $\boldsymbol{\Sigma}_S$ and $\mathbf{E}$ matrices reads as

$$\begin{aligned}
F &\propto (-) \, \mathrm{Tr}\left[N_1^i N_1^j \left(\delta^{jk} - 3\frac{R^j R^k}{R^2}\right) N_2^k N_2^l \left(\delta^{li} - 3\frac{R^l R^i}{R^2}\right)\right] \frac{\exp(-R/12)}{R^2} \\
&\propto (-) \left[\hat{N}_1 \cdot \hat{N}_2 - 3\left(\hat{N}_1 \cdot \hat{\mathbf{R}}\right)\left(\hat{N}_2 \cdot \hat{\mathbf{R}}\right)\right]^2 \frac{\exp(-R/12)}{R^2}
\end{aligned} \tag{3.17}$$

For surfaces parallel to each other, $\hat{N}_1 \cdot \hat{N}_2 \; = \; \hat{N}_1 \cdot \hat{\mathbf{R}} \; = \; \hat{N}_2 \cdot \hat{\mathbf{R}} \; = \; 1$. Hence, $F \propto (-)\dfrac{e^{-R/12}}{R^2}$. For surfaces perpendicular to each other, $\hat{N}_1 \cdot \hat{N}_2 = 0$ and either $\hat{N}_1 \cdot \hat{\mathbf{R}} = 0$ or $\hat{N}_2 \cdot \hat{\mathbf{R}} = 0$ depending on orientation of respective surface with respect to the radial vector. Hence, $F = 0$.

Part II

Molecular mean field theory for water and hydrophobic force between macroscopic surfaces

4

Molecular mean field theory for water

We address the hydrophobic force between large surfaces in a model theoretic study. This forms second part of the thesis. We first develop a theoretic description to analyze hydrogen-bond fluctuations in model water, called *molecular mean field theory*. The analysis is then extended to include macroscopic hydrophobic surfaces as boundaries and thermodynamic consequences of confinement are deduced.

The constituent particles of every fluid have a repulsive hard-core of finite radius due to Pauli exclusion principle obeyed by electrons. As a consequence of finite size, each particle has a maximum coordination number. If the particle possesses orientation-dependent attractive regions in its potential, such as hydrogen bonds, sulfur bonds, the particles can participate in a fixed number of bonds. Consequently, there are related steric constraints disallowing arbitrary number of coordinating or bonding partners from approaching an already coordinated/bonded particle. These facts can be formulated into sum rule(s) for the system. Density saturation and bond saturation effects are natural consequences of such sum rule(s). In case of water, a hydrogen bond occurs when a hydrogen arm of one molecule interacts with a lone-pair arm of another molecule. The specificity necessitates the density of hydrogen bonds (HB) and density of dangling bonds (DB) i.e., lone-pair and hydrogen arms which are not hydrogen-bonded, to be commensurate with molecular density (ρ). This can be stated as a sum rule, given by

$$\text{DB} + 2\,\text{HB} = 4\rho \tag{4.1}$$

Now, if we consider a bulk system of water molecules the above equation still

holds when DB, HB and ρ are appropriately defined per unit volume. In other words, the local topology of molecular interactions implies a sum rule which is also true in the bulk for any thermodynamic conditions such as temperature, pressure. Furthermore, this is also independent of other interactions in the dynamical system such as van der Waals' (vdW), Coulombic etc. These facts are not surprising since Eq.(4.1) is a topological constraint which is insensitive to details of dynamics.

Thermodynamic properties of solid phase (ice forms) are governed by periodic distribution of water molecules which also fixes HB. Hence, it is sufficient to envisage water density field alone in the description of solid phase. In low density phases (gas or vapor), the free energy is dominated by kinetic energy of the molecules. If hydrogen bonds are present, an appropriate density of bond dimers can be introduced and the thermodynamic phase behavior can be analyzed in a non-interacting system of monomers and dimers which satisfy the sum rule.

Liquid water, however, lacks the trivial structure of solid or the non-interacting nature of gas molecules. The hydrogen-bond (formation and breaking) dynamics in the liquid phase take place at picosecond timescales and contribute to entropy of the system. In order to analyze the hydrogen-bond fluctuations it is essential to envisage both density and orientational degrees of freedom of each water molecule. The fluctuations of density and orientational fields (the latter being inherently connected to HB and DB fluctuations) are not totally independent; their long wavelength fluctuations especially are to be consistent with the sum rule.

We propose a simple model Hamiltonian for water which incorporates essential features of hydrogen bonding interaction and analyze the fluctuations consistent with the sum rule [48]. To accomodate the hard-sphere repulsion we envisage all density fields on a hypercubic lattice and the model is essentially a slight generalization of the Pauling's model for water [49]. The partition function corresponding to the lattice model is analyzed by introducing appropriate discrete lattice fields. It is shown that the sum rule is automatically true in the bulk. Molecular mean field (MMF) approximation extremizes the partition functional in terms of defined dual fields. In addition, all the observables such as ρ, HB and DB are functionals of these dual fields. One of the mean field equation which implies sum rule also implicates the *equation of network* i.e., a relation between equilibrium densities HB and ρ. We study the equation of state and various mean field fluctuations in terms of dual field correlation functions. We also considered long range Coulomb

interaction and studied its consequences. Subsequently, an MC simulation study of the model is pursued and compared with the mean field theory quantitatively. We also discussed results of our analysis in the context of experiments and MD simulations.

4.1 Model for water
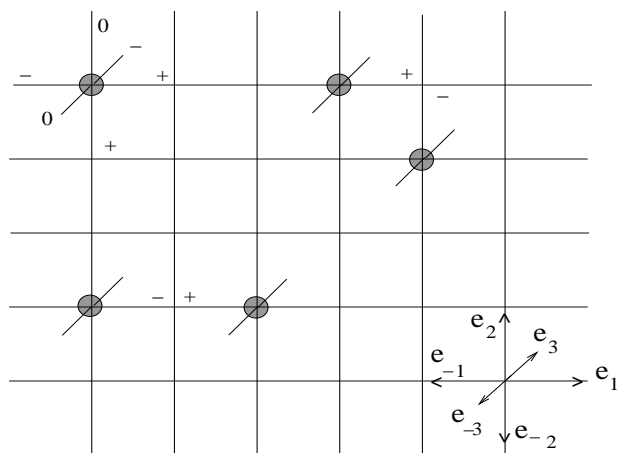
Figure 4.1: Allowed configurations : A water site with two hydrogen arms (+) and two lone-pair arms (-) on links around the site, consistent with constraints Eq.(4.2). A hydrogen bond occurs when a hydrogen arm (+) and a lone-pair arm (-) of two molecules meet at a site. (right bottom corner) Unit vectors on cubic lattice.

On a three-dimensional hypercubic lattice, we define the occupation field $W(r) = \{0, 1\}$ corresponding to water being absent or present respectively, at a site $r = (x, y, z)$. At each occupied site we define bond arms $H_\alpha(r) = \{0, \pm 1\}$, where $\alpha = \{\pm 1, \pm 2, \pm 3\}$ denotes the direction around the site. $H_\alpha(r) = 0$ corresponds to no arm on the corresponding link, $+1$ to that of hydrogen arm, and -1 for lone pair arm. The constraints between $W(r)$ and $H_\alpha(r)$ are

$$\sum_\alpha H_\alpha^2(r) = 4W(r) \tag{4.2a}$$

$$\sum_\alpha H_\alpha(r) = 0 \tag{4.2b}$$

which imply that every water molecule has two hydrogen arms and two lone-pair arms only. A hydrogen bond is realized when two water molecules two lattice units apart have one of each's hydrogen and lone-pair arms meet at a site, as shown in Fig.(4.1). When two molecules are on near neighbor sites they are not allowed to have any non-zero bond arm on the link between them. The constraint is given by

$$W(r) \left(\sum_\alpha H_\alpha^2(r + e_\alpha) \right) = 0 \tag{4.3}$$

We write a general interaction Hamiltonian in terms of the H_α field as

$$\mathcal{H} = \frac{\tilde{\lambda}}{2} \sum_r \sum_{\alpha,\alpha'} H_\alpha(r - e_\alpha) H_{\alpha'}(r - e_{\alpha'}) \tag{4.4}$$

where, $\tilde{\lambda}$ is the interaction strength and α and α' denote directions around a site. There are additional restrictions on H_α field, namely, (i) at any site no more than two bond arms meet i.e.,

$$0 \leq \sum_\alpha H_\alpha^2(r + e_\alpha) \leq 2 \tag{4.5}$$

and (ii) two non-zero bond arms of same type are disallowed from meeting at a site i.e., anti-bonds are disallowed:

$$-1 \leq \sum_\alpha H_\alpha(r + e_\alpha) \leq 1 \tag{4.6}$$

The grand canonical partition function for the system at a finite chemical potential $\tilde{\mu}$ for water and inverse temperature β is given by

$$Z = \prod_r \sum_{W(r), H_\alpha(r)}' \exp\left[-\beta \sum_r (\mathcal{H} - \tilde{\mu} W(r)) \right] \tag{4.7}$$

where the prime indicates that summation over $W(r)$ and $H_\alpha(r)$ has to be carried out in compliance with Eqs.(4.2), (4.3), (4.5), and (4.6). Evaluating Z amounts to enumerating all possible configurations that satisfy the above constraints and calculating the exponential in Eq.(4.7) for those configurations over the allowed
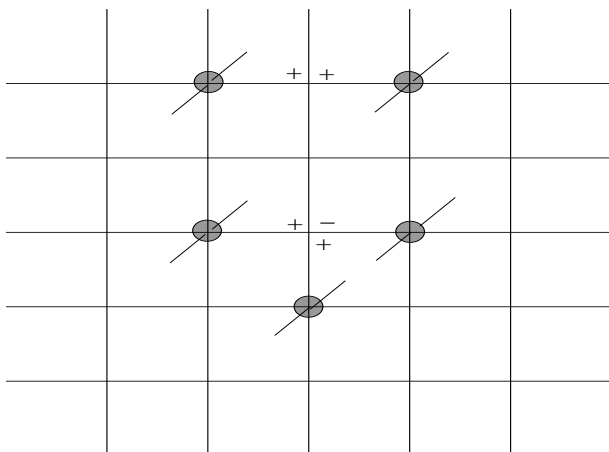
Figure 4.2: Disallowed configurations : non-zero bond arms of same type of two molecules meeting at a site; more than two non-zero arms meeting at a site.

range of W and H_α at fixed values of $\tilde{\mu}$, β and V the volume of the system.

The restrictions shown in Fig.(4.2) represented by Eqs.(4.3), (4.5), and (4.6) are at sites where there is no water. To implement them in our analysis it is useful to define two discrete integer fields $b(r)$, $q(r)$:

$$b(r) = \sum_\alpha H_\alpha^2(r + e_\alpha) \tag{4.8a}$$

$$q(r) = \sum_\alpha H_\alpha(r + e_\alpha) \tag{4.8b}$$

The discrete field $b(r)$ counts the number of non-zero arms in the neighborhood of site r, while $q(r)$ measures the net charge i.e, the difference between the number of hydrogen arms and lone-pair arms meeting at site r. By construction, $b(r)$ varies between 0 and 6 on a three dimensional hypercubic lattice and $q(r)$ in turn varies between $-b(r)$ and $b(r)$. By imposing the condition that $b(r) \leq 2$ in our analysis, we ensured that no more than two arms can meet at a site. Furthermore, for $b(r) = 2$ we demand $q(r) = 0$ to disallow anti-bond configurations. In terms of these variables, Eqs.(4.3), (4.5), and (4.6) can be rewritten as

$$W(r)b(r) = 0 \tag{4.9}$$

$$(b(r), q(r)) = \{(0,0), (1,1), (1,-1), (2,0)\} \tag{4.10}$$

The fields $b(r)$ and $q(r)$ are restricted only to the above set of mutually exclusive pairs. We now rewrite the partition function as

$$Z = \prod_r \sum_{\substack{W(r), H_\alpha(r) \\ b(r), q(r)}}' \exp\left[-\beta \sum_r \left(\mathcal{H} - \tilde{\nu}q^2(r) - \tilde{\mu}W(r)\right)\right] \qquad (4.11)$$

where we have additionally introduced a chemical potential $\tilde{\nu}$ for dangling bond configuration i.e., $(b, q) = (1, \pm 1)$. The fields b and q are to be summed over their allowed range [Eq.(4.10)] and the prime over the summation indicates that Eqs.(4.2), (4.8), and (4.9) act as constraints in the evaluation. Note that, since only hydrogen-bond interaction is envisaged in the model, the Hamiltonian $\mathcal{H}$ can be rewritten as a simple expression:

$$\mathcal{H} = -\tilde{\lambda} \sum_r \delta(b(r), 2) \qquad (4.12)$$

where the Kronecker delta function denoted here as $\delta(p, q)$ is defined as $\delta(p, q) = 1$ for $p = q$ and 0 otherwise. All the possible hydrogen-bond configurations are implied from solving the non-local constraints Eq.(4.8). These constraints are enforced in the partition function by introducing dual fields, as given below:

$$\delta\left(b(r), \sum_\alpha H_\alpha^2(r + e_\alpha)\right) = \frac{1}{2N+1} \sum_{\eta(r)} \exp\left[-i\frac{\pi}{N}\eta(r)\left(b(r) - \sum_\alpha H_\alpha^2(r + e_\alpha)\right)\right]$$
$$(4.13a)$$

$$\delta\left(q(r), \sum_\alpha H_\alpha(r + e_\alpha)\right) = \frac{1}{2N+1} \sum_{\phi(r)} \exp\left[-i\frac{\pi}{N}\phi(r)\left(q(r) - \sum_\alpha H_\alpha(r + e_\alpha)\right)\right]$$
$$(4.13b)$$

where $\eta(r)$ and $\phi(r)$ act as dual fields to the density and net charge of bond arms in a local neighborhood. The discrete η and ϕ fields take integer values in the range $[-N, N]$ at every site, where N is any suitably large integer (greater than 8).

The partition function can be rewritten in terms of new variables and dual
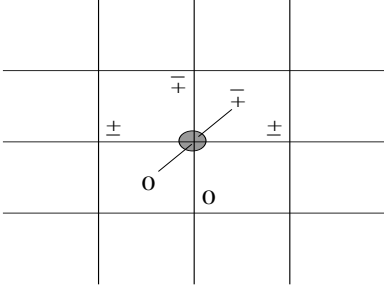
Figure 4.3: A set of orientations consistent with Eq.(4.2) and corresponding to the term proportional to μ in Eq.(4.16).

fields as

$$
\begin{aligned}
Z = & \left[\prod_r \underset{\substack{W(r), H_\alpha(r) \\ b(r), q(r)}}{\sum{}'} \frac{1}{(2N+1)^2} \sum_{\eta(r), \phi(r)} \right] \exp \sum_r \left[-\beta(\mathcal{H} - \tilde{\nu}q^2(r) - \tilde{\mu}W(r)) \right. \\
& \left. + i\frac{\pi}{N}\eta(r) \left(\sum_\alpha H_\alpha^2(r+e_\alpha) - b(r) \right) + i\frac{\pi}{N}\phi(r) \left(\sum_\alpha H_\alpha(r+e_\alpha) - q(r) \right) \right] \quad (4.14)
\end{aligned}
$$

Here, the prime over the summation refers to the sum being restricted to local on-site constraints Eqs.(4.2) and (4.9) only. The introduction of dual fields $\eta(r)$ and $\phi(r)$ allows summation over other discrete fields $(W(r), H_\alpha(r), b(r), q(r))$ within their respective allowed range at each site *without* any restrictions from the neighborhood configurations i.e., as if there were a single site functional Z_{site}.

$$
Z = \left[\prod_r \frac{1}{(2N+1)^2} \sum_{\eta(r), \phi(r)} \right] \prod_r Z_{site}(\eta(r), \phi(r), \nabla_\alpha\eta, \nabla_\alpha\phi) \quad (4.15)
$$

The Z_{site} expression thus obtained is stated below. For brevity, in the following expression, $\frac{\pi}{N}\eta$ is written as η, $\frac{\pi}{N}\phi$ as ϕ.

$$
Z_{site} = 1 \ + 2\nu \exp(-i\eta(r))\cos(\phi(r)) \ + \lambda\exp(-2i\eta(r)) \ + \mu C(\eta, \phi, \nabla_\alpha\eta, \nabla_\alpha\phi)) \quad (4.16)
$$

$$C(\eta, \phi, \nabla_\alpha \eta, \nabla_\alpha \phi) = \sum_{\substack{H_\alpha = 0, \pm 1 \\ \alpha = \pm 1, \pm 2, \pm 3}}' \exp\left[i \sum_\alpha (H_\alpha^2(r)\eta(r + e_\alpha) + H_\alpha(r)\phi(r + e_\alpha))\right]$$

$$(4.17)$$

where $\nu \equiv \exp(\beta\tilde{\nu})$, $\lambda \equiv \exp(\beta\tilde{\lambda})$ and $\mu \equiv \exp(\beta\tilde{\mu})$ are fugacities of dangling bond, hydrogen bond and water states, respectively. Various terms in Eq.(4.16) follow from the fact that at any site r there are only the following contributions to the partition function : (i) unity for vacuum, (ii) ν term for unpaired hydrogen or lone-pair arms (dangling bonds), (iii) λ term for hydrogen bond and (iv) μ term for water with all its possible orientations suitably weighted. The orientational degrees of freedom of water yields $C(\eta, \phi, \nabla_\alpha \eta, \nabla_\alpha \phi)$ given by Eq.(4.17), where the summation is over orientations at site r. The prime over the summation indicates H_α's of each orientation satisfy Eq.(4.2). The exponential corresponds to an orientation and it is a function of dual fields at near-neighbor sites towards which non-zero bond arms of the orientation are directed. The densities of dangling bond (DB), hydrogen bond (HB) and water (ρ) are calculated from partial derivative of the partition function with respect to $\beta\tilde{\nu}$, $\beta\tilde{\lambda}$, $\beta\tilde{\mu}$, respectively.

$\eta(r)$ and $\phi(r)$ are discrete fields varying in the range $[-N, N]$. By construction the partition functional is independent of N for $N \geq 8$. In practice, it is convenient to evaluate this functional by taking $N \to \infty$, whereupon the effective $\eta(r)$ and $\phi(r)$ become continuous fields. We implement this limiting procedure and check if the sum rule is obeyed. In the $N \to \infty$ limit, summation over η and ϕ is replaced by integrals. The resulting functional integral has the following trivial property:

$$\left[\prod_r \int \frac{d\eta(r)}{2\pi} \frac{d\phi(r)}{2\pi}\right] \sum_{r_1} \frac{d}{d\eta(r_1)} \prod Z_{site} = 0 \qquad (4.18)$$

Taking derivatives explicitly in the above equation gives terms proportional to ν, λ, and μ. Since these terms are summed over at all lattice sites each of them can be regrouped in terms of derivatives of ν, λ, and μ as

$$i\left[-\nu\frac{\partial}{\partial\nu} - 2\lambda\frac{\partial}{\partial\lambda} + 4\mu\frac{\partial}{\partial\mu}\right] Z = 0 \qquad (4.19)$$

The μ-dependent term in the Eq.(4.19) has contributions from the four neighboring

sites. Since all sites are being summed over, the μ term in Eq.(4.18) gets each contribution four times. We notice that this equation is precisely the *sum rule* constraint [Eq.(4.1)]. This demonstrates that the sum rule in terms of continuous dual fields is automatically true.

4.2   Molecular mean field theory

We now evaluate the functional integral within the MMF approximation. The partition function's integrand can be envisaged as a product of field-dependent phase factors at each site. When we enumerate them site by site, corresponding to physically allowed configurations the phase factors cancel exactly. Evaluating along this procedure is analogous to the standard high temperature or Mayer-like expansion. Instead, we attempt an approximate method wherein we first notice that if we relax the constraint Eq.(4.8) and Eq.(4.10) the integrand still peaks for the same configurations that obey Eq.(4.8) strictly. Hence, in the thermodynamic limit, approximating the integrand suitably around the peaking configurations, we may reliably estimate the partition function. This reliability can be self-consistently established by computing the variance or correlation functions.

The leading contribution to the partition functional is expected to come from the extremum which maximizes the integrand Z_{site}. Furthermore, in order to describe fluid phase of the model we seek such spatial configurations in dual fields which have discrete translational and rotational symmetry. The integrand Z_{site} over a space-independent field configuration $\tilde{\eta}, \tilde{\phi}$ is given by

$$Z_{site}\big|_{\eta \,=\, \tilde{\eta},\, \phi \,=\, \tilde{\phi}} = \left(1 + 2\nu \exp\left(-i\tilde{\eta} \right) \cos \tilde{\phi} + \lambda \exp\left(-2i\tilde{\eta} \right) + 90\mu \exp\left(4i\tilde{\eta} \right) \right)$$
(4.20)

It is evident that the maximum of Z_{site} occurs at $\tilde{\eta} = \tilde{\phi} = 0$, since all fugacities are positive. Z_{site} at the maximum is given by Z_o:

$$Z_o = (1 + 2\nu + \lambda + 90\mu)$$
(4.21)

This provides zeroth-order contribution to the partition function in the form $Z = (Z_o)^V$. The extremization of Z_o with respect to $\tilde{\phi}$ is trivially true, while that with

respect to $\tilde{\eta}$ yields

$$2\nu + 2\lambda = 4(90\mu) \tag{4.22}$$

This is a consequence of the sum rule within the zeroth-order approximation. Using this relation, the densities of dangling bond, hydrogen bond and water are given upto zeroth-order as

$$\mathrm{DB} \;\equiv\; \nu\frac{\partial}{\partial\nu}(\ln Z) \;=\; \frac{4\nu}{2 + 5\nu + 3\lambda} \tag{4.23a}$$

$$\mathrm{HB} \;\equiv\; \lambda\frac{\partial}{\partial\lambda}(\ln Z) \;=\; \frac{2\lambda}{2 + 5\nu + 3\lambda} \tag{4.23b}$$

$$\rho \;\equiv\; \mu\frac{\partial}{\partial\mu}(\ln Z) \;=\; \frac{\nu + \lambda}{2 + 5\nu + 3\lambda} \tag{4.23c}$$

Eliminating λ from equations for DB and HB we obtain

$$\mathrm{HB} \;=\; 2\rho - \frac{\nu}{\nu + 1}(1 - 3\rho) \tag{4.24}$$

We call Eq.(4.24) as the *equation of network*. It is a manifestation of sum rule in terms of model parameters. The free energy is related to partition function as $\beta G = \ln(Z)$. The mean field free energy G_m per unit volume can be given in terms of densities as

$$\beta G_m = \ln(1 - 5\rho + \mathrm{HB}) = \ln\left(\frac{1 - 3\rho}{1 + \nu}\right) \tag{4.25}$$

From the sum rule, it follows that $0 \leq \mathrm{HB} \leq 2\rho$. Consequently, ρ here varies between $\nu/(5\nu + 2)$ and $1/3$. The upper bound on ρ ($= 1/3$) is indeed the highest possible density in the model, while the lower bound is a consequence of MMF approximation, meaning that this description is self-consistent only for densities greater than $\nu/(5\nu + 2)$. The non-analycities of free energy implied in Eq.(4.25) are precisely at the lower and higher limits of density. Without loosing any generality, we choose $\tilde{\lambda} = 1$ i.e, measure all energies in the units of hydrogen-bond energy. Then, we make the observation that if temperature (β^{-1}) is always positive, we can show that ρ is greater than $1/5$. Furthermore, as $\beta \to \infty$, from Eq.(4.23) we see that $\rho \to 1/3$, $\mathrm{HB} \to 2/3$ and $\mathrm{DB} \to 0$. The saturation density $\rho = 1/3$ is verified to be exactly true by explicit construction of such configurations.

Thus, the equation of network is a manifestation and density saturation effect is a direct consequence of the sum rule.

4.2.1 Fluctuations

Next, we evaluate the functional integral of the partition function by considering small fluctuations about the mean field and obtain one-loop correction to the free energy [50]. At any arbitrary site we expand Z_{site} upto quadratic order in dual fields and obtain

$$
Z_{site} \simeq 1 \ + \ 2\nu \ + \ \lambda \ + \ 90\mu + 2\nu \left(-i\eta - \frac{\eta^2}{2} - \frac{\phi^2}{2} \right) + \lambda \left(-2i\eta - 2\eta^2 \right)
$$

$$
+ 90\mu \left[4i\eta + \frac{2}{3}i\sum_\alpha \nabla_\alpha \eta - \frac{8}{3} \left(\sum_\alpha \eta\nabla_\alpha \eta \right) - 8\eta^2 - \frac{1}{5} \left(\sum_\alpha \nabla_\alpha \eta \right)^2 \right.
$$

$$
\left. - \frac{2}{15}\sum_\alpha (\nabla_\alpha \eta)^2 + \frac{1}{15} \left(\sum_\alpha \nabla_\alpha \phi \right)^2 - \frac{2}{5}\sum_\alpha (\nabla_\alpha \phi)^2 \right]
$$

$$
\simeq \ Z_o \exp \left\{ -i\eta(x) \left(\nu' + 2\lambda' - 4\mu' \right) - \frac{2i\mu'}{3}\sum_\alpha \nabla_\alpha \eta \right.
$$

$$
- \frac{1}{2} \left[\left(\nu' + 4\lambda' + 16\mu' \right) \eta^2(x) + \frac{2\mu'}{5} \left(\sum_\alpha \nabla_\alpha \eta \right)^2 + \frac{4\mu'}{15}\sum_\alpha (\nabla_\alpha \eta)^2 \right.
$$

$$
+ \frac{16\mu'}{3} \left(\sum_\alpha \eta\nabla_\alpha \eta \right) - \left((\nu' + 2\lambda' - 4\mu')\eta(x) - \frac{2\mu'}{3}\sum_\alpha \nabla_\alpha \eta \right)^2
$$

$$
\left. \left. + \nu'\phi^2(x) + \frac{4\mu'}{5}\sum_\alpha (\nabla_\alpha \phi)^2 - \frac{2\mu'}{15} \left(\sum_\alpha \nabla_\alpha \phi \right)^2 \right] \right\} \qquad (4.26)
$$

where $\nu' = 2\nu/Z_o$, $\lambda' = \lambda/Z_o$, $\mu' = 90\mu/Z_o$ are the reduced fugacities, such that all of them are less than 1 and their sum is also less than 1. In the above expression, we used the notation $\nabla_\alpha \eta(r) = (\eta(r + e_\alpha) - \eta(r))$ and similarly for ϕ field.

Inserting the above expression for Z_{site} in Eq.(4.14) and evaluating the resulting Gaussian integral by Fourier transformation in a periodic box, the free energy per unit volume is given by

$$
\beta G = \beta G_m + \frac{1}{2} \int\limits_{-\pi}^{\pi} \frac{d^3k}{(2\pi)^3} \left[\ln(P_{\eta\eta}(\Delta)) + \ln(P_{\phi\phi}(\Delta)) \right] \qquad (4.27)
$$

where

$$P_{\eta\eta}(\Delta) = \left[64\mu'\Delta^2 \left(\frac{9}{10} - \mu' \right) + 64\mu'\Delta \left(-\frac{9}{10} + \mu' - \frac{\nu'}{4} - \frac{\lambda'}{2} \right) \right.$$

$$\left. + \nu' + 4\lambda' + 16\mu' - \left(\nu' + 2\lambda' - 4\mu' \right)^2 \right] \tag{4.28a}$$

$$P_{\phi\phi}(\Delta) = \left[\frac{96\mu'}{5} \Delta \left(1 - \Delta \right) + \nu' \right] \tag{4.28b}$$

and $\Delta = \frac{1}{6} \sum_{i=1}^{3} (1 - \cos(k_i))$, k_i are vector components of $\vec{k}$. Equation (4.27) gives the free energy density to one-loop order. $P_{\eta\eta}$ and $P_{\phi\phi}$ are correlation functions for η and ϕ fields, respectively, in the momentum space and are called propagators.

4.2.2 Correlation functions

The position space correlation functions for η and ϕ field fluctuations are given by

$$\mathcal{G}_\eta(r_1, r_2) \equiv \langle \eta(0)\eta(r) \rangle = \int_{-\pi}^{\pi} \frac{d^3 k}{(2\pi)^3} \frac{\exp\left(i\vec{k} \cdot (\vec{r_1} - \vec{r_2})\right)}{P_{\eta\eta}(\vec{k})} \tag{4.29}$$

where, $\vec{r_1}$, $\vec{r_2}$ are position vectors for any two sites. Similarly for ϕ field in terms of $P_{\phi\phi}$.

We note that to zeroth-order $\mu' \simeq \rho$, $\lambda' \simeq \text{HB}$, $\nu' \simeq \text{DB}$ and using Eq.(4.22), leading order expressions for the propagators are given by

$$P_{\eta\eta}(\vec{k}) \simeq 64\rho \left(\frac{9}{10} - \rho \right) \left[\left(\Delta - \frac{9}{20(\frac{9}{10} - \rho)} \right)^2 + \frac{3(\frac{9}{25} - \rho)}{8(\frac{9}{10} - \rho)^2} \right] \tag{4.30a}$$

$$P_{\phi\phi}(\vec{k}) \simeq \frac{96\rho}{5} \left[\Delta(1 - \Delta) + \frac{5(\text{DB})}{96\rho} \right] \tag{4.30b}$$

The asymptotic behavior of $\mathcal{G}_\eta$ and $\mathcal{G}_\phi$ correlators can be obtained by pursuing small-k expansion of the integrand in Eq.(4.29) and noting that for small $\vec{k}$, $\Delta \simeq \frac{1}{12} \sum_i k_i^2$. The $\mathcal{G}_\eta$ correlator for large $r = |\vec{r_1} - \vec{r_2}|$ is of functional form

$$\mathcal{G}_\eta(0, r) \propto \frac{\exp(-r/\xi_\eta)}{r} \sin(\omega_\eta r) \tag{4.31}$$

where

$$(\xi_\eta)^{-1} = \sqrt[4]{\frac{\frac{3}{8}}{\frac{9}{10} - \rho}} \ \sin\left(\frac{1}{2}\tan^{-1}\sqrt{\frac{50}{27}\left(\frac{9}{25} - \rho\right)}\right) \tag{4.32}$$

$$\omega_\eta = \sqrt[4]{\frac{\frac{3}{8}}{\frac{9}{10} - \rho}} \ \cos\left(\frac{1}{2}\tan^{-1}\sqrt{\frac{50}{27}\left(\frac{9}{25} - \rho\right)}\right) \tag{4.33}$$

This indicates that $\mathcal{G}_\eta$ has periodic peaks whose amplitudes are exponentially falling off.

The $\mathcal{G}_\phi$ correlator takes the following asymptotic form for large r, in addition to oscillatory behavior prominent at short distances:

$$\mathcal{G}_\phi(0, r) \propto \frac{\exp(-r/\xi_\phi)}{r} \tag{4.34}$$

where

$$(\xi_\phi)^{-1} = \sqrt{6\left(\sqrt{1 + \frac{5\,\mathrm{DB}}{24\rho}} - 1\right)} = \sqrt{6\left(\sqrt{1 + \frac{5}{24}(4 - h)} - 1\right)} \tag{4.35}$$

where $h = 2\mathrm{HB}/\rho$.

All correlations in the system can be deduced as functions of $\mathcal{G}_\eta$ and $\mathcal{G}_\phi$. The water density correlation can be calculated as given below.

$$\langle W(r_1)W(r_2)\rangle = \left\langle \frac{\mu\{\ldots\}}{Z_{site}(r_1)} \frac{\mu\{\ldots\}}{Z_{site}(r_2)} \right\rangle \tag{4.36}$$

The non-zero value of W-field at each site picks only the term proportional to μ in Z_{site} [Eq.(4.16)], denoted by $\{\ldots\}$ in the above equation. The connected part of the correlation is given by $\langle W(r_1)W(r_2)\rangle_c \equiv \langle W(r_1)W(r_2)\rangle - \langle W(r_1)\rangle\langle W(r_2)\rangle$. The explicit expression for the correlation function is given in Appendix (4.4.3). The expression suggests that, to the leading order, only η field contributes to the density correlations.

Similarly, orientational correlations can also be deduced using the expression for orientational weight given by Eq.(4.17). The asymptotic behavior of orientational correlations is dominated by ϕ field correlation.

The dangling bond correlation is a direction function of $\mathcal{G}_\phi$. A dangling bond configuration is identified by non-zero value of $q(r)$ field. Hence, the dangling bond correlation is given by

$$\langle q(0)q(r)\rangle \;=\; \left\langle \frac{\nu\{\ldots\}}{Z_{site}(0)}\frac{\nu\{\ldots\}}{Z_{site}(r)}\right\rangle \;\simeq\; -(\text{DB})^2\mathcal{G}_\phi(0,r) \qquad (4.37)$$

The correlation function falls-off exponentially at large distances, as implied in Eq.(4.35).

4.2.3 Fraction of molecules with i hydrogen bonds

Another useful quantity namely the fraction of water molecules with i hydrogen bonds can also be calculated. Consider a water molecule in a configuration in which i arms are hydrogen bonded to neighboring molecules and the other $(4-i)$ arms remain of dangling type. A weight can be associated with each such configuration defined in terms of appropriate site fields and summed over all possible orientations of the molecule. We denote this weight averaged with respect to the full partition function for each i as p_i. For instance, the averaged weight assigned to a molecule which is hydrogen bonded to only two other molecules is given by

$$p_2 \;=\; \sideset{}{'}\sum_{\{\alpha_1,\alpha_2,\ldots,\alpha_6\}} \langle W(r)\,\delta(b(r+e_{\alpha_1}),0)\,\delta(b(r+e_{\alpha_2}),0)\,\delta(b(r+e_{\alpha_3}),2)\,\delta(q(r+e_{\alpha_3}),0)$$
$$\times\delta(b(r+e_{\alpha_4}),2)\,\delta(q(r+e_{\alpha_4}),0)\,\delta(b(r+e_{\alpha_5}),1)\,\delta(b(r+e_{\alpha_6}),1)\rangle \quad (4.38)$$

The prime over summation means dissimilar α. The probability for an i-bonded molecule at any site r is the probability that any two directions around central site have zero arms, each denoted by $\delta(b(x+e_\alpha),0)$, that i other directions have a hydrogen bond denoted by $\delta(b(x+e_\alpha),2)\,\delta(q(x+e_\alpha),0)$, and that the remaining $(4-i)$ sites are of dangling bond type denoted by $\delta(b(x+e_\alpha),1)$. The summation over the set $\{\alpha_1,\alpha_2,\ldots,\alpha_6\}$ implies summing over all possible rearrangements of hydrogen bond and dangling bonds among all the directions. With $\begin{bmatrix}6\\2\end{bmatrix}$ ways of choosing two empty sites in the neighborhood, $\begin{bmatrix}4\\2\end{bmatrix}$ ways for there being two

hydrogen bond sites, p_2, to the leading order, is given by

$$p_2 \simeq \begin{bmatrix} 6 \\ 4 \end{bmatrix} \begin{bmatrix} 4 \\ 2 \end{bmatrix} (\text{HB})^2 (\text{DB})^2 = \frac{1}{2^4} 15(6)\rho^4 h^2 (4-h)^2 \tag{4.39}$$

where $h = 2\text{HB}/\rho$. Similarly, other p_i values can be enumerated and computed up to leading order. For $i = 0, 1, 2, 3, 4$,

$$p_i = \frac{1}{2^4} \, 15 \begin{bmatrix} 4 \\ i \end{bmatrix} \rho^4 h^i (4-h)^{4-i} \tag{4.40}$$

Thereupon, f_i, which is fraction of i-bonded molecules, can be calculated from the relation

$$f_i \;=\; \frac{Vp_i}{\sum_{i=0}^{4} Vp_i} \;=\; \begin{bmatrix} 4 \\ i \end{bmatrix} h^i (4-h)^{4-i} \tag{4.41}$$

Note that the above expression is obtained to zeroth-order approximation within the model. There exist one-loop corrections to it which can be calculated from MMF theory, but they are small numerically. The binomial distribution suggested by Eq.(4.41) agrees well with MD simulations [51]. Furthermore, molecular clusters such as trimers, tetramers, pentamers are also known to exist in liquid water [52]. The probabilities for such cluster configurations can also be calculated within MMF theory along the same lines as above calculation.

4.2.4 Coulomb interaction

In this section, we consider the influence of long range Coulomb interaction between the bond arm charges H_α. The interaction potential is given in terms of electronic charge Q as

$$\mathcal{H}_{Col} = \frac{Q^2}{2} \sum_{r_1,r_2}' \sum_{\alpha,\alpha'} \frac{H_\alpha(r_1)H_{\alpha'}(r_2)}{|r_1 + e_\alpha - r_2 - e_{\alpha'}|} \tag{4.42}$$

where the prime over the summation means $r_1 \neq r_2$. In our model we envisage the charges at the tip of bond arms. The interaction potential can be incorporated in

our analysis by using an auxiliary field technique.

$$\exp\left(-\beta\mathcal{H}_{Col}\right) \;\rightarrow\; \sqrt{\det(-\Box + m^2)}\prod_r \int \frac{d\chi(r)}{\sqrt{2\pi}} \tag{4.43}$$

$$\times \exp\sum_r \left[-\frac{1}{2}\chi(r)(-\Box + m^2)\chi(r) + i\sqrt{\beta Q^2}\sum_\alpha H_\alpha(r+e_\alpha)\chi(r)\right]$$

where the Laplacian operator $\Box\chi(r) = \sum_\alpha \left(\chi(r+e_\alpha) - \chi(r)\right) = \sum_\alpha \nabla_\alpha \chi(r)$ and m is a parameter that regulates the range of interaction. The interaction potential behaves as $\exp(-mr)/r$ for large distances, which when $m = 0$ reduces to Coulomb interaction with a short distance cut off. If the lattice constant and m are both taken to be zero, then it reduces to exact Coulomb interaction for all r.

By inserting the above in our partition function Eq.(4.14), all the interactions of water degrees of freedom remain unchanged with the following transformation: $\eta \rightarrow \eta$, $\phi \rightarrow \phi + \chi\sqrt{\beta Q^2}$. The extremum of the new partition function is still at $\tilde{\eta} = \tilde{\phi} = \tilde{\chi} = 0$. The leading zeroth-order term remains unchanged; the one-loop correction about the mean field gets additional contributions due to quadratic terms corresponding to $\phi\chi$ and $\chi\chi$ in the Gaussian expansion, given by

$$P_{\chi\chi} \;=\; \left(12\Delta + m^2\right) + \frac{96\mu' \beta Q^2}{5}\Delta\left(1 - \Delta\right) \tag{4.44}$$

$$P_{\phi\chi} \;=\; \frac{96\mu'\sqrt{\beta Q^2}}{5}\Delta\left(1 - \Delta\right) \tag{4.45}$$

The free energy density with Coulomb interactions to one-loop order is given by

$$\beta G = \beta G_m + \frac{1}{2}\ln(12\Delta + m^2) - \frac{1}{2}\int\limits_{-\pi}^{\pi}\frac{d^3k}{(2\pi)^3}\left[\ln(P_{\eta\eta}(\Delta)) + \ln(P(\Delta))\right] \tag{4.46}$$

where

$$\begin{aligned}
P(\Delta) \;&\equiv\; P_{\phi\phi}P_{\chi\chi} - P_{\phi\chi}^2 \tag{4.47}\\
&=\; \frac{96\mu'}{5}(12\Delta + m^2)\left[\Delta\left(1 - \Delta\right) + \frac{5\nu'}{96\mu'} + \frac{\beta Q^2\nu'}{12\Delta + m^2}\Delta\left(1 - \Delta\right)\right]
\end{aligned}$$

44

which to leading order can be written as

$$P(\vec{k}) \simeq \frac{96\rho}{5}(12\Delta + m^2)\left[\Delta(1-\Delta) + \frac{5(\text{DB})}{96\rho} + \left(\frac{\beta Q^2(\text{DB})}{12\Delta + m^2}\right)\Delta(1-\Delta)\right] \quad (4.48)$$

The factor Q^2 being small, the strength of Coulomb interaction in comparison with other interactions is weak. Furthermore, all charge effects are proportional to $\beta Q^2(\text{DB})$, wherein $\beta(\text{DB})$ is always finite since, as $\beta \to \infty$, $\text{DB} \to 0$. Consequently, the effect of Coulomb interactions on thermodynamic properties such as the equation of network and the equation of state is small. The coordination peaks and asymptotic behavior of the correlation functions are modified slightly.

4.3   Results

We understand from Eqs.(4.24) and (4.25) that the equation of network is a manifestation and density saturation is a consequence of sum rule. The saturation effect is independent of the dangling bond energy which is an arbitrary parameter in the model. We may choose $\tilde{\nu} = 0$ and measure temperature (β^{-1}) in the units of hydrogen-bond strength ($\tilde{\lambda}$). To the zeroth-order, the theory is now parameter free and all the densities can be obtained as a function of temperature only. The one-loop correction to the densities ρ, HB, and DB can be calculated from the free energy function given by Eq.(4.27) using the propagator expressions [Eq.(4.28)] [see Appendix (4.4.2)]. To the zeroth-order, the relation between ρ and HB is simply given by the equation of network. This equation can be recast as a simple relation between ρ and $h = \frac{2\text{HB}}{\rho}$ as

$$h = 7 - \frac{1}{\rho} \quad (4.49)$$

Temperature is conjugate to HB and hence, it can be fixed self-consistently for given h [Fig.(4.4)]. By model definition, the maximum value of h is 4 and the above equation indicates that $h = 4$ is attained at maximum density $\rho = 1/3$. In this limit the residual entropy per site at highest density is in agreement with known results in ice models [see Appendix (4.4.4)]. However, we find that the highest density in our model is not that of a unique crystal configuration. Instead, from explicit

construction we find that there are infinitely many configurations corresponding to different spatial and orientational arrangements of water molecules [Appendix (4.4.5)].

The lattice constant in the model is arbitrary. By computing physical length-scales such as correlation lengths it can be fixed. The asymptotic behavior of density and orientational correlations is deduced in Eqs.(4.31) and (4.34) in terms of ξ_η and ξ_ϕ [Eqs.(4.32) and (4.35)]. The expressions for ξ_η and ξ_ϕ are deduced from leading order expressions for propagators [Eq.(4.30)]. Their precise values can be obtained using Eq.(4.28) for propagators. We plot these lengths in Fig.(4.4) as a function of h. ξ_η is only about one lattice unit in liquid phase and does not vary considerably with h, while ξ_ϕ increases with h. In MD simulation no correlation length is seen for density correlation; this is consistent with MMF result since ξ_η is equal to the minimum length possible in the model and also independent of h. Orientational correlation lengths inferred from MD simulation are 5.2 Å and 24 Å, of which the latter is weaker in strength (one-tenth) relative to the shorter one [see Eq.(2.4) of Chapter 2]. In our water model, we have only one orientational correlation length ξ_ϕ which we relate to 5.2 Å. For liquid water, h value is suggested to be about 3.6 [31]. From Fig.(4.4), $h = 3.58$ corresponds to $\xi_\phi \simeq 3.3$ lattice units. Consequently, we infer that 1 lattice unit $\simeq \frac{5.2}{3.3} = 1.57$ Å. It should be noted that these predictions are not robust as the coefficients such as $\frac{5}{24}$ in the expression for ξ_ϕ [Eq.(4.35)] vary with topology of the underlying lattice.

We make the observation from Eq.(4.30) that the correlation functions of the mean field theory diverge if $\rho \to 0$ i.e., even the local fluctuations about the mean field are very large rendering the approximation invalid. Indeed, the theory fails well before $\rho = 0$ because it violates the sum-rule already at $\rho = \nu/(5\nu + 2)$ [Eq. 4.24]. Our mean field description is consistent only at high densities closer to the saturation value within the model.

The mean field configuration and fluctuations about it are self-consistently calculated for arbitrary densities in the model. The expansion is neither about low density nor high density. However, we find that the description is consistent only at higher densities. In the free energy expression [Eq.(4.27)], the zeroth-order contribution is energy component and one-loop correction due to fluctuations (say, βG_f) is entropy component. The reliability of mean field approximation can be understood by comparing magnitudes of the energy and entropy components,
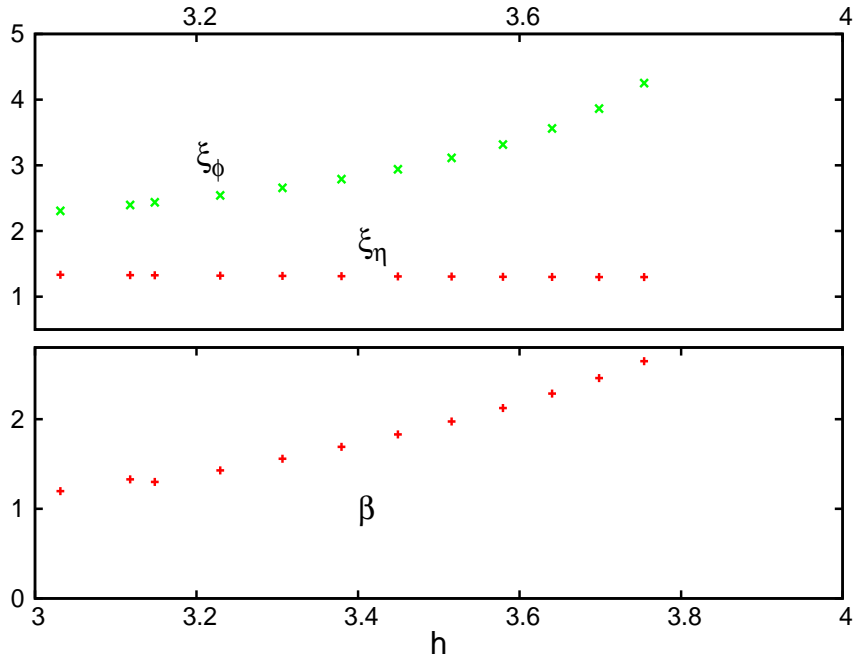
Figure 4.4: Inverse temperature β and the lengthscales ξ_η, ξ_ϕ as a function of h. β is measured in units of hydrogen-bond strength $\tilde{\lambda}$ in the model. The lengths are expressed in lattice units.

given in Table (4.1). We see that, in the region where MMF approximation is consistent, the entropy component is always smaller than the energy component and as saturation density is approached, fluctuations gradually decrease, while the energy contribution is significantly larger.

In order to attest important results deduced within MMF theory we carry out exact MC simulations for the water model. The simulations are performed with dangling bond energy set to zero and all other energies are measured in the units of hydrogen-bond energy. The simulation details and corresponding results are discussed in Chapter (5).

β^{-1}	ρ	HB	ρ/ρ_{max}	h	βG_m	βG_f
1.844	0.2183	0.27	0.6549	2.47	2.210	1.190
0.835	0.2534	0.384	0.76	3.03	2.570	1.155
0.642	0.2719	0.45	0.8158	3.30	2.800	1.137
0.47	0.294	0.527	0.883	3.58	3.320	1.122
0.378	0.309	0.581	0.929	3.75	3.660	1.110

Table 4.1: State points and their corresponding thermodynamic data

4.4 Appendix

4.4.1 Orientational weight $C(\eta, \phi)$

The orientational weight for the water state in bulk water is given by

$$C(\eta, \phi) = \sum_{\substack{H_\alpha = 0, \pm 1 \\ \alpha = \pm 1, \pm 2, \pm 3}}^{\prime} \exp\left[i \sum_\alpha (H_\alpha^2(r)\eta(r + e_\alpha) + H_\alpha(r)\phi(r + e_\alpha)) \right]$$

where the summation is over all possible orientations and the prime indicates that the summation is subject to constraints Eq.(4.2).

About the mean field configuration $\eta = \phi = 0$, the dual fields are expanded upto quadratic order. $C(\eta, \phi)$ is then given by

$$C(\eta, \phi) \simeq 90 \left[1 + \frac{2i}{3} \sum_\alpha \eta_\alpha - \frac{1}{3} \sum_\alpha \eta_\alpha^2 - \frac{2}{5} \sum_{\alpha,\beta} \eta_\alpha \eta_\beta - \frac{1}{3} \sum_\alpha \phi_\alpha^2 + \frac{2}{15} \sum_{\alpha,\beta} \phi_\alpha \phi_\beta \right]$$
(4.50)

where $\eta_\alpha \equiv \eta(r + e_\alpha)$ and $\phi_\alpha \equiv \phi(r + e_\alpha)$.

Note that there exists a linear term in ϕ field in the weight for each orientation. Upon summation over all possible orientations, the linear ϕ terms cancel out exactly since the bond arm charges of a molecule take all possible directions around the site of occupation.

4.4.2 Densities upto one-loop correction

The densities ρ, HB, and DB deduced from free energy upto one-loop correction are given by

$$\rho = \mu' - \frac{1}{2}\left[(-\nu'\mu')T_1 + (-\lambda'\mu')T_2 + \mu'(1-\mu')T_3\right] \qquad (4.51a)$$

$$\text{HB} = \lambda' - \frac{1}{2}\left[(-\nu'\lambda')T_1 + \lambda'(\lambda'-1)T_2 + (-\lambda'\mu')T_3\right] \qquad (4.51b)$$

$$\text{DB} = \nu' - \frac{1}{2}\left[\nu'(1-\nu')T_1 + (-\nu'\lambda')T_2 + (-\nu'\mu')T_3\right] \qquad (4.51c)$$

where

$$T_1 = (1 - 2(\nu' + 2\lambda'))\mathcal{G}_\eta(r,r) + \frac{4\mu'}{3}\sum_\alpha \mathcal{G}_\eta(r, r+e_\alpha) + \mathcal{G}_\phi(r,r) \qquad (4.52a)$$

$$T_2 = (4 - 4(\nu' + 2\lambda'))\mathcal{G}_\eta(r,r) + \frac{8\mu'}{3}\sum_\alpha \mathcal{G}_\eta(r, r+e_\alpha) \qquad (4.52b)$$

$$\begin{aligned}
T_3 = &\frac{4\mu'}{3}(\nu' + 2\lambda')\sum_\alpha \mathcal{G}_\eta(r, r+e_\alpha) + \frac{4}{15}\sum_\alpha \mathcal{G}_\eta(r+e_\alpha, r+e_\alpha) \\
&+ \frac{2}{15}\left(1 - \frac{20\mu'}{9}\right)\sum_{\alpha,\alpha'} \mathcal{G}_\eta(r+e_\alpha, r+e_{\alpha'}) - \frac{2}{15}\sum_{\alpha,\alpha'} \mathcal{G}_\phi(r+e_\alpha, r+e_{\alpha'}) \\
&+ \frac{4}{5}\sum_\alpha \mathcal{G}_\phi(r+e_\alpha, r+e_\alpha) \qquad (4.52c)
\end{aligned}$$

and $r = (x, y, z)$ is a site position, $r + e_\alpha$ is a near-neighbor site in e_α direction. The Green's functions are computed using Eq.(4.29).

The densities are computed consistent with the sum rule for water. The numerical procedure for the computation can be conveniently carried out in the parameter space of the reduced fugacities ν', λ', and μ', all of which are less than 1 and their sum is also less than 1. They are optimally varied in their allowed range such that the solutions for ρ, HB, and DB are consistent with the sum rule.

4.4.3   Density correlations

From Eq.(4.53), the density correlation function is given by

$$\langle W(r_1)W(r_2)\rangle = \left\langle \frac{\mu\{\ldots\}}{Z_{site}(r_1)}\frac{\mu\{\ldots\}}{Z_{site}(r_2)} \right\rangle \tag{4.53}$$

where $\mu\{\ldots\}$ is the term proportional to μ in Z_{site} [Eq.(4.16)]. The dual fields are expanded upto quadratic order and the leading other expression for the connection part of correlation is given by

$$\langle W(r_1)W(r_2)\rangle_c \simeq -(\mu')^2 \left[(\nu'+2\lambda')^2 \mathcal{G}_\eta(r_1,r_2) + \left(\frac{2\mu'}{3}\right)^2 \sum_{\alpha,\alpha'}\mathcal{G}_\eta(r_1+e_\alpha, r_2+e_{\alpha'}) \right.$$

$$\left. + 2\left(\frac{2\mu'}{3}\right)(\nu'+2\lambda')\sum_{\alpha'}\mathcal{G}_\eta(r_1,r_2+e_{\alpha'}) \right] \tag{4.54}$$

where r_1 and r_2 are arbitrary sites on same interface; r_1+e_α and $r_2+e_{\alpha'}$ are their respective near-neighbor sites in the directions e_α and $e_{\alpha'}$ respectively. $\mathcal{G}_\eta(r_1,r_2)$ can be computed from Eq.(4.29).

Orientational correlations can also be evaluated using the expression for orientational weight given in Appendix (4.4.1). The linear terms in η and ϕ fields in the weights for each orientation provide leading contribution to the correlation function. However, the asymptotic behavior is dominated by ϕ field only.

4.4.4   Residual entropy at highest density

We calculate entropy per site to the zeroth-order as below.

$$S = \beta^2 \frac{\partial}{\partial \beta}(G_m) = \ln\left(1 + \frac{5\nu}{2} + \frac{3}{2}\exp(\beta)\right) - \beta\frac{3\exp(\beta)}{2+5\nu+3\exp(\beta)} \tag{4.55}$$

In the limit $\beta \to \infty$, ρ reaches its maximum value and the entropy at the highest density tends to a constant value $\ln(3/2)$. This result compares exactly with that of Pauling's estimate for tetrahedral ice model [49] and agrees well with the numerical estimate by Nagle i.e., $\ln(1.50685 \pm 0.00015)$ [53]. We note that our zeroth-order results are independent of the lattice dimension; hence, in two dimensions the

constant also compares well with the exact result for square ice by Lieb [54].

4.4.5 Highest density configurations

A configuration corresponding to highest density in the model is one with all the lattice sites either in a water state or in a hydrogen bond state. All the bond arms of each molecule are hydrogen bonded. No site is either in a dangling bond or void state. For each molecule one site corresponds to water state, tips of its four bond arms are at four neighboring sites. The bond arms are hydrogen bonded. Hence the share of hydrogen bond state for each molecule is 'half the site'. Collectively, each molecule effectively occupies three lattice sites. Hence, the maximum density possible in the model is 1/3.

There are infinitely many possible spatial and orientational arrangements at the highest density. We illustrated a portion of few configurations in Figs.(4.5), (4.6), and (4.7). In the illustrations, W denotes a water state and all other sites are in the hydrogen bond state. An arrow pointed away from W implies that the molecule is donating a proton (hydrogen arm) to the hydrogen bond present on the neighboring site in the direction of arrow. An arrow pointing inward implies that W is accepting a proton i.e., lone-pair of W. In the two dimensional plane shown in the figures each molecule is shown to participate in two hydrogen bonds. The molecule's other two arms are in the third dimension. The planes in the third dimension which flank the given one have a complementary arrangement of water and hydrogen bond states i.e., a W in the given plane is to be replaced by a hydrogen bond state in the other two planes and vice versa.

In each spatial configuration of W and hydrogen bond states, a set of consecutive forward arrows implies a path on the lattice. The set of all such paths represents an orientational arrangement for the configuration. A complete reversal of one or more paths results in a new orientational arrangement. Thus, a given configuration has infinitely many orientational possibilities.

Different configurations can be obtained by ensuring that no voids or dangling bonds are present and that the orientations obey the constraints and restrictions defined for the model.
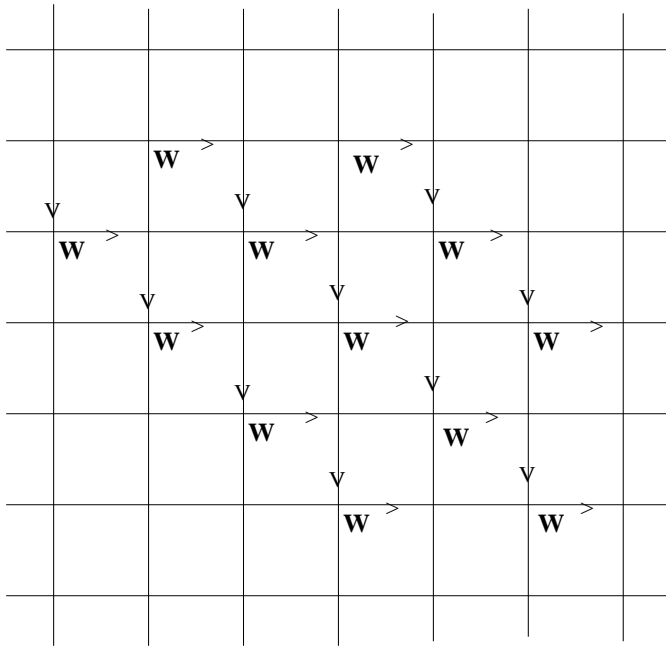
Figure 4.5: An illustration of a spatial and orientational arrangement at highest density in the model. W denotes a water state and H denotes a hydrogen bond state.
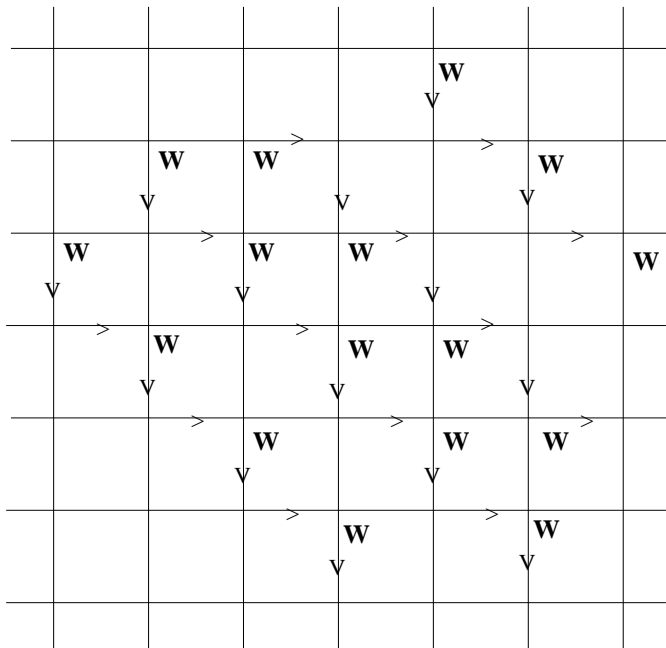
Figure 4.6: An illustration of a spatial and orientational arrangement at highest density in the model.
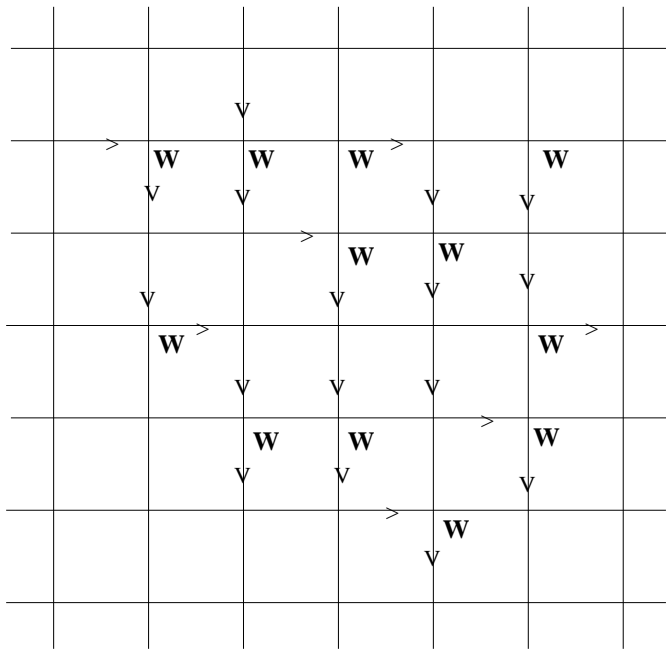
Figure 4.7: An illustration of a spatial and orientational arrangement at highest density in the model.

<div style="text-align: right; font-size: 4em; color: gray;">5</div>

Monte Carlo simulation of the water model

We validate the results of MMF theory by performing Monte Carlo simulations for the water model exactly accounting for all the constraints imposed on the lattice fields. The sum rule is explicitly respected during the simulation. The MC results are seen to be consistent and in semi-quantitative agreement with the results of MMF theory [48].

5.1   Methods

The water model is simulated using a standard Monte Carlo procedure for a grand canonical ensemble i.e., a $\tilde{\mu}VT$ ensemble [39, 55]. We choose to measure all energies in units of hydrogen-bond energy i.e., $\tilde{\lambda} = 1$. Furthermore, we set $\tilde{\nu} = 0$. The theory is now essentially parameter free. The temperature ($\beta^{-1} > 0$) and chemical potential for water ($\tilde{\mu}$) are varied as per needs of the simulation. We employ suitable local configurational moves on a randomly chosen site on lattice in order to smoothly explore the configurational space of the model. The moves are INSERT, DELETE, ROTATE.

- If there is no water molecule or dangling bond or hydrogen bond on the chosen site we perform INSERT operation i.e., put $W = 1$ on the site, provided there are four free directions among the six available directions around the site. That is, the neighboring sites in any four directions should be unoccupied to ensure that the constraint Eq.(4.3) is not violated in the neighborhood.

Those neighboring sites shouldn't already have more than one bond arm in their direction so that the restriction Eq.(4.5) is complied with. Then, in the four free directions four non-zero bond arms are placed randomly such that two of them are of hydrogen type $H_\alpha = 1$ and other two are of lone-pair type $H_\alpha = -1$, in compliance with Eq.(4.2).

- When there is a water molecule on the chosen site we perform either DELETE or ROTATE operation with equal probability.

  - In a DELETE operation we set $W = 0$ on the site and set $H_\alpha = 0$ along all directions around the site.

  - In a ROTATE operation, the directions of non-zero bond arms in the existing configuration are altered to a new configuration implying a rotation of the molecule. We ensure that the constraints Eqs.(4.3), (4.5), and (4.6) are not violated in the neighborhood.

Beginnning with a valid initial configuration the moves ensure that the constraints Eqs.(4.2) and (4.3) and restrictions Eqs.(4.5) and (4.6) are always respected and result in only valid network configurations at each simulation step. These local moves allow the system to explore all possible configurations at all sites and hence, ensemble averages given by MC procedure are expected to provide reliable estimates for the desired thermodynamic quantities.

We employ importance sampling MC procedure using Metropolis criterion to satisfy the detailed balance condition during each move. According to the criterion if total energy change of the system during the move is negative the new configuration is accepted. If the energy change is positive then the new configuration is accepted with a probability equal to Boltzmann weight over the energy change. To compute the energy change of the system during each move, we note that the moves are local and hence, they cause only local changes in particle number and/or hydrogen bonds and anti-bonds in the immediate neighborhood. Hence, we assign a local energy function to initial and final configurations and compute energy change in terms of chemical potential and interaction energies due to hydrogen bonds and anti-bonds. An acceptance rate of about $30 - 40\%$ is achieved during simulation runs in the parameter regime of interest.

Some of the important thermodynamic observables are ρ, HB, DB, total energy, density of molecules with $i(= 0, 1, 2, 3, 4)$ hydrogen bonds. After a sufficient equilibration run the densities are updated every $50 - 300$ MC steps over a simulation time of $10^5 - 10^6$ MC steps. The sampling rate is varied according to acceptance rate. Running averages and variances are computed at every sampling step to determine the efficiency of the sampling procedure. It is ensured that there is no observable overall rise or fall in the averages and variances and that the results smoothly converge to within a relative error of $10^{-2} - 10^{-3}$.

The size dependence of the averages is ascertained and an optimal lattice size of 20 sites per side is found to closely reproduce averages up to the fourth decimal place relative to bigger lattice sizes.

We explore constant temperature curves to facilitate computation of pressure using the Gibbs-Duhem procedure [56]. The pressure at a desired density is obtained from the relation

$$\mathcal{P} = \int\limits_{\tilde{\mu}_i}^{\tilde{\mu}_f} \rho(\tilde{\mu}) \, d\tilde{\mu} \tag{5.1}$$

where a ρ versus $\tilde{\mu}$ curve is integrated between chemical potentials $\tilde{\mu}_i$ and $\tilde{\mu}_f$ to obtain pressure at $\rho(\tilde{\mu}_f)$. The pressure is normalized to zero at zero density. The volume is kept fixed and chemical potential is varied in steps. Since a range of chemical potentials is to be explored the step size is appropriately adjusted so that a quench-like situation is avoided. The system evolves smoothly in configuration space without any unwanted domains persisting. At chosen chemical potential the simulation is initialized using an end configuration from the simulation at previous chemical potential value. This successive seeding procedure accelerates equilibration considerably compared to any random seed configuration. The end averages remain unchanged when the seeding procedure is carried out in an alternative parameter space; for example, instead of the chemical potential, the temperature can be varied in small steps. This confirms the absence of any possible bias created by our successive seeding procedure in most part of the parameter space (except near first-order phase transitions where hysteresis exists).

We also compute spatial correlation functions as an ensemble average over equilibrium configurations. The underlying lattice structure dominates the correlation functions. To facilitate comparision with MMF results we extract rotationally

invariant part of the correlation using the following projection procedure.

$$R(r_0) = \sum_{\vec{r}} \Theta(|\vec{r}| - r_0) \; \Theta((r_0 + \delta r) - |\vec{r}|) \tag{5.2a}$$

$$f(r_0) = \frac{1}{R(r_0)} \sum_{\vec{r}} f(\vec{r}) \; \Theta(|\vec{r}| - r_0) \; \Theta((r_0 + \delta r) - |\vec{r}|) \tag{5.2b}$$

where $\vec{r} \equiv (x, y, z)$ is position index for a lattice site, $|\vec{r}|$ is its magnitude in Euclidean metric. $f(r)$ is any function defined on the lattice and r_0 is the distance where correlation is desired; δr is a small distance window. Θ is the Heaviside step function defined as $\Theta(x - a) = 1$ for $x \geq a$ and 0 for $x < a$. $R(r)$ is weight function for distance r.

5.2 Results
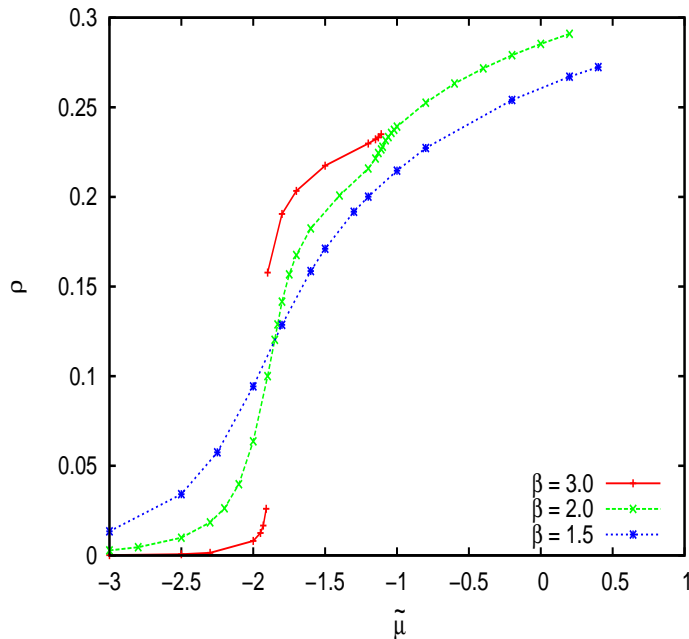
Figure 5.1: First order phase transition in MC simulation seen for $\beta > 2$: Isotherms correspond to $\beta = 3.0, 2.0, 1.5$. The $\beta = 3.0$ isotherm (red curve) shows discontinuity near $\tilde{\mu} = -1.91$ when density changes from $\rho \sim 0.025$ to $\rho \sim 0.16$.

We made preliminary investigations in studying phase transitions in the model. A set of representative constant temperature curves are shown in Fig.(5.1). Each

curve has two prominent shoulders where significant slope change occurs. Beyond a certain $\tilde{\mu}$ value, no more equilibriated configurations could be traced and the density starts shooting up to the saturation value. For inverse temperature $\beta > 2$ the curves exhibit discontinuity. For instance, at $\beta = 3$ the system jumps from a $\rho \sim 0.025$ to $\rho \sim 0.16$ upon an infinitesmal increase about $\tilde{\mu} \sim -1.91$. The rise in density is higher for higher β. Hysteresis is also seen when retracing the curve by decreasing the $\tilde{\mu}$. This indicates the presence of first-order phase transition in the region. We interpret this as a liquid-gas transition in the model. Within our limited exploration of the phase diagram we find that $\rho > 0.16$ corresponds to liquid phase. MMF theory is seen to be consistent in this region only i.e., for $\rho > 1/5$.

The equation of state deduced within MMF theory [Eq.(4.25)] is compared with that computed from MC simulation. In the theory pressure is simply negative of the free energy density. Their magnitude is same since the free energy is deduced in infinite volume limit. The comparison between MMF theory and MC simulation is put forth in Fig.(5.2). It shows that the high pressure states at each ρ show qualitatively same profile as predicted by MMF theory. A quantitative comparison of equation of state between MMF theory and MC simulation is unreliable because pressure from MMF theory absurdly vanishes at $\rho = 1/7$ whereas, physically the pressure is zero in this model only at $\rho = 0$. As discussed earlier, MMF approximation fails for small densities. Therefore, a consistent normalization between various schemes of calculation is not present. Thus, the qualitative picture obtained from MMF calculation is only indicative, nevertheless consistent with MC results.

One of the important expositions of the MMF theory is the equation of network. From Eq.(4.24), at $\tilde{\nu} = 0$, the mean field equation of network is given by

$$\text{HB} = \frac{7\rho}{2} - \frac{1}{2} \tag{5.3}$$

We plot the ρ and the HB data obtained from MC simulation against the equation of network. This is shown in Fig.(5.3). The equation of network is a manifestation of sum rule and it is deduced within MMF approximation in the infinite volume limit. The linear relation between ρ and HB is borne out in MC simulation by configurations with lowest free energy (or high pressure) at each ρ. There is excellent quantitative agreement between MMF and MC results in this regard.
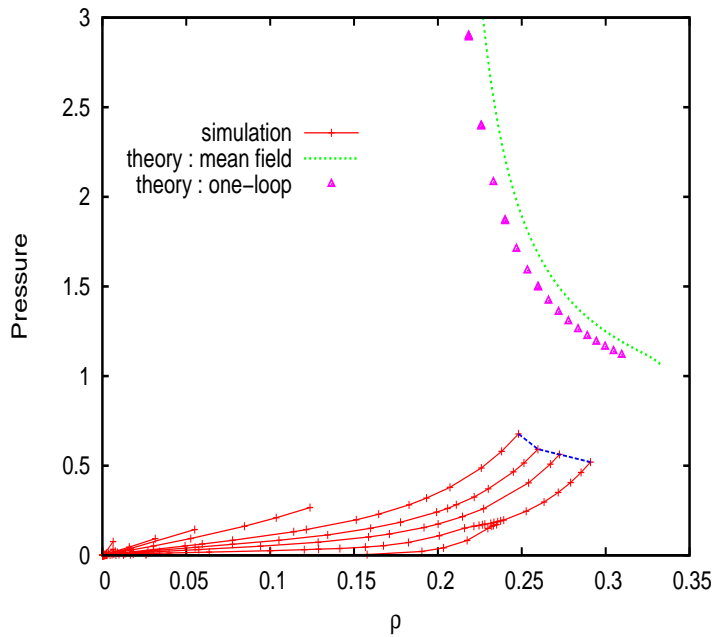
Figure 5.2: Equation of state : (green, dotted line) MMF theory zeroth order; (magenta, filled triangles) MMF theory upto one-loop correction; (red lines) isotherms in MC simulation with temperature increasing from top to bottom; (blue, dashed line) high pressure states at each density in MC simulation.

We also pursued a preliminary study of equation of network obtained from experiments and MD simulations. The density of hydrogen bonds is indirectly probed and inferred under varying external conditions in experiments [57] and is also computed in MD and MC simulations [51, 58]. The data are put in perspective by converting the mass densities to number densities using the known radius of a water molecule. As shown in Fig.(5.4), in the region of high molecular density i.e., corresponding to liquid water we find that ρ and HB are linearly related to each other. A linear fit function is used for the HB versus ρ curve and compared with that of the MMF equation [Eq.(4.24)]. We infer a dangling bond fugacity ν in the range $(0.06, 0.18)$, implying that the corresponding energy $\tilde{\nu}$ is positive and large compared to the thermal energy. This implies that dangling bonds are highly disfavored in liquid water. Due to anomalous thermal expansion the functional relation between HB and ρ in liquid water is expected to exhibit non-linearity at higher densities.

The highest density state in the model exhibits infinite degeneracy in spatial
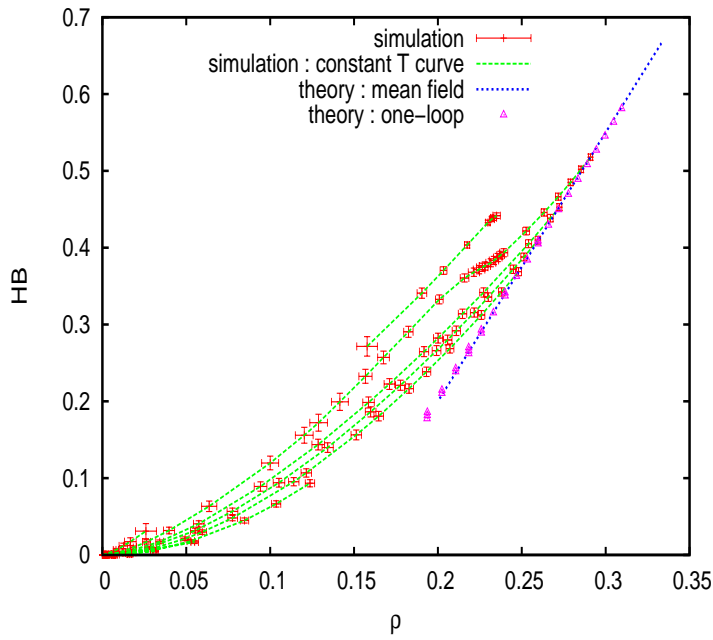
Figure 5.3: Equation of network for $\tilde{\nu} = 0$: (green, dashed lines) MC simulation isotherms (temperatures increasing from bottom to top); (blue, dotted line) mean field equation; (magenta, open triangles) with one-loop correction.
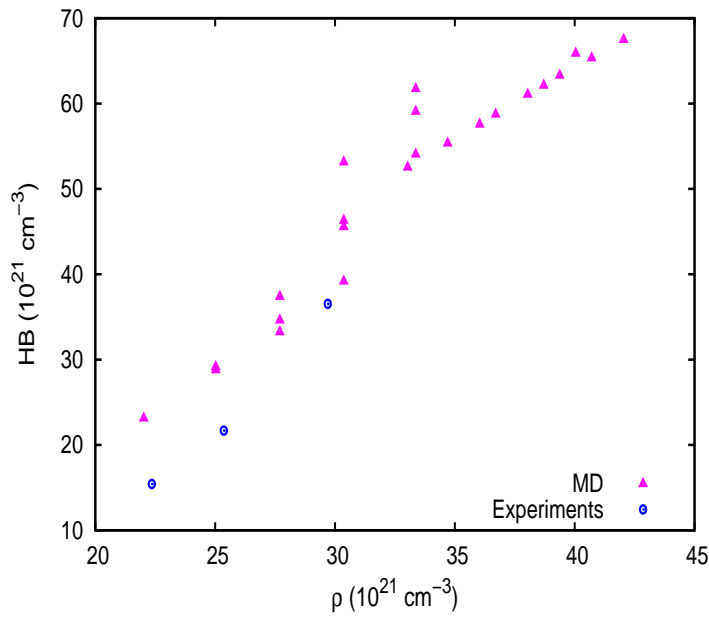
Figure 5.4: Equation of network : (blue, filled circles) Experiments and (magenta, filled triangles) MD simulations.

arrangement of molecules and their orientations [see Appendix 4.4.5 in Chapter 4]. The presence of large set of crystalline states suggests that there could be a liquid-glass transition at high densities or near zero temperature in our model. In MC simulation we witnessed dynamical slowing down at low temperatures, consistent with our speculation. Furthermore, in this region MMF theory indicates a second order transition as seen from $q(x)$ correlator [Eq.(4.35)], wherein for $\beta \to \infty$, $\rho \to 1/3$ and DB $\to 0$ implying that $\xi_\phi \to \infty$. The implications of this analytic structure to low temperature phase behavior of the model need to be studied in detail.

The important correlations in the model are $\langle W(0)W(r) \rangle$ and $\langle q(0)q(r) \rangle$. In the MMF theory they are explicit functions of dual field correlations $\mathcal{G}_\eta$ and $\mathcal{G}_\phi$ [Eqs.(4.37) and (4.53)]. They are computed numerically and shown in Figs.(5.5) and (5.7). In MC simulation the correlation functions are computed from the projection scheme given by Eq.(5.2) and are displayed in Figs.(5.6) and (5.8). The correlation functions within MMF theory and in MC simulation are computed at comparable values of ρ and HB. We find that the positions of coordination peaks in density correlation function are in agreement and are in compliance with the constraints in the model and underlying lattice topology. The density correlation function with characterstic hydration peaks appears qualitatively similar to radial distribution function of fluids. It does not show any long distance behavior. This is consistent with MMF result since ξ_η is only one lattice unit which is minimum length in the model. The charge correlations both in MMF theory and MC simulation show an asymptotic fall-off with distance. MMF theory predicts an exponential fall-off [Eq.(4.35)] consistent with MD simulations for liquid water. It is encouraging to see that a consistent qualitative picture of fluctuations could be obtained from a simple analytical calculation. It is however observed that the quantitative details of correlation functions depend on the underlying lattice, but the analytic structure is amenable to interpretation in the continuum as well.
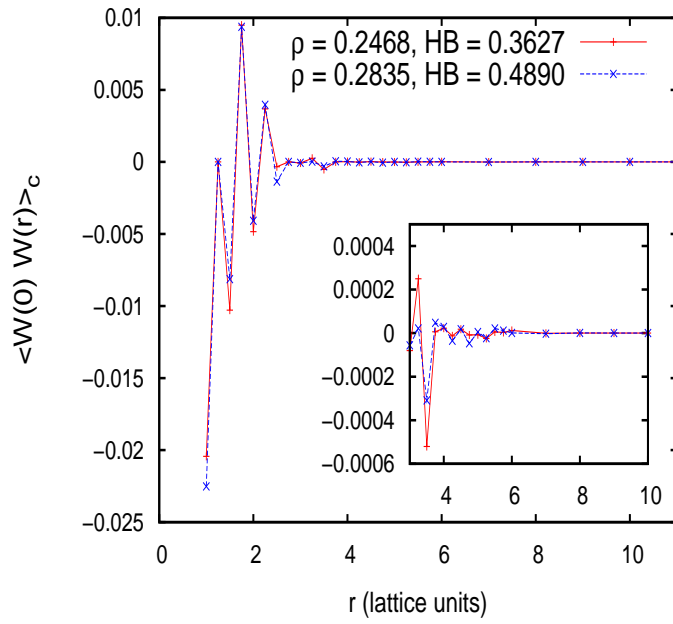
Figure 5.5: MMF theory : $\langle W(0)W(r)\rangle$ correlation at two representative densities.
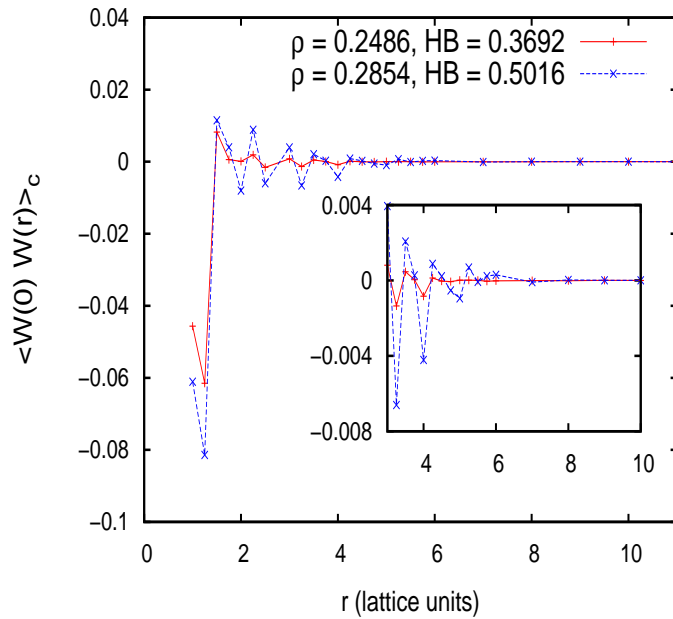
Figure 5.6: MC simulation : $\langle W(0)W(r)\rangle$ correlation.
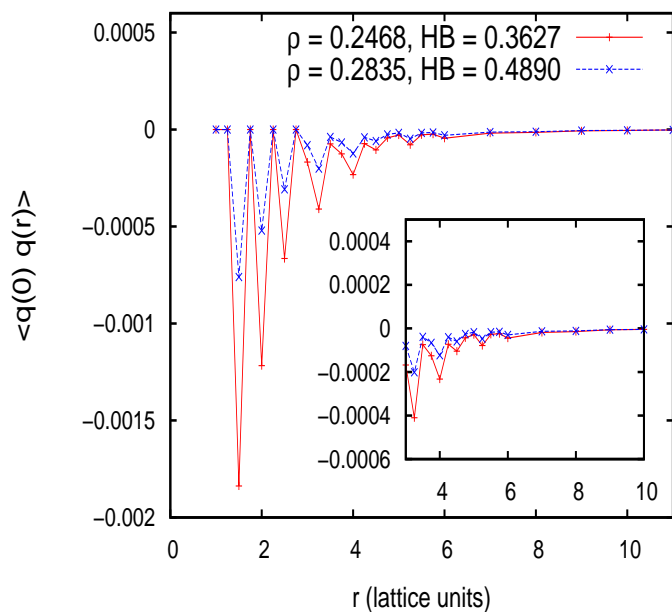
Figure 5.7: MMF theory : $\langle q(0)q(r)\rangle$ (dangling bond) correlation
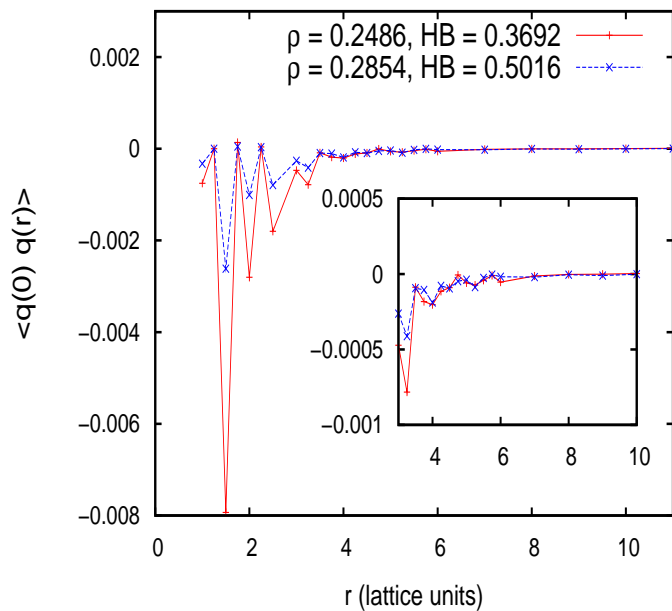
Figure 5.8: MC simulation : dangling bond correlation.

6

Hydrophobic force between macroscopic surfaces

In this chapter we address hydrophobic force between large surfaces using the framework of MMF theory. The water model analyzed in the previous chapters is envisaged here. In our model study we analyze the consequences of confining hydrogen-bond fluctuations in presence of large hydrophobic surfaces and infer that hydrophobic force is a manifestation of Casimir-like force largely influenced by the long-distance correlations of orientational fluctuations.

When water is confined between large hydrophobic surfaces the inherent field fluctuations vanish on surfaces. Furthermore, water molecules at the interface with each surface have restricted orientational entropy owing to repulsive hydrophobe-water interactions. This effect gives rise to modified fluctuations at each interface. We study the collective consequences of these effects on the overall free energy of the system in a model study. Two macroscopic surfaces are envisaged as boundaries in a spatial dimension and water is confined between them. The change in free energy due to the presence of surfaces is calculated and is seen to be composed of three important contributions : (i) Casimir part, which arises solely from discretization of fluctuation modes between boundaries and is generic to all surfaces; (ii) Interfacial free energy, which is free energy change due to modified fluctuations at hydrophobe-water interface. It is dependent on nature of surface-water interaction and to a small extent, also on separation distance between the surfaces; (iii) Interfacial fluctuations-induced free energy, which is due to correlation between modified fluctuations at both interfaces. It depends on type of both surfaces and

their interaction with water. The results are discussed for different types of sur-
faces such as hydrophobic and hydrophilic. We find that the Casimir part is leading
contribution and is an inverse power-law function of separation distance. However,
numerically the magnitude of Casimir part is significant for distances only upto
four times the longest correlation length in the model. The interfacial free energy
also varies with separation distance, but its variation is numerically insignificant.
The interfacial fluctuations-induced contribution is seen to be exponentially decay-
ing with distance, analogous to the force form deduced for mesoscopic surfaces [see
Chapter 3]. Furthermore, we find that all the contributions are of comparable order
of magnitude consistent with experimental values. The dependence of the force on
fluid conditions like temperature, average hydrogen bonds is also discussed. Our
results indicate that hydrophobic force qualitatively imitates Casimir-like force be-
havior [59]. It is desirable to emulate the computation within more realistic models
of water possibly with the help of MD simulations. We also looked at transverse
density profile for confined water and show that an increase in density occurs near
interfaces.

6.1   Water confined between macroscopic surfaces

We envisage surfaces in the (x, y) plane of rectangular coordinate system; one
present at $z = 0$ and other at $z = L$ [Fig.(6.1)]. Each surface excludes water from
its region of occupation. Hence, $W = 0$ on surface sites. On the immediate layer,
i.e., at $z = 1$ or $z = L - 1$ called the *interface* layer, water can be present and
can take various orientations. For a hydrophobic surface if a non-zero bond arm
of interface water is directed towards the surface, there would be a dangling bond
on surface site; else a void state occurs. There can never be a hydrogen bond on
surface i.e., $b \neq 2$ on surface. We will take care of these possibilities explicitly in
our analysis. Consequently, we need not introduce η and ϕ integrals [Eq.(4.13)] on
the surface. Alternatively, we set $\eta = \phi = 0$ on surfaces.

The calculation of partition function begins with formulating the site functional
Z_{site} at each site, which comprises weights corresponding to each allowed state in
the model. The site functional for all the sites in bulk region is of same form as
given by Eq.(4.16). On the interface sites, weights corresponding to the void state,
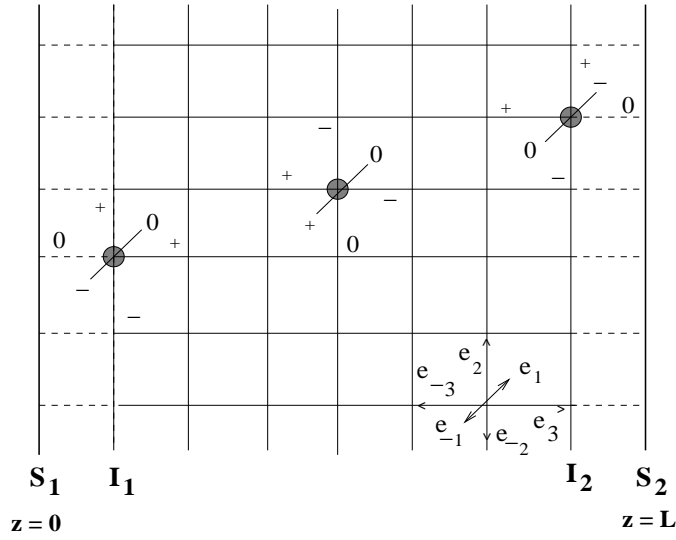
Figure 6.1: Water confined between macroscopic surfaces. S_1, S_2 are surface planes at $z = 0$ and $z = L$ respectively; I_1, I_2 are their respective interfaces at $z = 1$ and $z = L - 1$.

the dangling bond and the hydrogen bond states remain unaltered. When a water molecule is present on an interface site its bond arms can orient in all possible ways. Only if one of the arms is towards the surface we assign a weight $\exp(\beta\tilde{\nu}_S)$ to the corresponding orientation. For an ideal hydrophobic surface i.e., which is indifferent to bond arms of vicinal water, $\tilde{\nu}_S = 0$ (in general, $\tilde{\nu}_S$ can be positive or negative). Consequently, orientational weights for a water state on any interface site (with surface in e_3 direction) are given by

$$
\begin{aligned}
C(\eta,\phi)|_{\text{interface}} &= \left(\sideset{}{'}\sum_{\substack{\alpha \neq 3 \ H_\alpha = 0,\pm 1 \\ H_3 = 0}} + \exp(\beta\tilde{\nu}_S) \sideset{}{'}\sum_{\substack{\alpha \neq 3 \ H_\alpha = 0,\pm 1 \\ H_3 = \pm 1}} \right) \\
&\qquad \exp\left[i\sum_\alpha (H_\alpha^2(r)\eta(r+e_\alpha) + H_\alpha(r)\phi(r+e_\alpha)) \right] \\
&= C(\eta,\phi) + \nu_S \sideset{}{'}\sum_{\substack{\alpha \neq 3 \ H_\alpha = 0,\pm 1 \\ H_3 = \pm 1}} \exp\left[i\sum_\alpha (H_\alpha^2(r)\eta(r+e_\alpha) + H_\alpha(r)\phi(r+e_\alpha)) \right] \\
&\equiv C(\eta,\phi) + \nu_S C'(\eta,\phi)
\end{aligned}
\tag{6.1}
$$

where the prime over the H_α sum implies the constraints Eq.(4.2), $C'(\eta, \phi)$ corresponds to affected orientations only i.e., those with $H_3 = \pm 1$, and $\nu_S \equiv \exp(\beta \tilde{\nu}_S) - 1$ is a function of surface-water interaction strength. The site functional Z_I for any interfacial site can be arranged as

$$Z_I \;=\; Z_{site} + \nu_S \mu C'(\eta, \phi) \tag{6.2}$$

By definition, ν_S ranges from -1 to ∞. We remark that for a perfect hydrophobic surface, $\nu_S = 0$.

The modified site functional at the interface sites can be recast in the expression for full partition function such that the following decomposition is deduced.

$$\begin{aligned}
Z_{\parallel} \;&=\; \int [\mathcal{D}\eta][\mathcal{D}\phi] \prod_r Z_{site} \prod_{r_1 \in I_1} (1 + \Gamma(r_1)) \prod_{r_2 \in I_2} (1 + \Gamma(r_2))) \\
&=\; Z \left\langle \exp\left(\sum_{r_1 \in I_1} \ln(1 + \Gamma(r_1)) + \sum_{r_2 \in I_2} \ln(1 + \Gamma(r_2)) \right) \right\rangle
\end{aligned} \tag{6.3}$$

where $Z_{\parallel}$ is partition function for the system with the surfaces, Z is for the corresponding unperturbed case ($\nu_S = 0$) with $\eta = \phi = 0$ on the surface sites, and $\Gamma(r)$ is defined only on the interface sites. It is relative orientational weight of the affected orientations with respect to Z_{site}, i.e.,

$$\Gamma(r) \;=\; \frac{\nu_S \mu C'(\eta, \phi)}{Z_{site}(r)} \tag{6.4}$$

The partition function for the unperturbed case Z can be evaluated using the MMF technique. The leading mean field energy is obtained from the maximum of Z_{site} at each site and the fluctuations in η and ϕ fields are analyzed subject to vanishing boundary conditions on the surfaces. The interfaces-dependent part in $Z_{\parallel}$ is evaluated using cluster technique and the corresponding free energy is obtained. The resulting form of total free energy G_{tot} per unit lattice area is organized to be

$$G_{tot} = G_o + G_C + \gamma_{S_1} + \gamma_{S_2} + G_\Gamma \tag{6.5}$$

where $G_o + G_C$ is the free energy obtained from the evaluation of Z, analogous to Eq.(4.27). G_o includes leading terms proportional to L and constants obtained

in the large L limit. They contribute only to bulk pressure of the system. G_C is the remaining L-dependent part. γ_{S_1}, γ_{S_2} are free energy contributions due to surface-water interaction and evaluated only on the sites of respective interfaces I_1 and I_2 respectively. G_Γ constitutes terms which involve sites of both interfaces. Expression for each of the terms is deduced in the remaining section and their relevance to hydrophobic interaction is elucidated.

We first evaluate Z using the MMF technique described in the previous section. We identify the maximum of the functional to be at $\eta = \phi = 0$. It yields mean field free energy per unit area, which to the leading order is given by LG_m [Eq.(4.25)]. The dual fields are then expanded upto quadratic order about their maximum and the resulting Gaussian integrand functional for Z is integrated over all the field configurations which are consistent with the boundary conditions. This yields the one-loop contribution to the free energy. In the process, the following Fourier transformation is employed which satisfies the vanishing boundary conditions in the z direction.

$$\eta(\vec{r}) \;=\; \frac{2}{L} \sum_{n=1}^{L-1} \int_{-\pi}^{\pi} \frac{(dk_1)(dk_2)}{(2\pi)^2} \; \tilde{\eta}(\vec{k}) \exp(ik_1 x + ik_2 y) \sin(n\pi z/L) \qquad (6.6)$$

where $\vec{r} = (x, y, z)$ is position vector for an arbitrary site and $\vec{k} = (k_1, k_2, k_3 = \frac{n\pi}{L})$ denote modes in the momentum space. Similarly for ϕ field.

The entropy contribution to the free energy for the unperturbed system is a discrete analog of the corresponding expression for bulk water [Eq.(4.27)], in that the integral over the wavevector in z-direction is replaced by a summation over a restricted number of wavevectors i.e., $k_3 = \frac{\pi}{L}, \frac{2\pi}{L}, \ldots, \frac{\pi(L-1)}{L}$. To analyze the L-dependence, we define entropy contribution per unit area in each mode in z-direction as

$$S(k_3) \;=\; \frac{1}{2} \int_{-\pi}^{\pi} \frac{(dk_1)(dk_2)}{(2\pi)^2} \ln\left(P_{\eta\eta}(\vec{k})P_{\phi\phi}(\vec{k})\right) \qquad (6.7)$$

where the propagators $P_{\eta\eta}$ and $P_{\phi\phi}$ are same as those deduced in the case of bulk water. Total entropy contribution to the free energy of confined water is $S(k_3)$ summed over the allowed values of k_3. Its large-L behavior can be enumerated

using Euler-Maclaurin series expansion [60].

$$\sum_{k_3=\frac{\pi}{L}}^{\frac{\pi}{L}(L-1)} S(k_3) \;=\; L \int_0^\pi \frac{dk_3}{\pi} S(k_3) - \frac{1}{2}\left(S(0) + S(\pi)\right) + \beta G_C \tag{6.8}$$

On the right hand side of Eq.(6.8), the first term is the total entropy contribution in the same volume of bulk water. $S(0)$ and $S(\pi)$ are free energy densities in the modes $k_3 = 0$ and $k_3 = \pi$ respectively. They are independent of L. From Eq.(6.8) we infer G_C to be the net difference in entropy contribution per unit area between confined water and bulk water in the same volume. G_C can be calculated as a series expansion in $\frac{1}{L}$, in which the leading term is

$$\beta G_C \;\simeq\; \frac{\pi}{B_2 L}\left[\left.\frac{\partial}{\partial k_3}S(k_3)\right|_{k_3=\pi} - \left.\frac{\partial}{\partial k_3}S(k_3)\right|_{k_3=0} \right] \quad \text{for large L} \tag{6.9}$$

where $B_2 = 2$ is the first Bernoulli constant. G_C is analogous to the Casimir interaction energy derived in case of conducting plates confining electromagnetic fluctuations [26]. Hence, we call G_C the *Casimir part* of the free energy. It falls off asymptotically as $\frac{1}{L}$ for large L.

In the expression for the partition function [Eq.(6.3)], the average over the interface terms is now pursued. At each interfacial site, $\ln(1 + \Gamma(r)) \simeq \Gamma(r)$ is the leading order term. This is justified because in Eq.(6.4) for $\Gamma(r)$, we note that $\frac{\mu C'(\eta,\phi)}{Z_{site}} \simeq \frac{\rho C'(\eta,\phi)}{90}$ whose maximum value is always less than 1, since $\rho < \frac{1}{3}$ and $\left|\frac{C'(\eta,\phi)}{90}\right| < \frac{2}{3}$, $C'(0,0) = 60$. The leading order contribution from the interface terms in Eq.(6.3) is then given by

$$\frac{Z_\parallel}{Z} \;=\; \left\langle \exp\left(\sum_{r_1 \in I_1} \Gamma(r_1) + \sum_{r_2 \in I_2} \Gamma(r_2) \right) \right\rangle \tag{6.10}$$

The average can be evaluated using cluster technique[1]. Terms that involve sites of the same interface and those involving sites of both interfaces are segregated. γ_S

---

[1]If A and B are functions of a random variable whose probability distribution is known, the average $< \exp(A + B) >$ over the probability distribution is given by : $\langle \exp(A + B) \rangle = \exp\left[< A > + < B > +\frac{1}{2}(< A^2 > - < A >^2 + < B^2 > - < B >^2) + < AB > - < A >< B > +\ldots\right]$

is defined to constitute terms corresponding to sites on the same interface. Each of them is proportional to ν_S or its higher order. γ_S is given to the leading order as

$$-\beta\gamma_S A = \left[\left\langle \sum_{r \in I} \Gamma(r) \right\rangle + \left\langle \sum_{\substack{r_1, r_2 \in I \\ r_1 \neq r_2}} \Gamma(r_1)\Gamma(r_2) \right\rangle - \left\langle \sum_{r \in I} \Gamma(r) \right\rangle^2 \right] \qquad (6.11)$$

where A is area of the surface. γ_S arises due to surface-water interaction and consequent effect on orientational fluctuations in the interfacial region.

Each of the averages in Eq.(6.11) can be evaluated using a functional integration relation[2]. For an interface site with surface in e_3 direction, using Eqs.(6.1) and (6.4) $\langle \Gamma(r) \rangle$ is given to the leading order as

$$\langle \Gamma(r) \rangle = \left(\frac{\nu_S \rho}{90} \right) \sideset{}{'}\sum_{\substack{\alpha \neq 3 \ H_\alpha = 0, \pm 1 \\ H_3 = \pm 1}} \exp\left[\sum_{\alpha, \alpha'} \left(H_\alpha^2(r) H_{\alpha'}^2(r) \mathcal{G}_\eta(r + e_\alpha, r + e_{\alpha'}) \right. \right.$$
$$\left. \left. + H_\alpha(r) H_{\alpha'}(r) \mathcal{G}_\phi(r + e_\alpha, r + e_{\alpha'}) \right) \right]$$
$$(6.12)$$

where the H_α summation is over the affected orientations at site r. The prime over the summation indicates that the H_αs of each orientation satisfy the constraints Eq.(4.2). The exponential in Eq.(6.12) corresponds to one such orientation. H_α and $H_{\alpha'}$ are bond arms of the same orientation; $r + e_\alpha$ and $r + e_{\alpha'}$ are the bond arm locations.

---

[2] If ϕ is a random field whose action is known and when a constant external field J couples to ϕ such that their interaction is $iJ\phi(r)$, then $< \exp(iJ(\phi(r_1) + \phi(r_2))) > = \exp[-\frac{1}{2}J^2(< \phi(r_1)\phi(r_1) > + < \phi(r_2)\phi(r_2) + 2 < \phi(r_1)\phi(r_2) >) + \ldots]$. If the two-point correlation is leading order among the correlations, then the subsequent terms of higher order denoted by $(\ldots)$ can be ignored

The average $\langle \Gamma(r_1)\Gamma(r_2) \rangle$ is given to leading order as

$$
\langle \Gamma(r_1)\Gamma(r_2) \rangle = \left(\frac{\nu_S \rho}{90}\right)^2 \sum_{\substack{\alpha \neq 3 \ H_\alpha = 0, \pm 1 \\ H_3 = \pm 1}}^{'} \sum_{\substack{\kappa \neq 3 \ H_\kappa = 0, \pm 1 \\ H_3 = \pm 1}}^{'} \exp \Bigg[
$$

$$
\sum_{\alpha,\alpha'} \left(H_\alpha^2(r_1) H_{\alpha'}^2(r_1) \mathcal{G}_\eta(r_1 + e_\alpha, r_1 + e_{\alpha'}) + H_\alpha(r_1) H_{\alpha'}(r_1) \mathcal{G}_\phi(r_1 + e_\alpha, r_1 + e_{\alpha'}) \right)
$$

$$
+ \sum_{\kappa,\kappa'} \left(H_\kappa^2(r_2) H_{\kappa'}^2(r_2) \mathcal{G}_\eta(r_2 + e_\kappa, r_2 + e_{\kappa'}) + H_\kappa(r_2) H_{\kappa'}(r_2) \mathcal{G}_\phi(r_2 + e_\kappa, r_2 + e_{\kappa'}) \right)
$$

$$
+ \sum_{\alpha,\kappa} \left(H_\alpha^2(r_1) H_\kappa^2(r_2) \mathcal{G}_\eta(r_1 + e_\alpha, r_2 + e_\kappa) + H_\alpha(r_1) H_\kappa(r_2) \mathcal{G}_\phi(r_1 + e_\alpha, r_2 + e_\kappa) \right) \Bigg]
$$

$$(6.13)$$

where H_α and $H_{\alpha'}$ are bond arms of an affected orientation at site r_1; H_κ and $H_{\kappa'}$ are those of an orientation at site r_2. The exponential corresponds to the product of the two orientations and the summation is over all possible products. The two-point Green's function $\mathcal{G}_\eta(r_1, r_2)$ for the η-field fluctuations between any two arbitrary sites $r_1 = (x_1, y_1, z_1)$ and $r_2 = (x_2, y_2, z_2)$ is given by

$$
\mathcal{G}_\eta(r_1, r_2) = \frac{2}{L} \sum_{n=1}^{L-1} \int_{-\pi}^{\pi} \frac{(dk_1)(dk_2)}{(2\pi)^2} \exp\left(ik_1(x_1 - x_2) + ik_2(y_1 - y_2)\right)
$$

$$
\times \frac{\sin(n\pi z_1/L)\sin(n\pi z_2/L)}{P_{\eta\eta}(\vec{k})} \qquad (6.14)
$$

Similarly, $\mathcal{G}_\phi(r_1, r_2)$ for ϕ field can be defined using the propagator $P_{\phi\phi}(\vec{k})$.

The expression for γ_S indicates that it varies with separation distance, owing to the L-dependent Green's functions. The asymptotic value of the γ_S is the interfacial tension for the hydrophobic surface in contact with water. The leading correction term is proportional to $\frac{1}{L}$ for large-L and contributes to force between the surfaces.

From the cluster expansion of the partition function, terms that involve sites

of both interfaces are grouped as G_Γ. It is given to the leading order as

$$-\beta G_\Gamma A = \left[\left\langle \sum_{r_1 \in I_1} \Gamma(r_1) \sum_{r_2 \in I_2} \Gamma(r_2) \right\rangle - \left\langle \sum_{r_1 \in I_1} \Gamma(r_1) \right\rangle \left\langle \sum_{r_2 \in I_2} \Gamma(r_2) \right\rangle \right] \quad (6.15)$$

Effectively, G_Γ is the connected correlation between orientational fluctuations of both interfaces. Hence, we call this contribution *interfacial fluctuations-induced part* of the free energy. The averages in Eq.(6.15) can be evaluated using the Eq.(6.12) with ν_S corresponding to each interface and using the Eq.(6.13) with proportionality factor $(\nu_{S_1} \nu_{S_2})$ instead of $(\nu_S)^2$. The identity of the sites is as per given in the expression for G_Γ [Eq.(6.15)].

The long-distance behavior of G_Γ is dominated by the $\phi(r)$ correlations, the $\eta(r)$ being short-ranged. Between two hydrophobic surfaces, to the leading order, G_Γ is proportional to the square of orientational correlations i.e., $(\mathcal{G}_\phi(r))^2$, where $\mathcal{G}_\phi(r)$ is an exponentially falling-off function for large r [see section (4.2.2) in Chapter 4].

For the case of mesoscopic surfaces, hydrophobic force is shown to arise from orientational correlations between water molecules present at the interfaces of both surfaces [see Chapter 3]. The force is seen to decay exponentially with the separation distance, asymptotically [Eq.(3.6)]. G_Γ is thus analogous to the hydrophobic interaction free energy of mesoscopic surfaces. However, for macroscopic surfaces, in addition to G_Γ, hydrophobic force obtains contributions from the Casimir part and the interfacial free energy. This aspect distinguishes the hydrophobic interaction between large surfaces from that of between small surfaces, both qualitatively and quantitatively. The non-additive nature of hydrophobic interaction with increasing size of surfaces has attracted considerable attention [17, 61] and our work provides a direction to elucidate the size dependence in terms of hydrogen-bond fluctuations in water.

6.1.1 Hydrophilic surfaces

We can envisage surfaces of generic heterogeniety in our calculation. The heterogeniety could be in terms of space-dependent ν_S and/or charge on the surface. One of the simplest cases is a homogeneous hydrophilic surface with a fixed charge at each site. We first consider the case of a positively charged hydrophilic surface. On its interface, the site functional comprises weights corresponding to all states. When a

water molecule is present on interface, its hydrogen arm is restricted from pointing in the surface direction. We assign an energetic penalty to such orientations and the site functional can be arranged, analogous to the case of a hydrophobic surface, as given below:

$$Z_I = Z_{site} + \nu_S \mu C'(\eta, \phi)$$

Here, $\nu_S \in (-1, 0)$ (ideally, $\nu_S = -1$) and the orientational weight corresponding to the affected orientations $C'(\eta, \phi)$ is given by

$$C'_+(\eta, \phi) = \sum_{\substack{\alpha \neq 3 \ H_\alpha = 0, \pm 1 \\ H_3 = 1}}^{'} \exp\left[i \sum_\alpha (H_\alpha^2(r)\eta(r + e_\alpha) + H_\alpha(r)\phi(r + e_\alpha))\right]$$

(6.16)

The above expression is for an interface site with surface in e_3 direction. A negatively charged hydrophilic surface can also be envisaged such that, for an interface water molecule, orientations with lone-pair arm in the surface direction are energetically penalized. Here, the orientational weight for the affected orientations is given by

$$C'_-(\eta, \phi) = \sum_{\substack{\alpha \neq 3 \ H_\alpha = 0, \pm 1 \\ H_3 = -1}}^{'} \exp\left[i \sum_\alpha (H_\alpha^2(r)\eta(r + e_\alpha) + H_\alpha(r)\phi(r + e_\alpha))\right]$$

(6.17)

We now compute the free energy components G_C, γ_{S_1}, γ_{S_2}, and G_Γ using their respective expressions for different types of surfaces. ν_S is an arbitrary parameter in the calculation. It is chosen close to its ideal value for each surface type. The properties of water enter the computation via Green's functions $\mathcal{G}_\eta$ and $\mathcal{G}_\phi$. These are computed within the model using Eq.(6.14). Due to the L-dependent modes in the confined direction, all the free energy components that depend on fluctuations are expected to vary with the separation distance L.

6.2 Results : Hydrophobic force, interfacial tension

We first mention that this computation is totally parameter free on lattice. The equation of network uniquely fixes HB as a function of ρ. Temperature in the model is conjugate to HB and can be self-consistently fixed for a given $h(= 2HB/\rho)$. Hence, we describe our results in terms of h to relate to water. All the free energy components given by Eqs.(6.8, (6.11), and (6.15) are evaluated from the partition function upto one-loop order using the corresponding expressions for the propagators [Eq.(4.28)].
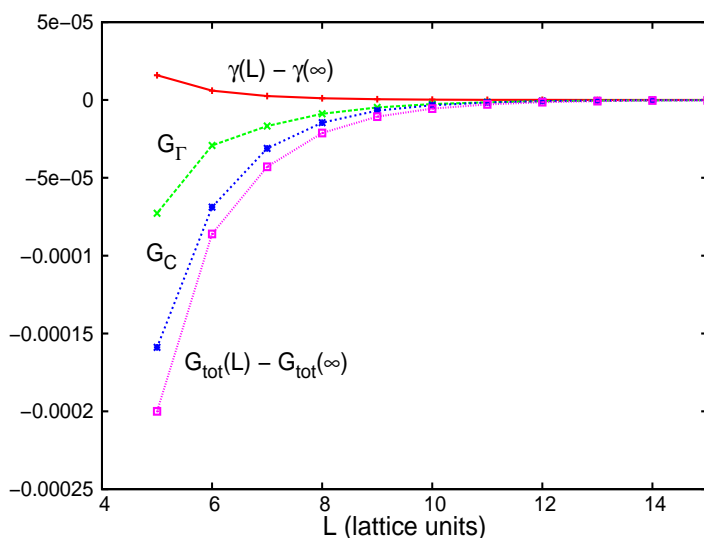
Figure 6.2: Different contributions to G_{tot} for two hydrophobic surfaces ($\nu_{S_1} = \nu_{S_2} = -0.5$). The curves are plotted for $h = 3.58$. In the order from top to bottom the curves correspond to $\gamma_S(L) - \gamma_S(\infty)$, G_Γ, G_C, and $G_{tot}(L) - G_{tot}(\infty)$ respectively. The free energy densities are measured per unit hydrogen-bond strength.

In Fig.(6.2) various contributions to the interaction free energy and their relative magnitudes are plotted as a function of the separation distance L between the surfaces. The plot is presented for $h = 3.58$. The Casimir part G_C is leading attractive component of the total interaction, followed by G_Γ, while the interfacial free energy γ_S is repulsive, albeit very small. G_C and γ_S fall off as $\frac{1}{L}$ for large L from our analytic calculation. Numerically, beyond 15 lattice units they are insignificant. All the plots are presented for the lattice distance $L \geq 5$. For smaller

L the results are predominantly influenced by surface effects. In the model, for $L = 4$ there is only one layer which can have free orientations (besides two interface layers), while for $L \geq 5$ there are two or more such free layers.
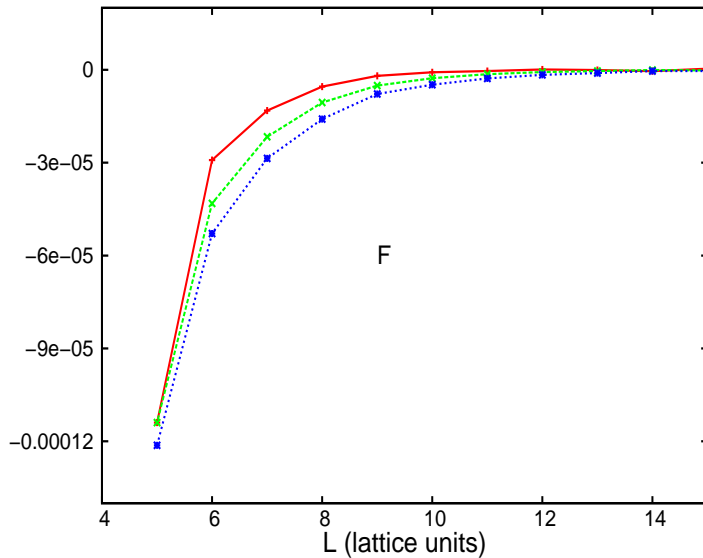
Figure 6.3: Force between two hydrophobic surfaces ($\nu_{S_1} = \nu_{S_2} = -0.5$). Top (red) curve corresponds to $h = 3.03$, middle (green) curve : $h = 3.58$, bottom (blue) : $h = 3.75$. Force is measured per unit hydrogen-bond strength per unit lattice distance.

Force between the surfaces is computed as discrete derivative of the total free energy with respect to L and plotted in Fig.(6.3) for various h. The curves effectively show that the force can manifest upto a length of about 15 lattice units which translates to about four times the orientational correlation length in the model. All the free energy components and the force obtain major contributions from orientational fluctuations.

Figures (6.4), (6.5), and (6.6) display the h-dependence of G_C, γ_S, and G_Γ functions. The Casimir part G_C monotonically increases in magnitude with h. The interfacial free energy γ_S decreases and is always slightly repulsive. Interfacial fluctuations-induced part G_Γ increases with h for $L \geq 6$. At shorter distances it decreases with increasing h. This indicates that the adhesion strength of G_Γ is higher for higher temperatures. This behavior is qualitatively similar to the temperature dependence of interaction free energy for mesoscopic hydrophobic surfaces [2, 62]. This reaffirms our interpretation that G_Γ is analogous to the
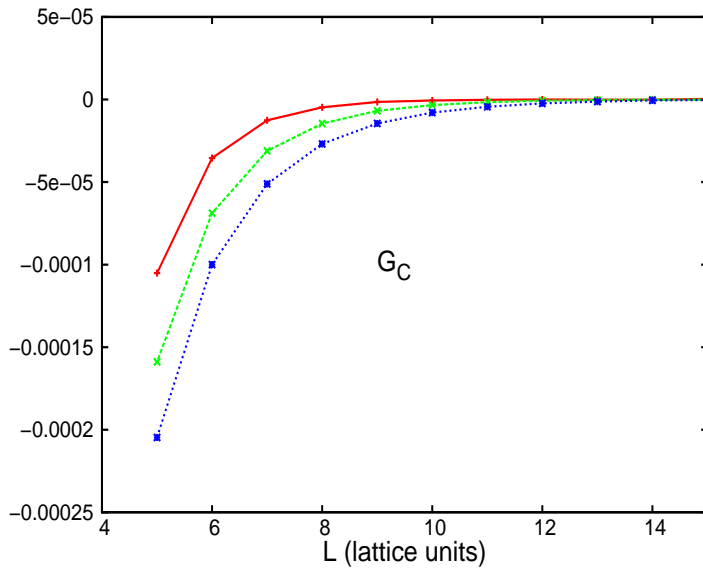
Figure 6.4: G_C as a function of L. Top (red) curve corresponds to $h = 3.03$, middle (green) curve : $h = 3.58$, bottom (blue) : $h = 3.75$.

hydrophobic interaction free energy for mesoscopic surfaces.

Figure (6.7) is the plot for G_Γ contribution between two hydrophilic surfaces for two cases: (i) Both surfaces are of the same type i.e., both are either hydrogen donor type or hydrogen acceptor type, and (ii) Both surfaces are of dissimilar type. G_Γ in both cases is proportional to $\mathcal{G}_\phi$ and hence, the correlation length is twice as longer in range than in the case of hydrophobic surfaces (where G_Γ is proportional to $(\mathcal{G}_\phi)^2$). At short distances, this contribution is seen to be attractive for both combinations of hydrophilic surfaces. However, for large distances, it is weakly repulsive between like-charged surfaces, in contrast to attraction between oppositely charged surfaces. Fig.(6.8) depicts the force between hydrophilic surfaces for both similar and dissimilar combinations. As expected, the dissimilar pair of surfaces have marginally larger attraction than that of similar surfaces. It is interesting to note that like-charged hydrophilic surfaces also have a net attraction. This is due to dominance of the Casimir part G_C which is indifferent to surface charge.

Figure (6.9) displays force between a hydrophobic and hydrophilic surface. It bears similar profile as in the case of two hydrophobic surfaces. This is expected because essentially G_Γ is qualitatively same for both cases i.e., proportional to $(\mathcal{G}_\phi)^2$. For all surface combinations the force is seen to increase in magnitude with
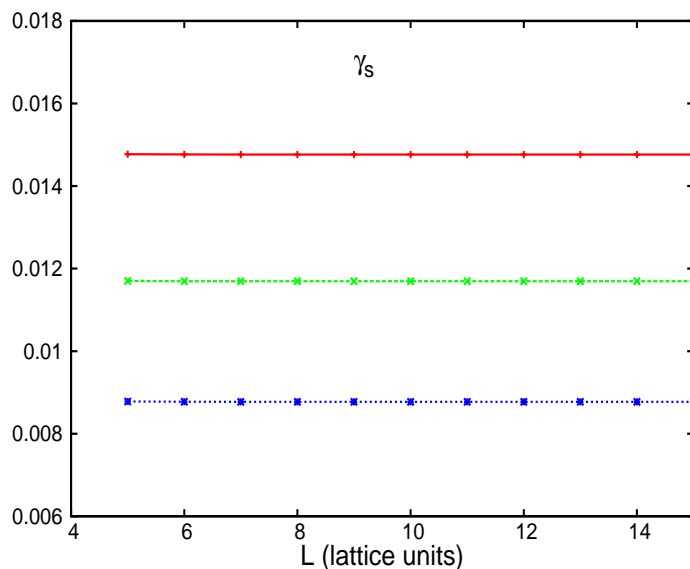
Figure 6.5: γ_S for a hydrophobic surface ($\nu_S = -0.5$). Top (red) curve corresponds to $h = 3.03$, middle (green) curve : $h = 3.30$, bottom (blue) : $h = 3.58$.

h, dominantly due to the Casimir part which is leading contribution in all the cases and is indifferent to surface types. This is a consequence of the fact that the entropy induced forces are largely charge neutral.

Next, we make an attempt to relate our computational results to those of experiments. The free energy values presented in the graphs are in the units where hydrogen-bond strength is unity. Generally, dimensionful quantities in lattice models and those in corresponding continuum models are not the same. So, it is best to compare dimensionless quantities. In our instance, for $h = 3.58$ and $L = 6$ lattice units which translates to $6 \times 1.57\text{Å} \simeq 9.5\text{Å}$, $\dfrac{|G_{tot}(6) - G_{tot}(\infty)|}{\gamma_S(\infty)} \simeq \dfrac{9 \times 10^{-5}}{8.5 \times 10^{-3}} \simeq 10^{-2}$. From experiments, the interaction free energy estimate when two hydrophobic plates are about 10 Å apart is about 1 mJ m^{-2} [9], while the interfacial tension is in the range $50 - 100$ mJ m^{-2} [63]; their ratio agrees with our computation. In experiments the free energy values are also measured for larger distances all the way up to 100 Å. Unfortunately, our model is not good for these distances. This discrepancy was already noticed when our results were compared with the MD simulation. The simple water model has only one orientational correlation length, while there are more than one in both MD simulations [see Eq.(2.4) in Chapter 2] and surface force apparatus experiments [7]. We conclude that while the order
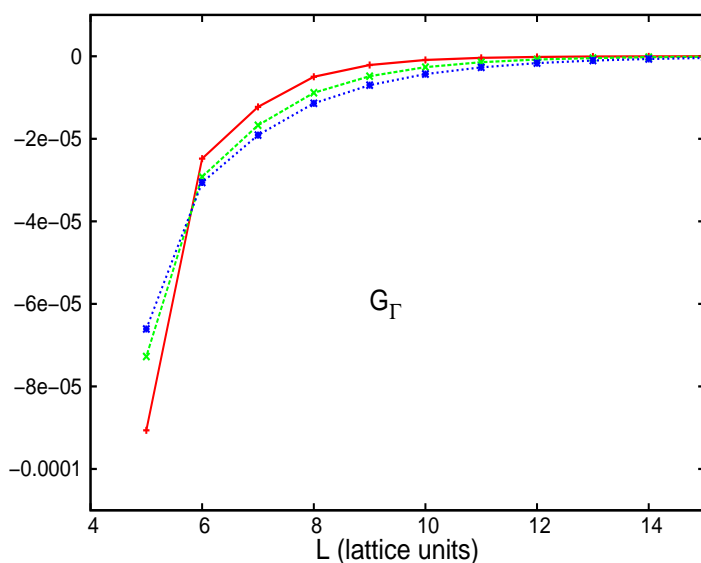
Figure 6.6: G_Γ for two hydrophobic surfaces ($\nu_{S_1} = \nu_{S_2} = -0.5$). For $L \geq 6$, top (red) curve corresponds to $h = 3.03$, middle (green) curve : $h = 3.58$, bottom (blue) : $h = 3.75$.

of magnitude estimate of the strength of hydrophobic force is in agreement with Casimir-like energies envisaged here, a few more important details are perhaps missing in our simple model of water.

6.3   Transverse density profile

We also deduce expression for water density profile along the confinement direction. $\rho(z)$ is obtained by assuming chemical potential for water $\tilde{\mu}$ to be z-dependent and then, a partial derivative of $\ln(Z_{||})$ is taken with respect to $\beta\tilde{\mu}(z)$. At both interfaces i.e., $z = 1$ and $z = L - 1$, the modified fugacity provides additional correction to the average density. The expression for the density profile is given by

$$\rho(z) \equiv \frac{\partial(\ln(Z_{||}))}{\partial(\beta\tilde{\mu}(z))} = \rho_C(z) + \frac{1}{A}\left\langle \frac{\partial}{\partial(\beta\tilde{\mu}(z))}\left(\sum_{r_1 \in I_1}\Gamma(r_1) + \sum_{r_2 \in I_2}\Gamma(r_2)\right)\right\rangle + \dots \tag{6.18}$$

ρ_C is obtained from differentiating Z in Eq.(6.3). It is the density profile between ideal hydrophobic surfaces ($\nu_S = 0$) and is the dominant contribution at all positions. The explicit expression for $\rho_C(z)$ upto the one-loop order is same as given
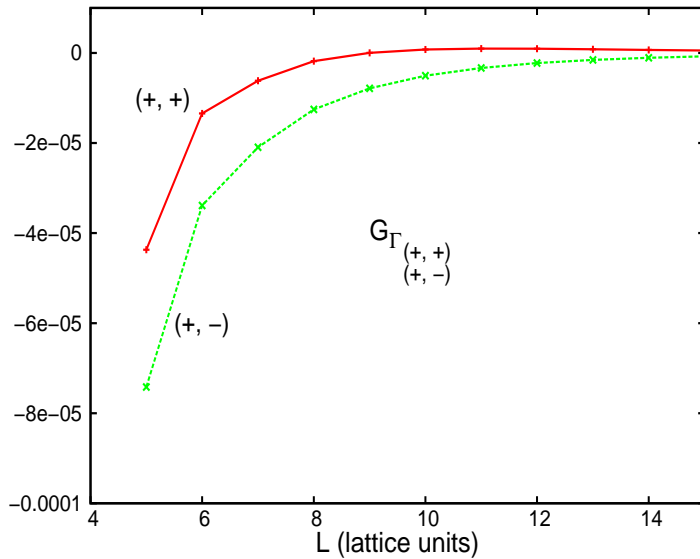
Figure 6.7: G_Γ for hydrophilic surfaces ($\nu_{S_1} = \nu_{S_2} = -0.9$). $(+, +)$ curve corresponds to similar type of hydrophilic surfaces and $(+, -)$, to dissimilar type. Both curves are plotted for $h = 3.58$.

in the Appendix (4.4.2) [see Chapter 4]. The Green's functions $\mathcal{G}_\eta$ and $\mathcal{G}_\phi$ in the expression are to be computed from Eq.(6.14). The interfaces-dependent term in Eq.(6.18) can be analyzed using Eq.(6.12). This contribution is only at $z = 1$ and $z = L - 1$.

The transverse density profile is shown in Fig.(6.10) after scaling $\rho(z)$ with respect to the bulk density value. At both interfaces there is a characterstic rise in density. From the expressions for $\rho_C(z)$ and the interface terms [Eq.(6.12)] it is evident that the net contribution of ϕ field correlations is numerically small, since, density is a charge-neutral quantity and linear ϕ-dependent terms tend to cancel each other. Hence, away from the interfaces, density reaches bulk density value rapidly within a distance ξ_η. Many a model simulations in the past computed the transverse density profile for water confined between model hydrophobic surfaces. The short-distance density increase is generically observed [64, 65]. At ambient conditions the magnitude of the interfacial density is seen to be typically 1.3 times the bulk density value in case of surfaces with alkane headgroups [65] and is independent of L. In our model study we see an L-independent increase of magnitude 1.2 for an ideal hydrophobic surface. The under-estimation could possibly be due to discrete orientational freedom envisaged in our model. Also, the alkane head-

79
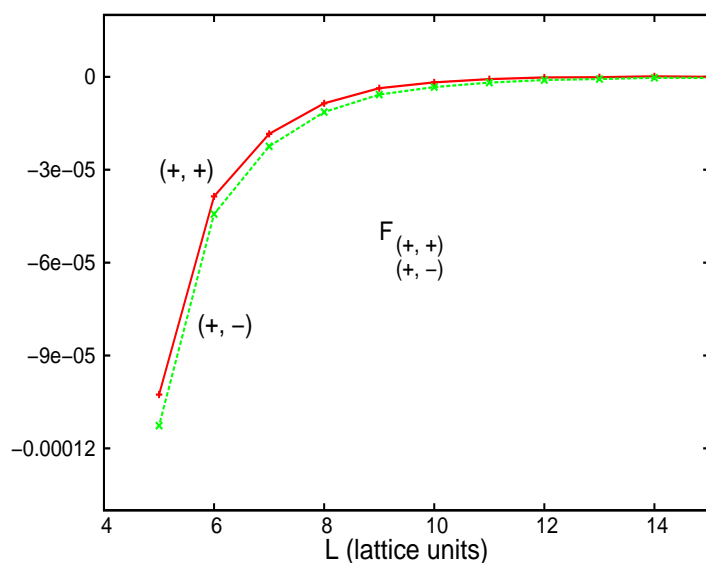
Figure 6.8: Force between two hydrophilic surfaces ($\nu_{S_1} = \nu_{S_2} = -0.9$). $(+, +)$ indicates similar type of hydrophilic surfaces and $(+, -)$ indicates dissimilar type. Both curves correspond to $h = 3.58$.

groups in simulations may have an extra entropy due to fluctuating short-length polymer chains.

The rise in interfacial density is also seen for water in the vicinity of hydrophilic surfaces [65, 66]. In our model study, $\rho(z)$ between hydrophilic surfaces also displays qualitatively similar profile and a lower magnitude of interfacial density compared to that near an ideal hydrophobic surface. In all the cases, the phenomenon is seen to be a consequence of the fact that the water density has to vanish on the surface. This is compensated by an increase at the interface and the system comes back to its bulk equilibrium density value within a distance ξ_η from the interface.

We also calculate density correlations within the interfacial plane and between sites on interface and away from the interface. Density correlations between any two sites r and $r^{'}$ can be calculated as given below.

$$\langle W(r)W(r^{'})\rangle \;\; = \;\; \left\langle \frac{\mu\{\ldots\}}{Z_{site}(r)} \frac{\mu\{\ldots\}}{Z_{site}(r^{'})} \right\rangle \tag{6.19}$$

where $Z_{site}(r)$ is the site functional at r. To compute density correlations on same interface, the site functional at both sites is given by Eq.(6.2). For density correlations between one site on interface and another site away from interface,
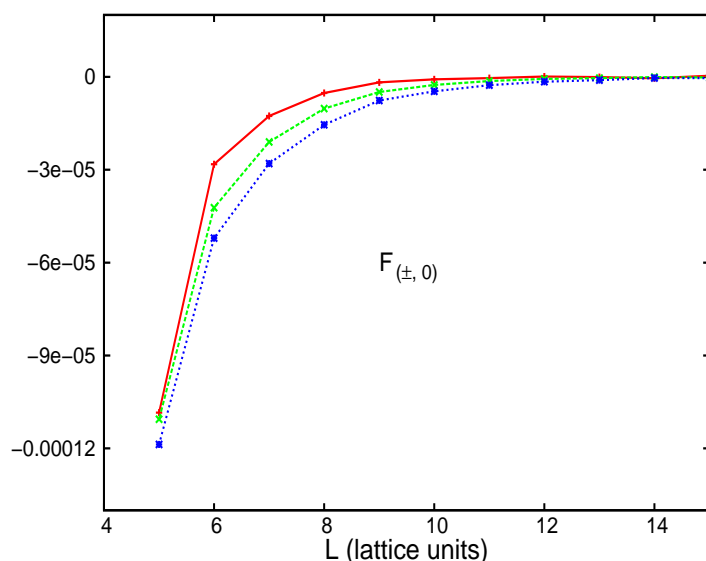
Figure 6.9: Force between a hydrophilic ($\nu_{S_1} = -0.9$) and a hydrophobic surface ($\nu_{S_2} = -0.5$). Top (red) curve corresponds to $h = 3.03$, middle (green) curve : $h = 3.58$, bottom (blue) : $h = 3.75$. $(\pm, 0)$ indicates that force is between a positively (negatively) charged hydrophilic surface and a hydrophobic surface.

the site functionals are given by Eqs.(6.2) and (4.16) respectively. $\mu\{\ldots\}$ refers to the term proportional to μ in the respective site functional. The connected part of the correlation is given by $< W(r)W(r^{'}) >_c \equiv (< W(r)W(r^{'}) > - < W(r) >< W(r^{'}) >)$. The explicit expression in each context is deduced upto one-loop order in terms of $\mathcal{G}_\eta$, $\mathcal{G}_\phi$ and are given in Appendix (6.4.2).

Density correlations scaled appropriately with respect to the bulk density value are plotted in Fig.(6.11). The plot corresponds to $h = 3.58$. The figure essentially indicates that density correlations do not extend beyond few molecular diameters from the interface. Also, there is no significant difference between correlations within an interface and that of between interface and non-interface sites.

Similarly, orientational correlations can also be analyzed using the expressions for orientational weights given in Appendix (6.4.1). Their effect persists upto longer distances away from interface, proportional to the long correlation length of the ϕ field.
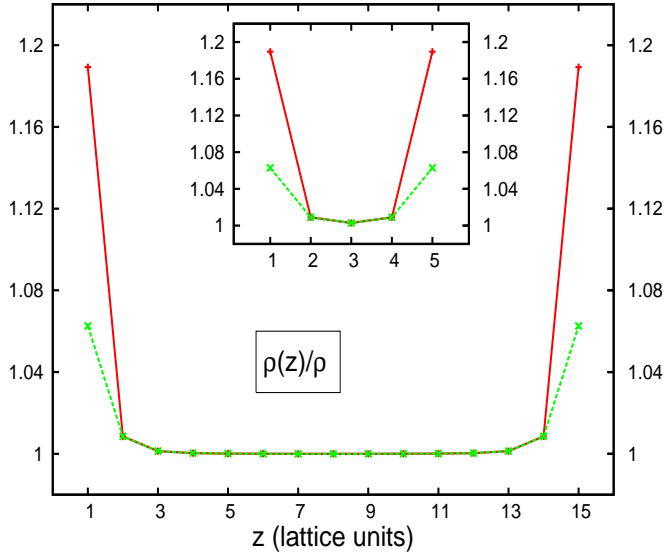
Figure 6.10: Transverse density profile for water between two hydrophobic surfaces separated by distance $L = 16$ and (inset) $L = 6$. Here, $h = 3.58$. The steeper (red) curve corresponds to ideal case $\nu_{S_1} = \nu_{S_2} = 0$ and the other (green) curve corresponds to $\nu_{S_1} = \nu_{S_2} = -0.5$.

6.4 Appendix

6.4.1 Orientational weight on interface

The orientational weight for the water state in bulk water is given by

$$C(\eta, \phi) = \sum_{\substack{H_\alpha = 0, \pm 1 \\ \alpha = \pm 1, \pm 2, \pm 3}}^{'} \exp\left[i \sum_\alpha (H_\alpha^2(r)\eta(r + e_\alpha) + H_\alpha(r)\phi(r + e_\alpha))\right]$$

where the prime indicates the summation is subject to constraints Eq.(4.2).

About the mean field configuration $\eta = \phi = 0$, the dual fields are expanded upto quadratic order. $C(\eta, \phi)$ is then given by

$$C(\eta, \phi) \simeq 90\left[1 + \frac{2i}{3}\sum_\alpha \eta_\alpha - \frac{1}{3}\sum_\alpha \eta_\alpha^2 - \frac{2}{5}\sum_{\alpha,\beta} \eta_\alpha \eta_\beta - \frac{1}{3}\sum_\alpha \phi_\alpha^2 + \frac{2}{15}\sum_{\alpha,\beta} \phi_\alpha \phi_\beta\right]$$

$$(6.20)$$

where $\eta_\alpha \equiv \eta(r + e_\alpha)$ and $\phi_\alpha \equiv \phi(r + e_\alpha)$.
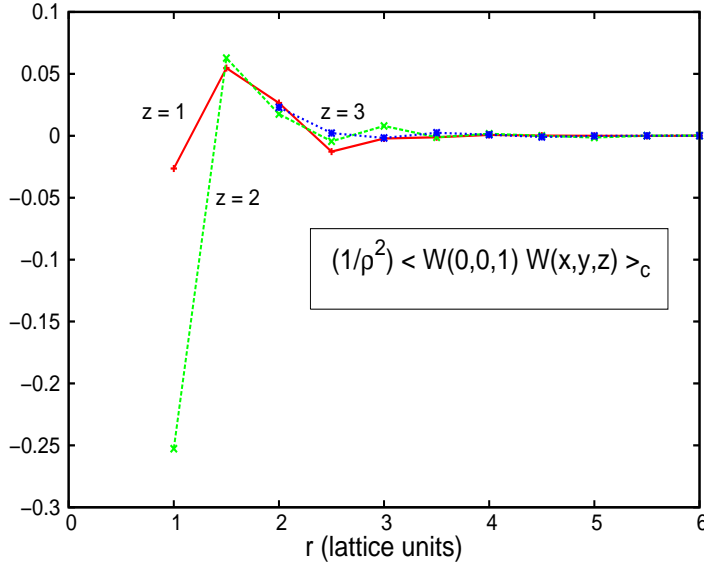
Figure 6.11: Density correlations near a hydrophobic interface ($\nu_S = -0.5$) scaled appropriately with respect to bulk density value at $h = 3.58$. Correlations are between a reference site on interface ($z = 1$) and an arbitrary site on a plane defined by its z coordinate. Distance between the two sites is measured using Euclidean metric.

The orientational weight for the affected orientations for an interfacial water near hydrophobic surface are denoted by $C'(\eta, \phi)$. With boundary conditions $\eta = \phi = 0$ on surface sites, it is given by

$$C'(\eta, \phi) \simeq 60 \left[1 + \frac{3i}{5} \sum_{\alpha} \eta_\alpha - \frac{3}{10} \sum_{\alpha} \eta_\alpha^2 - \frac{3}{10} \sum_{\alpha,\beta} \eta_\alpha \eta_\beta - \frac{3}{10} \sum_{\alpha} \phi_\alpha^2 + \frac{1}{10} \sum_{\alpha,\beta} \phi_\alpha \phi_\beta \right] \tag{6.21}$$

Near a hydrophilic surface, the orientational weight is given by

$$
\begin{aligned}
C'_\pm(\eta, \phi) \simeq 30 \left[1 + \frac{3i}{5} \sum_{\alpha} \eta_\alpha - \frac{3}{10} \sum_{\alpha} \eta_\alpha^2 - \frac{3}{10} \sum_{\alpha,\beta} \eta_\alpha \eta_\beta - \frac{3}{10} \sum_{\alpha} \phi_\alpha^2 \right. \\
\left. + \frac{1}{10} \sum_{\alpha,\beta} \phi_\alpha \phi_\beta \mp \frac{i}{5} \sum_{\alpha} \phi_\alpha \right] \tag{6.22}
\end{aligned}
$$

6.4.2 Interfacial density correlations

The connected part of density correlation function between sites on same interface, to leading order, is given by

$$
\langle W(r)W(r^{'})\rangle_c \simeq
$$
$$
-(\mu^{'})^2 \left[(\nu^{'} + 2\lambda^{'})^2 \mathcal{G}_\eta(r,r^{'}) + \left(\frac{2}{3}\left(1 + \frac{3\nu_S}{5} - \mu^{'} \right) \right)^2 \sum_{\alpha,\alpha^{'}} \mathcal{G}_\eta(r + e_\alpha, r^{'} + e_{\alpha^{'}}) \right.
$$
$$
\left. + 2\left(\frac{2}{3}\left(1 + \frac{3\nu_S}{5} - \mu^{'} \right) \right)(\nu^{'} + 2\lambda^{'}) \sum_{\alpha^{'}} \mathcal{G}_\eta(r, r^{'} + e_{\alpha^{'}}) \right] \tag{6.23}
$$

where r and $r^{'}$ are arbitrary sites on same interface; $r + e_\alpha$ and $r^{'} + e_{\alpha^{'}}$ are respective near-neighbor sites in the directions e_α, $e_{\alpha^{'}}$ respectively. $\mathcal{G}_\eta(r_1, r_2)$ and $\mathcal{G}_\phi(r_1, r_2)$ can be computed from Eq.(6.14). $\nu^{'}$, $\lambda^{'}$, and $\mu^{'}$ are the reduced fugacities [see section (4.2.1) in Chapter 4].

The density correlation function between a site on an interface and another site away from interface is given by

$$
\langle W(r)W(r^{'})\rangle_c \simeq
$$
$$
-(\mu^{'})^2 \left[(\nu^{'} + 2\lambda^{'})^2 \mathcal{G}_\eta(r,r^{'}) + \frac{2}{3}(1 - \mu^{'})\left(1 + \frac{3\nu_S}{5} - \mu^{'} \right) \sum_{\alpha,\alpha^{'}} \mathcal{G}_\eta(r + e_\alpha, r^{'} + e_{\alpha^{'}}) \right.
$$
$$
\left. + \frac{2}{3}(\nu^{'} + 2\lambda^{'})\left(2 + \frac{3\nu_S}{5} - 2\mu^{'} \right)\left(\sum_{\alpha} \mathcal{G}_\eta(r + e_\alpha, r^{'}) + \sum_{\alpha^{'}} \mathcal{G}_\eta(r, r^{'} + e_{\alpha^{'}}) \right) \right]
$$
$$
\tag{6.24}
$$

where r is any site on the interface and $r^{'}$ is away from interface; $r + e_\alpha$ and $r^{'} + e_{\alpha^{'}}$ are their respective near-neighbor sites.

Orientational correlations can also be evaluated using the expression for orientational weights given in Appendix (6.4.1) and can be computed using known expressions for Green's functions.

7

Results summary

- MD simulation study reveals that orientational correlations in liquid water are longer in range, whereas density correlations vanish beyond few molecular diameters (12 Å). The longitudinal dipolar correlation, in particular, exhibits two correlation lengths, one of order 5.2 Å and the other of 24 Å. MMF theory for a simple lattice water model predicts a correlation length for orientational fluctuations consistent with the shorter length. MC simulation of the model confirms this feature qualitatively. Coulomb interactions have no significant effect on the correlation length, asymptotically. This aspect is verified both within MD study and MMF theory.

- The finite particle size and finite number of bonds that particles can undergo in associating fluids imply sum rule(s) for the fluid. MMF theory for the water model explicitly respects the corresponding sum rule in the evaluation of partition function. The sum rule manifests in the form of equation of network, a relation between hydrogen bond density and molecular density. The same is borne out in experiments. Furthermore, as a consequence of the sum rule the equation of state correctly predicts the density saturation and the bond saturation in the model.

- Two mesoscopic hydrophobic surfaces in water are shown to experience a long range attractive force mediated by orientational correlations in water. The deduced force expression suggests that, for distances greater than the surface size itself, hydrophobic force falls off exponentially with a correlation length half that of orientational correlations i.e., about 12 Å. This distance

dependence is quantitatively consistent with experiments. The shape of the surfaces and their mutual orientation are also shown to influence the magnitude of the force.

- For the case of macroscopic hydrophobic surfaces Casimir-like fluctuations in the intervening region give rise to an attractive hydrophobic force. The force obtains contributions from : (i) Casimir part of free energy, which solely arises from discretization of fluctuation modes in the region between surfaces and is independent of nature of surfaces, (ii) Interfacial free energy, which arises due to surface-water interaction and is weakly distance-dependent, (iii) Interfacial fluctuations-induced part, which is due to correlation between orientational fluctuations at both interfaces and depends on nature of both surfaces. All contributions are of similar order of magnitude. The Casimir part is the leading contribution among them.

- The Casimir part is largely influenced by long range correlations of orientational fluctuations. It behaves as $\frac{1}{L}$, asymptotically. However, its strength is practically weak for distances beyond four times the longest correlation length in water.

- We also deduce interfacial free energy for hydrophobic and hydrophilic surfaces in contact with water. This contribution is seen to weakly depend on separation distance.

- The interfacial fluctuations-induced part is exponentially decaying with a correlation length half that of orientational correlations in water. This contribution is analogous to the force between mesoscopic surfaces.

- Our analysis can be carried out for generic surface types. In case of hydrophilic surfaces the Casimir part is the leading contribution. The interfacial fluctuations-induced part is seen to depend on charge symmetry between the surfaces and is longer in range compared to the case of hydrophobic surfaces i.e., its correlation length is same as that of orientational correlations.

- The transverse density profile of water in confinement direction is seen to display a characterstic rise near interfaces, concomitant with simulation studies. The density approaches the bulk value within a hydrogen bond length.

Bibliography

[1] Philip Ball. Water as an active constituent in cell biology. *Chem. Rev.*, 108:74–108, 2008.
S. J. Gill and P. L. Privalov. Stability of protein structure and hydrophobic interaction. *Adv. Protein Chem.*, 39:191–234, 1988.
C. Tanford. How protein chemists learned about the hydrophobic factor. *Protein Sci.*, 6:1358–1366, 1997.

[2] H. S. Frank and M. W. Evans. Free volume and entropy in condensed systems. III. Entropy in binary liquid mixtures; partial molal entropy in dilute solutions; structure and thermodynamics of aqueous eletrolytes. *J. Chem. Phys.*, 13:507–532, 1945.

[3] W. Kauzmann. Factors in interpretation of protein denaturation. *Adv. Protein Chem.*, 14:1–63, 1959.

[4] J. A. V. Butler. The energy and entropy of hydration of organic compounds. *Trans. Faraday Soc.*, 33:229–236, 1937.

[5] J. N. Israelachvili and R. Pashley. The hydrophobic interaction is long range, decaying exponentially with distance. *Nature*, 300:341–342, 1982.

[6] J. N. Israelachvili. *Intermolecular and Surface forces.* Academic Press, 2nd edition, U.S.A., 1992.

[7] H. K. Christenson and P. M. Claesson. Direct measurements of the force between hydrophobic surfaces in water. *Adv. Colloid Interface Sci.*, 91:391–436, 2001.

[8] E. E. Meyer, K. J. Rosenberg, and J. N. Israelachvili. Recent progress in understanding hydrophobic interactions. *Proc. Natl. Acad. Sci. U. S. A.*, 103:15739–15746, 2006.

[9] A. Chaimovich, M. S. Shell, J. N. Israelachvili, M. U. Hammer, and T. H. Anderson. The search for the hydrophobic force law. *Faraday Discuss.*, 146:299–308, 2010.

[10] M. S. Lin, N. L. Fawzi, and T. H.-Gordon. Hydrophobic potential of mean force as a solvation function for protein structure prediction. *Structure*, 15:727–740, 2007.

[11] W. Kauzmann and D. Eisenberg. *The structure and properties of water*. Oxford University Press, U.S.A., 1969.

[12] G. M. Bell. Statistical mechanics of water: Lattice model with directed bonding. *J. Phys. C: Solid State Phys.*, 5(9):889, 1972.
D. Bratko, L. Blum, and A. Luzar. A simple model for the intermolecular potential of water. *J. Chem. Phys.*, 83(12):6367–6370, 1985.
E. A. Jagla. Core-softened potentials and the anomalous properties of water. *J. Chem. Phys.*, 111(19):8980–8986, 1999.
T. M. Truskett, P. G. Debenedetti, S. Sastry, and S. Torquato. A single-bond approach to orientation-dependent interactions and its implications for liquid water. *J. Chem. Phys.*, 111(6):2647–2656, 1999.
N. Giovambattista, E. La Nave, S. Mossa, A. Scala, F. Sciortino, F. W. Starr, H. E. Stanley, S. V. Buldyrev, and M. Yamada. Application of statistical physics to understand static and dynamic anomalies in liquid water. *J. Stat. Phys.*, 110(3-6):1039–1054, 2003.

[13] Bertrand Guillot. A reappraisal of what we have learnt during three decades of computer simulations on water. *J. Mol. Liq.*, 101(1-3):219–260, 2002.
M. M. Conde, J. L. Aragones, C. Vega, and J. L. F. Abascal. What ice can teach us about water interactions: A critical comparison of the performance of different water models. *Faraday Discuss.*, 141:251–276, 2009.

[14] J.-P. Hansen and I. R. McDonald. *Theory of Simple Liquids, Third Edition*. Academic Press, U.K., 2006.
K. E. Gubbins and C. G. Gray. *Theory of Molecular Fluids. Volume 1: Fundamentals*. Oxford University Press, U.S.A., 1984.

[15] L. Blum, P. T. Cummings, and D. Bratko. A general solution of the molecular Ornstein–Zernike equation for spheres with anisotropic adhesion and electric multipoles. *J. Chem. Phys.*, 92(6):3741–3747, 1990.

J. Richardi, C. Millot, and P. H. Fries. A molecular Ornstein–Zernike study of popular models for water and methanol. *J. Chem. Phys.*, 110(2):1138–1147, 1999.

[16] M. S. Wertheim. Fluids with highly directional attractive forces. I. Statistical thermodynamics. *J. Stat. Phys.*, 35(1):19–34, 1984.
M. S. Wertheim. Fluids with highly directional attractive forces. II. Thermodynamic perturbation theory and integral equations. *J. Stat. Phys.*, 35(1):35–47, 1984.
M. S. Wertheim. Fluids with highly directional attractive forces. III. Multiple attraction sites. *J. Stat. Phys.*, 42(3):459–476, 1986.

[17] D. Chandler. Structures of molecular liquids. *Annu. Rev. Phys. Chem.*, 29(1):441–471, 1978.
H. S. Ashbaugh and L. R. Pratt. Scaled particle theory and the length scales of hydrophobicity. *Rev. Mod. Phys.*, 78:159–178, 2006.

[18] L. R. Pratt and D. Chandler. Theory of hydrophobic effect. *J. Chem. Phys.*, 67:3683–3704, 1977.

[19] H. K. Christenson and P. M. Claesson. Cavitation and the interaction between macroscopic hydrophobic surfaces. *Science*, 239:390–392, 1988.
K. Leung, A. Luzar, and D. Bratko. Dynamics of capillary drying in water. *Phys. Rev. Lett.*, 90:065502, 2003.

[20] K. Lum, D. Chandler, and J. D. Weeks. Hydrophobicity at small and large length scales. *J. Phys. Chem. B*, 103:4570–4577, 1999.

[21] S. Marčelja and N. Radić. Repulsion of interfaces due to boundary water. *Chem. Phys. Lett.*, 42(1):129–130, 1976.
J. C. Eriksson, S. Ljunggren, and P. M. Claesson. A phenomenological theory of long-range hydrophobic attraction forces based on a square-gradient variational approach. *J. Chem. Soc., Faraday Trans. 2*, 85:163–176, 1989.
N. A. M. Besseling. Theory of hydration forces between surfaces. *Langmuir*, 13(7):2113–2122, 1997.

[22] P. Attard. Long-range attraction between hydrophobic surfaces. *J. Phys. Chem.*, 93(17):6441–6444, 1989.

R. J. Podgornik. Electrostatic correlation forces between surfaces with surface specific ionic interactions. *J. Chem. Phys.*, 91:5840, 1989.

Y. H. Tsao, D. F. Evans, and H. Wennerström. Long-range attraction between a hydrophobic surface and a polar surface is stronger than that between two hydrophobic surfaces. *Langmuir*, 9:779, 1993.

[23] F. Despa, A. Fernandez, and R. S. Berry. Dielectric modulation of biological water. *Phys. Rev. Lett.*, 93:228104, 2004.

F. Despa and R. Berry. Hydrophobe-water interactions: Methane as a model. *Biophys. J.*, 95(9):4241–4245, 2008.

[24] P. Attard. Bridging bubbles between hydrophobic surfaces. *Langmuir*, 12:1693–1695, 1996.

J. W. G. Tyrrell and P. Attard. Images of nanobubbles on hydrophobic surfaces and their interactions. *Phys. Rev. Lett.*, 87:176104, 2001.

P. Attard, M. P. Moody, and J. W. G. Tyrrell. Nanobubbles: The big picture. *Physica A*, 314:696–705, 2002.

[25] G. Silbert, D. B.-Yaakov, Y. Dror, S. Perkin, N. Kampf, and J. Klein. Long-ranged attraction between disordered heterogeneous surfaces. *arXiv:1109.4715*, 2011.

[26] H. B. G. Casimir. On the attraction between two perfectly conducting plates. *Proc. K. Ned. Akad. Wet.*, 51:793, 1948.

[27] E. M. Lifshitz. The theory of molecular attractive forces between solids. *Soviet Phys.*, 2(1):73–83, 1956.

[28] M. Kardar and R. Golestanian. The "friction" of vacuum, and other fluctuation-induced forces. *Rev. Mod. Phys.*, 71(4):1233–1245, 1999.

[29] M. E. Fisher and P. G. de Gennes. Wall phenomena in a critical binary mixture. *C. R. Seances Acad. Sci.*, Ser. B 287:207–209, 1978.

[30] A. Rahman and F. H. Stillinger. Molecular dynamics study of liquid water. *J. Chem. Phys.*, 55(7):3336–3359, 1971.

F. H. Stillinger and A. Rahman. Improved simulation of liquid water by molecular dynamics. *J. Chem. Phys.*, 60(4):1545–1557, 1974.

[31] M. W. Mahoney and W. L. Jorgensen. A five-site model for liquid water and the reproduction of the density anamoly by rigid, non-polarizable potential functions. *J. Chem. Phys.*, 112(20):8910–8922, 2000.
S. Rick. A reoptimization of the five-site water potential (TIP5P) for use with Ewald sums. *J. Chem. Phys.*, 120:6085–6093, 2004.

[32] J. G. Kirkwood. The dielectric polarization of polar liquids. *J. Chem. Phys.*, 7:911–919, 1939.
P. L. Silvestrelli and M. Parrinello. Water molecule dipole in the gas and in the liquid phase. *Phys. Rev. Lett.*, 82:3308–3311, 1999.
M. Sharma, R. Resta, and R. Car. Dipolar correlations and the dieletric permittivity of water. *Phys. Rev. Lett.*, 98:247401, 2007.

[33] W. L. Jorgensen, J. Chandrasekhar, J. D. Madura, R. W. Impey, and M. Klein. Comparision of simple potential functions for simulating liquid water. *J. Chem. Phys.*, 79:926–935, 1983.

[34] M. P. Allen and D. J. Tildesley. *Computer Simulation of Liquids*. Oxford Science Publications. Clarendon Press, Oxford, I edition, 1987.
J. Kolafa and I. Nezbeda. Effect of short- and long-range forces on the structure of water. II. Orientational ordering and the dielectric constant. *Mol. Phys.*, 98:1505–1520, 2000.

[35] C. Huang, K. T. Wikfeldt, T. Tokushima, D. Nordlund, Y. Harada, U. Bergmann, M. Niebuhr, T. M. Weiss, Y. Horikawa, M. Leetmaa, M. P. Ljungberg, O. Takahashi, A. Lenz, L. Ojamäe, A. P. Lyubartsev, S. Shin, L. G. M. Pettersson, and A. Nilsson. The inhomogeneous structure of water at ambient conditions. *Proc. Natl. Acad. Sci. U. S. A.*, 106:15214–15218, 2009.

[36] L. Bosio, J. Teixeira, and H. E. Stanley. Enhanced density fluctuations in supercooled H_2O, D_2O, and ethanol-water solutions: Evidence from small-angle x-ray scattering. *Phys. Rev. Lett.*, 46:597–600, 1981.

[37] R. M. Lynden-Bell and P. G. Debenedetti. Computational investigation of order, structure, and dynamics in modified water models. *J. Phys. Chem. B*, 109(14):6527–6534.
Z. Yan, S. V. Buldyrev, P. Kumar, N. Giovambattista, and H. E. Stanley. Correspondence between phase diagrams of the TIP5P water model and a spherically symmetric repulsive ramp potential with two characteristic length scales. *Phys. Rev. E*, 77(4):042201, 2008.
A. B. de Oliveira, P. A. Netz, T. Colla, and M. C. Barbosa. Structural anomalies for a three dimensional isotropic core-softened potential. *J. Chem. Phys.*, 125(12):124503, 2006.
W. P. Krekelberg, T. Kumar, J. Mittal, J. R. Errington, and T. M. Truskett. Anomalous structure and dynamics of the gaussian-core fluid. *Phys. Rev. E*, 79(3):031203, 2009.

[38] E. Lindahl, B. Hess, and D. van der Spoel. GROMACS 3.0 : A package for molecular simulation and trajectory analysis. *J. Mol. Mod.*, 7:306–317, 2001.

[39] D. Frenkel and B. Smit. *Understanding Molecular Simulation (Computational Science Series, Vol 1)*. Academic Press, U.S.A., 2001.
A. Leach. *Molecular Modelling: Principles and Applications (2nd Edition)*. Prentice Hall, U.S.A., 2001.

[40] L. Kale, R. Skeel, M. Bhandarkar, R. Brunner, A. Gursoy, N. Krawetz, J. Phillips, A. Shinozaki, K. Varadarajan, and K. Schulten. Molecular dynamics programs design, NAMD2 : Greater scalability for parallel molecular dynamics. *J. Comput. Phys.*, 151:283, 1999.

[41] G. Mathias and P. Tavan. Angular resolution and range of dipole-dipole correlations in water. *J. Chem. Phys.*, 120:4393–4403, 2004.

[42] J. M. Pradeep Kanth, S. Vemparala, and Ramesh Anishetty. Long-distance correlations in molecular orientations of liquid water and shape-dependent hydrophobic force. *Phys. Rev. E*, 81(2):021201, 2010.

[43] Y. K. Cheng and P. J. Rossky. Surface topography dependence of biomolecular hydrophobic hydration. *Nature*, 392:696–699, 1998.

[44] A. Poynor, L. Hong, I. K. Robinson, S. Granick, Z. Zhang, and P. A. Fenter. How water meets a hydrophobic surface. *Phys. Rev. Lett.*, 97:266101, 2006.
Y. L. A. Rezus and H. J. Bakker. Observation of immobilized water molecules around hydrophobic groups. *Phys. Rev. Lett.*, 99:148301, 2007.
P. N. Perera, K. R. Fegaa, C. Lawrence, E. J. Sundstrom, J. T.-Phillips, and D. B.-Amotz. Observation of water dangling oh bonds around dissolved nonpolar groups. *Proc. Natl. Acad. Sci. U. S. A.*, 106(30):12230–12234, 2009.

[45] P. L. Chau. Computer simulation of the hydrophobic hydration of concave surfaces. *Mol. Phys.*, 99:1289–1298, 2001.
P. Jedlovszky. The hydrogen bonding structure of water in the vicinity of apolar interfaces: A computer simulation study. *J. Phys.: Condensed Matter*, 16:5389–5402, 2004.
T. M. Raschke and M. Levitt. Nonpolar solutes enhance water structure within hydration shells while reducing interactions between them. *Proc. Natl. Acad. Sci. U. S. A.*, 102:6777–6782, 2005.

[46] F. H. Stillinger. Structure in aqueous solutions of nonpolar solutes from the standpoint of scaled-particle theory. *J. Solution Chem.*, 2:141, 1973.

[47] N. Goldenfeld. *Lectures on Phase Transitions and the Renormalization Group (Frontiers in Physics)*. Perseus Books, U.S.A., 1992.

[48] J. M. Pradeep Kanth and Ramesh Anishetty. Molecular mean field theory for liquid water. *Physica A*, doi: 10.1016/j.physa.2011.08.027, 2011.

[49] L. Pauling. The structure and entropy of ice and of other crystals with some randomness of atomic arrangement. *J. Am. Chem. Soc.*, 57(12):2680–2684, 1935.

[50] P. M. Chaikin and T. C. Lubensky. *Principles of Condensed Matter Physics*. Cambridge University Press, 1st edition, 2000.

[51] R. L. Blumberg, H. E. Stanley, A. Geiger, and P. Mausbach. Connectivity of hydrogen bonds in liquid water. *J. Chem. Phys.*, 80(10):5230–5241, 1984.

[52] J. D. Smith, C. D. Cappa, K. R. Wilson, B. M. Messer, R. C. Cohen, and R. J. Saykally. Energetics of hydrogen bond network rearrangements in liquid water. *Science*, 306(5697):851–853, 2004.

[53] J. F. Nagle. Lattice statistics of hydrogen bonded crystals. I. The residual entropy of ice. *J. Math. Phys.*, 7(8):1484–1491, 1966.

[54] E. H. Lieb. Residual entropy of square ice. *Phys. Rev.*, 162(1):162–172, 1967.

[55] D. P. Landau and K. Binder. *A Guide to Monte Carlo Simulations in Statistical Physics*. Cambridge University Press, 3rd edition, 2009.

[56] J. J. de Pablo, Q. Yan, and F. A. Escobedo. Simulation of phase transitions in fluids. *Annu. Rev. Phys. Chem.*, 50(1):377–411, 1999.
A. Z. Panagiotopoulos. Monte carlo methods for phase equilibria of fluids. *J. Phys.: Cond. Matter*, 12(3):R25–R52, 2000.
M. Girardi, A. L. Balladares, V. B. Henriques, and M. C. Barbosa. Liquid polymorphism and density anomaly in a three-dimensional associating lattice gas. *J. Chem. Phys.*, 126(6):064503, 2007.

[57] W. T. King and R. E. Barletta. Oxygen isotope fractionation in H_2O and the structure of liquid water. *J. Chem. Phys.*, 67(1):180–187, 1977.
J. B. Brubach, A. Mermet, A. Filabozzi, A. Gerschel, and P. Roy. Signatures of the hydrogen bonding in the infrared bands of water. *J. Chem. Phys.*, 122(18):184509, 2005.
P. H. L. Sit, C. Bellin, B. Barbiellini, D. Testemale, J. L. Hazemann, T. Buslaps, N. Marzari, and A. Shukla. Hydrogen bonding and coordination in normal and supercritical water from x-ray inelastic scattering. *Phys. Rev. B*, 76(24):245413, 2007.
T. Tokushima, Y. Harada, O. Takahashi, Y. Senba, H. Ohashi, L. G. M. Pettersson, A. Nilsson, and S. Shin. High resolution x-ray emission spectroscopy of liquid water: The observation of two structural motifs. *Chem. Phys. Lett.*, 460(4-6):387–400, 2008.
B. M. Auer and J. L. Skinner. Water: Hydrogen bonding and vibrational spectroscopy, in the bulk liquid and at the liquid/vapor interface. *Chem. Phys. Lett.*, 470(1-3):13–20, 2009.

[58] J. Martí, J. A. Padro, and E. Guárdia. Molecular dynamics simulation of liquid water along the coexistence curve: Hydrogen bonds and vibrational spectra. *J. Chem. Phys.*, 105(2):639–649, 1996.
A. Kalinichev. Structure and hydrogen bonding of liquid water at high hydrostatic pressures: Monte Carlo NPT-ensemble simulations up to 10 kbar. *J. Mol. Liq.*, 82(1-2):57–72, 1999.
J. Martí. Dynamic properties of hydrogen-bonded networks in supercritical water. *Phys. Rev. E*, 61(1):449–456, 2000.

[59] J. M. Pradeep Kanth and Ramesh Anishetty. Hydrophobic force a Casimir-like effect due to hydrogen bond fluctuations. *arXiv:1109.2733*, 2011.

[60] R. P. Boas and C. Stutz. Estimating sums with integrals. *Am. J. Phys.*, 39(7):745–753, 1971.

[61] D. Chandler. Interfaces and the driving force of hydrophobic assembly. *Nature*, 437:640–647, 2005.

[62] B. Widom, P. Bhimalapuram, and K. Koga. The hydrophobic effect. *Phys. Chem. Chem. Phys.*, 5:3085–3093, 2003.

[63] A. Goebel and K. Lunkenheimer. Interfacial tension of the water/n-alkane interface. *Langmuir*, 13:369–372, 1997.

[64] I. V. Brovchenkoa, A. Geiger, and D. Paschek. Simulation of confined water in equilibrium with a bulk reservoir. *Fluid Phase Equilibria*, 183:331–339, 2001.
P. Kumar, S. V. Buldyrev, F. W. Starr, N. Giovambattista, and H. E. Stanley. Thermodynamics, structure, and dynamics of water confined between hydrophobic plates. *Phys. Rev. E*, 72:051503, 2005.

[65] R. Godawat, S. N. Jamadagni, and S. Garde. Characterizing hydrophobicity of interfaces by using cavity formation, solute binding, and water correlations. *Proc. Natl. Acad. Sci. U. S. A.*, 106(36):15119–15124, 2009.

[66] L. Lu and M. L. Berkowitz. Hydration force between model hydrophilic surfaces: Computer simulations. *J. Chem. Phys.*, 124:101101, 2006.